Dynamical Adaptive Backstepping-Sliding Mode Control of Pneumatic Actuator

BY

LIANG HE

A Thesis

Submitted to the Faculty of Graduate Studies

In Partial Fulfillment of the Requirements

For the Degree of

MASTER OF SCIENCE

*****

Department of Mechanical & Manufacturing Engineering

The University of Manitoba

Winnipeg, Manitoba

THE UNIVERSITY OF MANITOBA

FACULTY OF GRADUATE STUDIES
*****
COPYRIGHT PERMISSION PAGE

DYNAMICAL ADAPTIVE BACKSTEPPING-SLIDING MODE CONTROL OF PNEUMATIC ACTUATOR

BY

LIANG HE

A Thesis/Practicum submitted to the Faculty of Graduate Studies of The University of

Manitoba in partial fulfillment of requirements of the degree

of

Master of Science

For the Continuance

Abstract

Pneumatic actuators are popular due to their extensive use in production lines of automobile industry in 1950s. Advantages of pneumatic actuators over other power systems include high power to weight ratio, cleanness, low costs, and low maintenance. The challenges in pneumatic actuators are the high compressibility of fluid medium, the nonlinearities in the system dynamics (i.e., pressure dynamics and valve flow dynamics), and the modeling of those characteristics. Another great challenge in the pneumatic actuators is the stick-slip friction caused by pneumatic cylinder seals, which keep pressurized air inside the pneumatic cylinder chambers. As the motion of actuator commences and stops, a jerky motion caused by the stick-slip friction can create adverse effects to the performance of pneumatic actuators, e.g., instability, slow response, large tracking errors, and limit cycle. Conventionally, the friction caused adverse effects in mechanical systems are reduced by increasing the stiffness of the control mechanisms. However, due to the compliance nature of pneumatically operated system, an alternative approach via adaptive friction compensation is considered herein.

This thesis documents the development of a novel nonlinear controller for servo pneumatic actuators that give good reference tracking at low speed motion, where friction has strong effect to the system behaviors. The design of the nonlinear controller presented in this thesis is based on the formalism of Lyapunov stability theory. The controller is constructed through a dynamical adaptive backstepping-sliding mode control algorithm. The conventional Lyapunov-based control algorithm is often limited by the order of the dynamical system; however, the backstepping design concept allows the control algorithm to be extended to higher order dynamical systems. In addition, the friction is estimated on-line via the Lyapunov-based adaptive laws embedded in the controller; meanwhile, the sliding mode control provides high robustness to the system parameter uncertainties. The simulation results clearly demonstrating the improved system performance (i.e., fast response and the reduced tracking error) are presented. Finally, the integration of the controller with a Lyapunov-based pressure observer reduces the state feedback of the servo pneumatic actuator model to only the piston displacement.

Acknowledgements

First and foremost, I would like to express my deepest thanks to Dr. Nariman Sepehri, my thesis advisor, who gave me freedom to explore my thesis topic without restriction, allowed me to make mistakes so that I might learn from them, and provided guidance and direction when it was needed. I would also like to thank Dr. Sepehri for allowing me to partake in a number of other unrelated research endeavors, during the course of my program, that included the first publication in IEEE international conference on cognitive informatics (ICCI'10).

I would also like to thank my advisory committee members, Dr. S. Balakrishnan and Dr. W. Kinsner, for their review and suggestions.

Finally, no words can describe my thanks to my mom and dad for a lifetime of support which has made me who I am today.

Table of Contents

List of Figures

List of Tables

List of Symbols

a	shape parameter in stress-strain curve of Dahl's friction model
A	annulus area of the piston
A_v	variable area of valve orifice
b	viscous friction coefficient
c_p	specific heat at constant pressure
c_v	specific heat at constant volume
C_d	discharge coefficient
e	error variable
$f(\cdot)$	single-valued ordinary differential equation $R^n \rightarrow R$
$\boldsymbol{f}(\cdot)$	single-valued ordinary differential equation $R^n \rightarrow R^n$
$F(\cdot)$	set-valued differential inclusion $R^n \rightarrow R$
$\boldsymbol{F}(\cdot)$	set-valued differential inclusion $R^n \rightarrow R^n$
F_a	applied force
F_C	Coulomb friction
F_f	friction
F_N	normal force
F_S	static friction
F_{spring}	spring force
$F_{stribeck}$	friction due to Stribeck effect
$g(\cdot)$	function describing Stribeck effect in LuGre friction model
k	spring constant or control gain (depends on the circumstances when it is used)
k_v	control gain between valve spool and control input
L	scale factor in ramp reference trajectory
m	mass of air in pneumatic cylinder chamber
m_i	mass flow through orifice $(i = 1, 2)$
M	mass of piston
P	pressure
P_{atm}	atmospheric pressure

P_{cr}	critical pressure
P_i	pressures at cylinder chambers $(i = 1, 2)$
P_u, P_d	up-stream and down-stream pressures with respect to valve orifice
P_s	supply pressure
P_Δ	pressure differential across the piston
Q	heat transfer through cylinder wall
r	ratio of specific heat
R	universal gas constant
s	measure of combined tracking error or distance to the sliding surface
$sign(x)$	sign function with $sign(0) = 0$
$Sign(x)$	set-valued sign function
T	absolute temperature
u_v	control input to servo valve
U	energy potential
v	velocity
v^*	zero velocity interval
v_s	Stribeck velocity
$V(\cdot)$	Lyapunov function (or candidate)
V_1, V_2	volumes of chamber 1 and chamber 2, respectively
V_{o1}, V_{o2}	fixed volume of chambers 1 and 2, respectively
$W(\cdot)$	positive definite function
x	displacement
$\boldsymbol{x}$	column vector in R^n
z	average bristle deflection

Greek Symbols

α	thermal expansion coefficient
γ	positive constant gain
Γ	positive constant gain
ε	system state
θ	unknown parameter
λ	convergence rate (or eigenvalue)

μ_C	Coulomb friction coefficient or kinetic friction coefficient
μ_S	static friction coefficient
ρ	air density
σ	equivalent spring constant in Dahl's friction model
σ_0	equivalent spring constant of bristle
σ_1	equivalent damping coefficient of bristle
σ_2	viscous coefficient in LuGre friction model
τ	time constant of valve spool or time shift factor in ramp reference trajectory
ϕ	pseudo-potential in systems with irreversible energy
$\psi(\cdot,\cdot)$	normalized mass flow rate

Subscripts

d	desired (or reference) value
m	mass
p	piston
$ploy$	polynomial
r	relative motion
v	valve spool

Accent

$\hat{*}$	estimate value
$\tilde{*}$	estimation error
$\dot{*},\ddot{*},\dddot{*}$	time derivative (1^{st} , 2^{nd}, and 3^{rd})

Chapter 1. Introduction

1.1 Preliminary Remark

Pneumatic systems use pressurized gases to control and transmit power. As their name implies, pneumatic systems typically use air as the fluid medium because air is safe, no cost, readily available fluid, and easy to dispose. Due to its high force-output to weight ratios, servo pneumatic actuators are well suited for modern manufacturing and production plants, e.g., pneumatic lifting devices, pneumatic hammers, and pneumatic adjusting devices for car seats. However, due to its complex nonlinear dynamics, the control of servo pneumatic actuators remains a difficult task and an active area of fluid power research. A recurring issue with the servo pneumatic actuator is the level of friction in the system, which affects the stability, accuracy, and repeatability.

In a typical servo pneumatic actuator, as shown in Figure 1.1, the movement of the rod and the piston are subject to friction. The surface contact between the rod and the lip seal and the contact between the piston O-ring and seal and the cylinder wall as well as the viscous effects of the lubricant all generate friction.

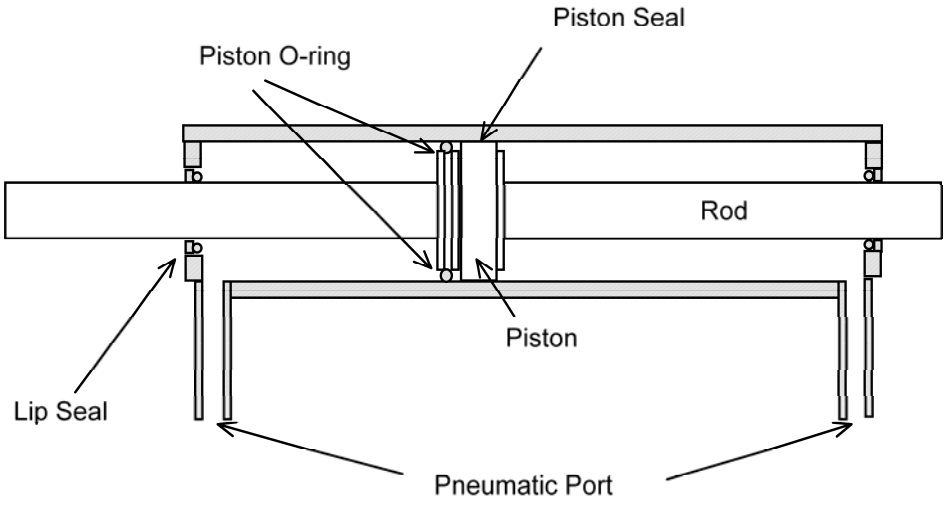

Figure 1.1 Cutoff view of pneumatic actuator.

Besides friction, some other non-idealities associated with pneumatic actuators include nonlinear valve flow dynamics, and nonlinear pressure dynamics. All of these problems impair the performance of the system. Recently, there is an increasing interest in the design and implementation of nonlinear control strategies that attempt to maintain the performance despite the influence of friction and the nonlinearities associated with the servo pneumatic actuator.

1.2 Friction in Mechanical Systems

Friction is present in all machines incorporating parts with relative motion. Although friction may be a desirable property, as it is for brakes, it is generally an impediment for servo control.

In a mechanical system under the influence of friction, the contacting surface is in the static friction regime before the motion commences, and an actuation force greater than the static friction is required to start the relative motion. The friction at static regime is determined by the very small displacement between contacting bodies, but the relative velocity or motion at this regime is considered to be zero. Therefore, friction in this regime is considered as a static force. As the motion commences, the friction suddenly decreases as it switches to the dynamic friction regime. In this regime, the friction is a function of relative velocity; in other words, the motion or the dynamics in the contacting bodies determines the dynamic evolution of friction, hence the name dynamic friction. The sudden change in friction results in a jerky actuator motion, which makes positional control and repeatability difficult.

The effect described above, is commonly referred to as stick-slip friction. The stick-slip friction is a nonlinear friction phenomenon and can be found in the servo pneumatic actuator moving at low speed. Modeling the sudden switching is difficult and precise control of the system usually involves complex system identifications and predictions [1]. It is therefore important for control engineers to understand friction phenomena and obtain the knowledge on how to deal with them effectively. The knowledge comes from stability theory, nonlinear control, nonlinear system identification, adaptive control, etc [2].

Model-oriented friction compensation techniques are based on the knowledge of suitable friction models that predict the real friction. Friction is quite often modeled as a static mapping of relative velocity. The static mapping of friction provides good representations for static friction, Coulomb friction, and viscous friction. In the last decade, the interests in dynamic friction model have increased. Some experimental observations of dynamic behaviors are Stribeck effect, static friction variation, and friction lag and memory [2]. These properties of friction are by no means complete but serve to illustrate many facets of friction behavior; however, these properties of friction cannot be described by the static mappings of friction. This is basically due to the fact that friction does not have an instantaneous response on a change of relative velocity, i.e., friction has internal dynamics [3]. Therefore, dynamic friction model is necessary to investigate the control associated with friction, and it has the potential to improve the quality of a control system [2]. Dahl [4] presented a solid friction model based on the stress and strain curve on ball bearings, and the dynamic behavior of static friction is considered in the model. The LuGre friction model is another dynamic friction model presented in [5], and the extensive analysis of the model and the applications to control systems with friction are discussed in [6].

From the mathematical perspective, a system with friction is often modeled as a non-smooth system, and the analysis of this type of system is taken into a different domain, the Filippov's system [7]. Consequently, the formalism of Lyapunov stability theory has to be extended to non-smooth dynamical systems via the construction of non-smooth Lyapunov functions [8]. The mathematical attempts to resolve the friction induced instability in control system are provided in [9]. With the knowledge obtained from aforementioned system analyses, it is possible to deal with friction effectively [2].

Conventionally, the friction induced adverse effects are reduced by increasing the stiffness of the control mechanism [2]; however, it becomes a difficult task for a servo pneumatic actuator to increase its stiffness in the face of high compressibility of air. Therefore, instead of bluntly increasing the stiffness of the control mechanism, nonlinear control techniques have been proposed for the servo pneumatic actuators to achieve tracking control and adaptive compensation of friction [10-12].

1.3 Control Strategies for Nonlinear Systems

The pneumatic system is highly nonlinear. A linear control approach can be applied to a nonlinear system through linearization; however, the approach will not cover higher order terms that may have great effects on the system's behavior. Therefore, it is quite advantageous to treat nonlinear problems directly with nonlinear controls. Some of the advantages of nonlinear control approaches over linear control approaches are listed as follows: (1) the validity of nonlinear model in large operation range, (2) the applications to nonlinearizable systems with discontinuous behavior, and (3) high tolerance to parameter uncertainties (e.g., a linear controller based on inaccurate model may show significant degradation or instability while a nonlinear robust controller can tolerate the model uncertainties by intentionally introducing nonlinearities to the controller) [13].

A simple and popular robust approach to the deterministic control of nonlinear system with uncertainties is the sliding mode control. This approach is based upon the special behavior of variable structure systems in the so-called sliding regime. The sliding mode control is synthesized by means of high-frequency discontinuous regulation signals, and a sliding layer can be created to make the control signal smooth. The sliding mode controller was implemented on a servo pneumatic actuator by Gulati et al.[12].

The general approach of a traditional Lyapunov-based nonlinear controller design is to construct a control Lyapunov function (CLF) according to the Lyapunov stability theory. The idea is to formulate a scalar positive energy-like function of the system states, and then choose a control law that makes the CLF decrease along the system trajectories. A nonlinear control system thus designed is stable in the sense of Lyapunov. However, this approach was only valid to systems with relative degree one or two (i.e., the control input can only be separated from the output of interest by one or two integrations). The design obstacle can be avoided via an order reduction [14]. Thereafter, a traditional Lyapunov-based controller can be designed through cascading the lower-order subsystems. Such a control approach is called cascade control. A cascade controller for a servo pneumatic actuator was introduced by Guenther et al. [11].

Krstic et al [15] introduced the concept of backstepping design that enabled the CLF design to be applied to higher-order systems. As its name suggests, the backstepping

design approach “steps back” toward the control input starting with the scalar equation of the output of interest, which is separated from the control input by the largest number of integrations. This design approach was used to construct a nonlinear controller for a servo pneumatic actuator by Rao et al. [10].

Lyapunov-based adaptive controls are often used to control nonlinear systems with parameter uncertainties including unknown bounds [13]. An algorithm for the synthesis of dynamical adaptive backstepping (DAB) controller was proposed by Rios-Bolivar et al. [16]. In order to provide robustness in the presence of undesirable disturbances, Rios-Bolivar [17] further proposed a combined dynamical adaptive backstepping-sliding mode control (DAB-SMC) algorithm. The application of this approach in adaptive-robust regulation of two nonlinear continuous chemical processes with uncertainties, and its validity was demonstrated via computer simulations [18]. The servo pneumatic actuator system is highly nonlinear and consists of parameter uncertainties. This suggests that the novel DAB-SMC algorithm may provide controllers that can improve the performance of the servo pneumatic actuator system.

1.4 Motivations and Objectives

Friction induced instability and low performance in servo pneumatic actuator suggest that a suitable compensation technique is necessary to achieve better trajectory tracking task. Although the use of nonmodel-based controllers, such as a PD controller [19] for the pneumatic system has met with a certain amount of success, nonmodel-based controllers cannot address the often significant nonlinearities associated with the servo pneumatic actuator system. Servo pneumatic actuators are governed by the nonlinear dynamics. The nonlinear model-based control techniques such as robust and/or adaptive control provide appealing features that can maintain the system performance in the face of modeling uncertainties [12]. In other words, it is highly desired to adapt nonlinear control techniques to solve nonlinear problems.

There are two objectives in this thesis. The first objective is to understand and analyze the mechanical system with friction. The second objective is to develop a novel nonlinear adaptive-robust control law to control the server pneumatic actuator with nonlinearities, uncertainties, and friction.

1.5 Thesis Layout

The remainder of this thesis is organized as follows. The operation of a typical servo pneumatic actuator is described in Chapter 2, and properties associated with this type of servo pneumatic actuator are characterized. Chapter 2 also develops a general mathematical model of the servo pneumatic actuator. Chapter 3 reviews the historical works exploring frictions and development of friction models that incorporate behavioral characteristics of friction. Chapter 4 considers friction in mathematical perspectives. By treating systems with friction as non-smooth dynamical systems, non-smooth analyses can be carried out. Chapter 4 also reviews the Lyapunov stability theory that provides the formalism for analyzing the stability and convergence properties of mechanical systems. Chapter 5 details the nonlinear controller design process, including previous works and the adapted dynamical adaptive backstepping-sliding mode controller synthesis. Subsequently, the controllers are implemented towards the control of the simulated mathematical model of the nonlinear servo pneumatic actuator in Chapter 6. The ability of the adapted controller to perform trajectory tracking and friction compensation as well as the performance of the servo pneumatic actuator is evaluated via computer simulations. The thesis is brought to an end by summarizing the study in Chapter 7.

Chapter 2. Servo Pneumatic Actuator

This chapter serves to familiarize the readers with servo pneumatic actuator. In Section 2.1, the components making up a typical servo pneumatic actuator are introduced and the operation of the circuit is described. The characteristics of the mass flow associated with the control valve in servo pneumatic actuator are given in Section 2.2. Section 2.3 develops a mathematical model for the servo pneumatic actuator.

2.1 Operation

The servomechanism considered in this study is a solenoid-driven proportional directional valve (i.e., servo valve) controlled pneumatic actuator (i.e., FESTO MPYE-5 valve and DNC actuator). An electrical signal u_v applied to the servo valve allows the positioning of the valve spool x_v. This modulates the flow of air into and out of the actuator chambers and creates a pressure differential across the piston. The force applied on the piston due to the pressure differential allows the piston position x_p to change.

The schematic of a typical servo pneumatic actuator is given in Figure 2.1. The servo

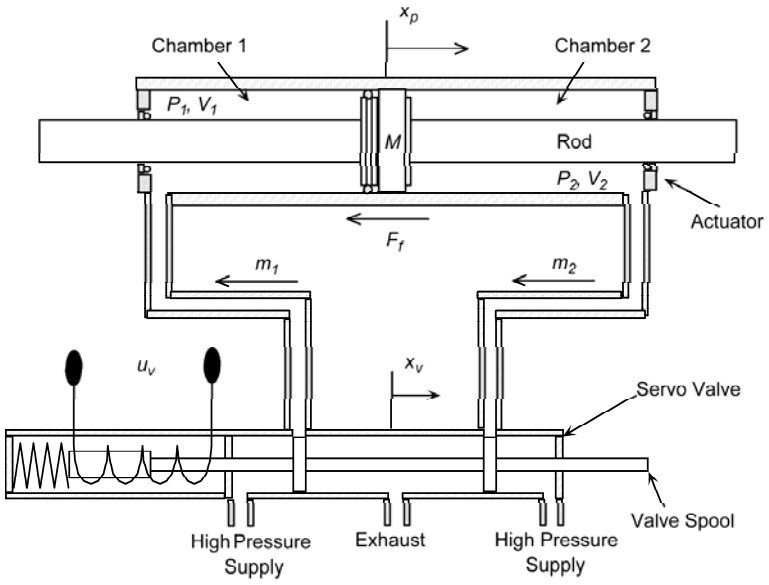

Figure 2.1 The schematics of pneumatic actuator controlled by a 5-port three-position servo valve.

pneumatic actuator consists of three main components, namely, the pneumatic power supply, the actuator, and the servo valve. The pneumatic power supply delivers compressed air to the high pressure supply port of the servo valve at a constant pressure, typically 500 to 700 kPa. The actuator cylinder consists of two chambers separated by a piston. A rod is attached to the piston to serve as the link between the actuator and the load. The servo valve is modeled as a 5-port three-position control valve, i.e., the valve has 5 openings and three operating positions, which regulate the motion of the actuator by controlling the air flow to and from the actuator chambers (see Figure 2.2).

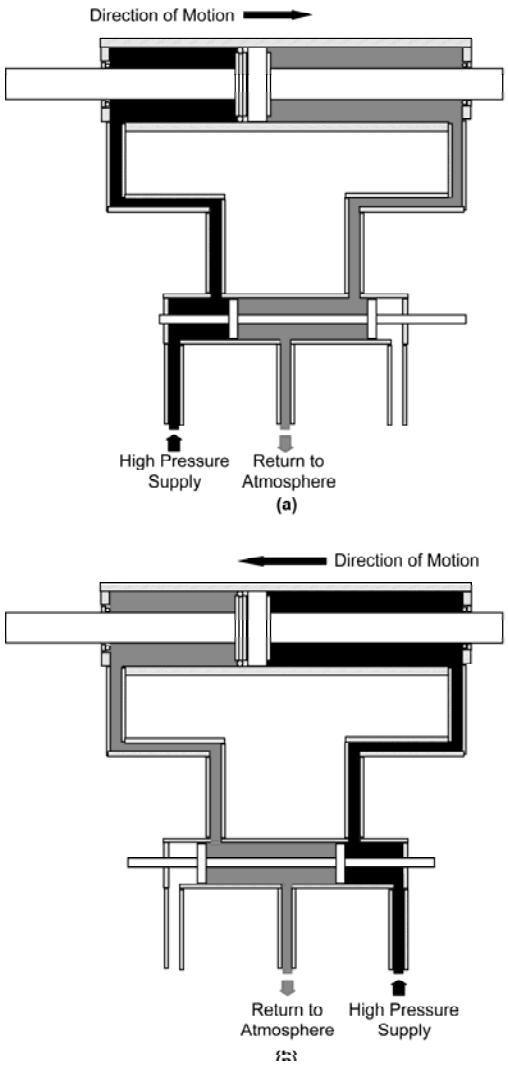

Figure 2.2 Operation of a typical pneumatic actuator system: (a) direction of air flows and actuator motion for positive valve spool displacement; (b) direction of air flows and actuator motion for negative valve spool displacement.

With reference to Figure 2.2 (a), when the valve spool is displaced to the positive position, the high pressure supply is connected to the left actuator chamber (chamber 1); meanwhile, the right actuator chamber (chamber 2) is connected to the exhaust port, which is directly open to the atmosphere. When the valve spool is displaced to the negative position, as shown in Figure 2.2 (b), the connections are reversed. When the valve spool is displaced, the net flow of fluid causes a pressure differential across the piston that causes the piston and rod to move. In contrary, the motion of the actuator stops when the valve spool is in the neutral position (see Figure 2.1), where there is no air flow into and out of the actuator chambers.

Position control of the servo pneumatic actuator is achieved by monitoring it through sensors and closing the loop through feedback control. To realize the closed-loop control, some means of positioning the valve spool is required. There are two types of electro-pneumatic valves that are commonly used to control the air flow in a pneumatic actuator. These are the on-off switching valves and the continuously acting servo/proportional valves.

The pulse width modulation (PWM) control approach is commonly used in on-off switching valves. The valves receive PWM signal as the control input to make the valve on and off successively. As a result, air mass is passed through the switching valve that is completely open or completely closed and is delivered to the actuator as discrete packets of air mass. The bigger pulse widths result in bigger packets of air mass. If the time rate of delivery of these packets is considerably faster than the dynamics of the actuator, then the system filters the discreteness of the packets and responds to the average of the input signal, similar to the continuously acting valve.

In this study, PWM is not pursued since the mathematical model is built upon the previous work [22], which uses a continuous acting valve. This task of continuous acting servo valve is accomplished by the solenoid-driven unit in a servo valve, shown schematically in Figure 2.3. The solenoid-driven valve converts an electrical command signal u_v into a proportional displacement of the valve spool x_v. With reference to Figure 2.3, the solenoid driven valve utilizes a linear motor arrangement to create the force imbalance required to position the valve spool and control air flow. The linear motor

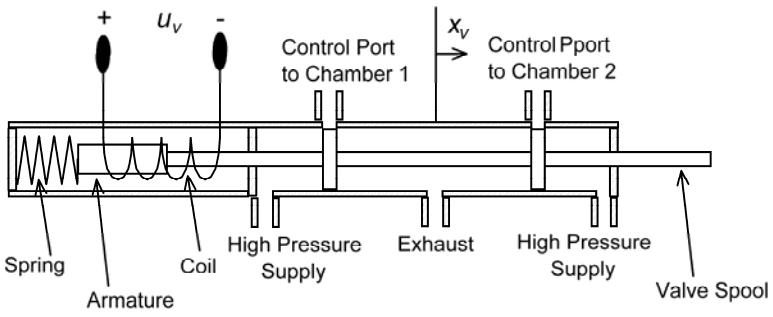

Figure 2.3 Schematic of the solenoid-driven proportional directional flow valve.

consists of a spring, an armature, and a DC current coil. The spring holds the armature in a neutral position originally. When a current is applied to the coil, a magnetic flux is generated which gives rise to a linear movement of the armature. Since the armature is coupled to the valve spool, the movement of the armature causes the displacement of valve spool from its neutral position. This displacement of valve spool connects the high pressure air to one control port and the exhaust port to the other control port. Finally, as the valve spool moves, the spring acts as a feedback and exerts a restoring force upon the armature. When the restoring force caused by the feedback spring is equal to the force exerted by the armature, the spool valve comes to a rest in the position proportional to the magnitude and corresponding polarity of current applied to the coil.

The relationship between the control input u_v and the valve spool position x_v, is often modeled as a simple gain k_v [20, 21]. However, the relevant manufacture's literature suggests that the dynamics of the valve spool are more adequately described by a 1st-order lag or 2nd-order lag [22]. In this study, the servo valve is modeled as a 1st-order lag:

$$\dot{x}_v = -\frac{x_v}{\tau} + \frac{k_v u_v}{\tau}, \tag{2.1}$$

where τ represents the valve spool 1st-order time constant.

Depending on the design of servo valve, an asymmetric flow deadband may exist [22]. Despite the existence of nonzero control signal in the deadband range, the flow through the orifice is zero. This suggests that the valve spool can be considered as always in the neutral position while control signal is in the deadband range. The modeling of flow deadband is accomplished by considering a null control signal inside the deadband.

Conventionally, the relationship between variable orifice area A_v of valve orifice and the valve spool displacement x_v in a servo valve is modeled according to the type of orifice used in the servo valve. Hence, an identification of the relationship is required prior to the modeling. In [22], visual inspection of the control valve reveals that the orifice area varies approximately linearly with the valve spool displacement x_v. Thus, the linear relationship between variable orifice area A_v and the valve spool displacement x_v is adapted in this study:

$$A_v = wx_v, \tag{2.2}$$

where w is the orifice area gradient of the corresponding control port.

2.2 Valve Flow Dynamics

To effect the motion of the actuator against the applied load, the chamber pressures P_i (where the subscript $i = 1, 2$ indicates chamber 1 and chamber 2, respectively) varies by charging and discharging the appropriate amount of control volume of air. The control volume of air is determined by the mass flow rate $\dot{m}_i$ of air passing through the variable area of valve orifice A_v. The mass flow rate $\dot{m}_i$ is a complex function of multiple variables, i.e., upstream pressure P_d, downstream pressure P_d, variable area of valve orifice A_v, etc.

The mathematical model for the mass flow rate $\dot{m}_i$ of air through the variable area of valve orifice is derived from normalized mass flow rate $\psi_i(P_u,\ P_d)$ of the fixed area of valve orifice. The downstream pressure P_d is equal to the chamber pressure P_i when charging and atmosphere pressure P_{atm} when discharging. Similarly, the upstream pressure P_u is equal to supply pressure P_s when charging and chamber pressure P_i when discharging. The behavior of the normalized mass flow rate $\psi_i(P_u,\ P_d)$ can be captured by the following switching rule:

$$\psi_i(P_u,\ P_d) = \begin{cases} \psi(P_s,\ P_i) & A_v \geq 0 \\ \psi(P_i,\ P_{atm}) & A_v < 0 \end{cases}, \tag{2.3}$$

where the signed variable area of valve orifice A_v serves to switch between charging ($A_v \geq 0$) and discharging ($A_v < 0$), respectively. According to the sign convention

defined in Figure 2.1, the switching rule (2.3) can be applied directly to chamber 1 while $-A_v$ is used for the flow switching rule applied to chamber 2.

The normalized mass flow rate $\psi_i(P_u,\ P_d)$ presents a hard nonlinearity due to a saturation of the mass flow through the fixed area of valve orifice. A critical pressure P_{cr} is compared with the ratio of the downstream pressure P_d to the upstream pressure P_u, P_d/P_u to determine the onset of the flow saturation. The critical pressure P_{cr} is calculated using the thermal expansion coefficient α of air. For adiabatic process (i.e., no heat exchange) of air, the thermal expansion coefficient α is given by the relation r:

$$\alpha_{adibatic} = r = \frac{c_p}{c_v}. \tag{2.4}$$

where c_v is the specific heat of air at constant volume and c_p is the specific heat of air at constant pressure. Both specific heat values account for the heat to temperature differential per unit mass of air.

Given the relation (2.4), the critical pressure of air flow for an adiabatic process is defined as

$$P_{cr} = \left(\frac{2}{r+1}\right)^{r/r-1}. \tag{2.5}$$

When the pressure ratio P_d/P_u is lower than the critical pressure P_{cr}, flow through the orifice is subsonic (unsaturated flow), and the flow depends only on upstream pressure. When the pressure ratio P_d/P_u is at the critical pressure, flow through the orifice become sonic (saturated flow). Beyond critical pressure the valve orifice is said to be saturated, mass flow rate is a function of both upstream pressure and downstream pressure. The commonly accepted normalized mass flow rate $\psi_i(P_u,\ P_d)$ is given as [12]

$$\psi_i(P_u, P_d) = \begin{cases} \frac{C_d P_u}{\sqrt{T}} \sqrt{\frac{r}{R}\left(\frac{2}{(\gamma+1)}\right)^{(r+1)/(r-1)}} & \frac{P_d}{P_u} \le P_{cr} \\ \frac{C_d P_u}{\sqrt{T}} \sqrt{\left(\frac{2r}{R(r+1)}\right)\left(\left(\frac{P_u}{P_d}\right)^{2/r} - \left(\frac{P_u}{P_d}\right)^{(r+1)/r}\right)} & \frac{P_d}{P_u} > P_{cr} \end{cases} \tag{2.6}$$

where T is the absolute temperature of the air and C_d is the discharge coefficient of the valve orifice, typically well characterized by the valve manufacturer. The parameter C_d

reflects a contraction of the flow path downstream of the orifice that reduces the effective flow area. The relationship between the orifice area and the mass flow rate of air is derived by assuming that the flow through the valve is an ideal gas undergoing an isentropic process (reversible adiabatic process), which leads to the variable area mass flow rate expression:

$$\dot{m}_1 = A_v \psi_1(P_u, P_d)$$
$$\dot{m}_2 = -A_v \psi_2(P_u, P_d). \tag{2.7}$$

2.3 Pneumatic Cylinder Dynamics

Thermodynamics provides the principle of converting thermal energy to other forms of energy (e.g., mechanical energy). In this study thermodynamic laws in adiabatic process is used to describe the compression and expansion of air in pneumatic cylinder, the changes of pressure value, and the required mechanical work. The ideal gas law, the conservation of mass and energy equations must be considered simultaneously to model the control volumes defined by the servo pneumatic actuator chambers. In the following the pressure dynamics of one pneumatic cylinder chamber is derived, and the resulting pressure differential equation can be applied equally to the other chamber. Assuming that the gas is ideal and the pressure and temperature are homogeneous (i.e., no variations in distributions of pressure and temperature) in the chamber, the ideal gas law is written as

$$PV = mRT, \tag{2.8}$$

where P is the chamber pressure, V is the volume of the chamber, m is the mass of the fluid in the chamber, and R is the ideal gas constant. For ideal gas, the following relationship holds for the gas constant R:

$$R = c_p - c_v. \tag{2.9}$$

Alternatively, the ideal gas law (2.8) may be expressed in terms of the air density ρ:

$$\frac{P}{R} = \frac{m}{V}T = \rho T. \tag{2.10}$$

Neglecting the potential energy and kinetic energy terms, the conservation of mass and energy equation is

$$\frac{d}{dt}(c_v V\rho T) = c_p \dot{m} T - P\dot{V} + \dot{Q}, \tag{2.11}$$

where $\frac{d}{dt}(c_v V\rho T)$ represents the rate of change of internal energy of air in the chamber, $c_p \dot{m} T$ is the internal energy of the air flows into or out of the chamber, $P\dot{V}$ is the rate at which work is done on the moving piston, and $\dot{Q}$ is the rate of heat transfer across the cylinder wall. With reference to the previous work in this area [23], the charging and discharging process are assumed to be adiabatic; therefore, $\dot{Q}$ can be ignored thereafter. Equation (2.11) becomes

$$\frac{d}{dt}(c_v V\rho T) = c_p \dot{m} T - P\dot{V}. \tag{2.12}$$

Substituting equation (2.10) into equation (2.12),

$$\frac{d}{dt}\left(\frac{c_v}{R} PV\right) = c_p \dot{m} T - P\dot{V}. \tag{2.13}$$

The term on left hand of equation (2.13) can be rearranged into

$$\frac{d}{dt}\left(\frac{c_v}{R} PV\right) = \frac{c_v}{R}\frac{d}{dt}(PV) = \frac{c_v}{R}\left(\dot{P}V + P\dot{V}\right). \tag{2.14}$$

Substituting equation (2.14) into equation (2.12),

$$\frac{c_v}{R}\left(\dot{P}V + P\dot{V}\right) = c_p \dot{m} T - P\dot{V} \tag{2.15}$$

Rearranging equation (2.15), the air pressure dynamics in the chamber is found to be

$$\dot{P} = \frac{c_p RT}{c_v V}\dot{m} - \frac{R}{c_v}\left(1 + \frac{c_v}{R}\right)\frac{P}{V}\dot{V}. \tag{2.16}$$

Given the relations in equations (2.4) and (2.9), equation (2.16) in an adiabatic process can be simplified as

$$\dot{P} = \frac{rRT}{V}\dot{m} - \frac{rP}{V}\dot{V}. \tag{2.17}$$

Choosing the middle of the stroke of the actuator as the datum of piston displacement x_p, the volumes of the actuator chambers can be expressed as

$$\begin{aligned} V_1 &= V_{o1} + A\left(\frac{L}{2} + x_p\right) \\ V_2 &= V_{o2} + A\left(\frac{L}{2} - x_p\right), \end{aligned} \tag{2.18}$$

where L is the full stroke length, A is the piston annulus area, and terms V_{o1} and V_{o2} denote a fixed volume at the end of chamber 1 and chamber 2, respectively.

Substituting equation (2.18) into equation (2.17), the differential equations that define the pressure dynamics of chamber 1 and chamber 2 are given respectively as

$$\begin{aligned} \dot{P}_1 &= \frac{rRT}{V_{o1}+A\left(\frac{L}{2}+x_p\right)}\dot{m}_1 - \frac{rP_1}{V_{o1}+A\left(\frac{L}{2}+x_p\right)}\dot{V}_1 \\ \dot{P}_2 &= \frac{rRT}{V_{o2}+A\left(\frac{L}{2}-x_p\right)}\dot{m}_2 - \frac{rP_2}{V_{o2}+A\left(\frac{L}{2}-x_p\right)}\dot{V}_2. \end{aligned} \tag{2.19}$$

With reference to equation (2.18), the volumetric change rate $\dot{V}_1$ and $\dot{V}_2$ can be obtained from the time derivative of equation (2.18):

$$\begin{aligned} \dot{V}_1 &= Av_p \\ V_2 &= -Av_p \end{aligned} \tag{2.20}$$

where $v_p = \dot{x}_p$ is the velocity of the piston. Substituting equation (2.20) into equation (2.19),

$$\begin{aligned} \dot{P}_1 &= \frac{rRT}{V_{o1}+A\left(\frac{L}{2}+x_p\right)}\dot{m}_1 - \frac{rP_1A}{V_{o1}+A\left(\frac{L}{2}+x_p\right)}v_p \\ \dot{P}_2 &= \frac{rRT}{V_{o2}+A\left(\frac{L}{2}-x_p\right)}\dot{m}_2 + \frac{rP_2A}{V_{o2}+A\left(\frac{L}{2}-x_p\right)}v_p. \end{aligned} \tag{2.21}$$

According to equation (2.21), the control valve regulates the mass flow rate $\dot{m}_i$ (i = 1, 2) of air to the corresponding actuator chambers, and hence controls the time evolution of the pressure differential dynamics, $\dot{P}_1$ and $\dot{P}_2$. However, $\dot{P}_1$ and $\dot{P}_2$ cannot be controlled independently due the specific configuration of the servo valve under study [22].

The dynamics of the piston and piston rod may be modeled as a 2nd-order differential equation:

$$\begin{aligned} \dot{v}_p &= \frac{1}{M}\left(P_\Delta A - F_f\right) \\ \dot{x}_p &= v_p \end{aligned} \tag{2.22}$$

where $\dot{v}_p$ is the acceleration of the piston, M is the combined mass of the piston and rod assembly, $P_\Delta = P_1 - P_2$ is the absolute pressure differential across the piston, and F_f represents the friction associated with servo pneumatic actuator. Given equations (2.1)-(2.22), the nonlinear equations representing the servo pneumatic actuator are given as follows:

$$
\begin{aligned}
&\dot{x}_v = -\frac{x_v}{\tau} + \frac{k_v u_v}{\tau} \\
&A_v = w x_v \\
&\psi_i(P_u,\ P_d) = \begin{cases} \psi(P_s,\ P_i) & A_v \geq 0 \\ \psi(P_i,\ P_{atm}) & A_v < 0 \end{cases} \\
&\psi_i(P_u, P_d) = \begin{cases} \frac{C_d P_u}{\sqrt{T}} \sqrt{\frac{r}{R}\left(\frac{2}{(r+1)}\right)^{(r+1)/(r-1)}} & \frac{P_d}{P_u} \leq P_{cr} \\ \frac{C_d P_u}{\sqrt{T}} \sqrt{\left(\frac{2r}{R(r+1)}\right)\left(\left(\frac{P_u}{P_d}\right)^{2/r} - \left(\frac{P_u}{P_d}\right)^{(r+1)/r}\right)} & \frac{P_d}{P_u} > P_{cr} \end{cases} \\
&\dot{m}_1 = A_v \psi_1(P_u, P_d) \\
&\dot{m}_2 = -A_v \psi_2(P_u, P_d) \\
&\dot{P}_1 = \frac{rRT}{V_{o1} + A\left(\frac{L}{2} + x_p\right)} \dot{m}_1 - \frac{r P_1 A}{V_{o1} + A\left(\frac{L}{2} + x_p\right)}\ v_p \\
&\dot{P}_2 = \frac{rRT}{V_{o2} + A\left(\frac{L}{2} - x_p\right)} \dot{m}_2 + \frac{r P_2 A}{V_{o2} + A\left(\frac{L}{2} - x_p\right)}\ v_p \\
&\dot{v}_p = \frac{1}{M}\left(P_\Delta A - F_f\right) \\
&\dot{x}_p = v_p
\end{aligned}
\tag{2.23}
$$

2.4 Summary

In this chapter, the mathematical model of the servo pneumatic actuator system is developed according to the physical laws. The mathematical model of the servo pneumatic actuator system shows high nonlinearities, which suggests that advanced nonlinear control techniques should be considered to control the actuator system. Besides the nonlinearities due to pressure dynamics and flow dynamics discussed in this chapter, friction associated with mechanical part of the pneumatic actuator system still remains as an untouched component in the system model. Friction can give adverse effect to the performance of the mechanical systems if it is not understood or modeled realistically. In the following chapter, friction associated with mechanical systems is explored.

Chapter 3. Friction in Mechanical Systems

Friction presents in the motion of all mechanical systems in contact, e.g., bearings, transmissions, hydraulic and pneumatic cylinders, valves, brakes, and wheels. Friction is a natural phenomenon with a long history, and the investigation on friction phenomena can be traced back to Da Vinci's time. Section 3.1 gives a brief historical review of friction. The physical phenomena of stick-slip motion are explained through tribology in Section 3.2. Section 3.3 provides representative friction models, which mathematicians use for system analysis and control engineers use for design of friction compensations in tracking control.

3.1 Investigation of Friction

Da Vinci (1452-1519) was one of the first scholars to study friction systematically. He realized how important friction was for the working machines. He made the observation that different materials moved with different ease. He summarized that this was a result of roughness of the material in question; thus, smoother material would have lower friction. Da Vinci stated the two basic laws of friction 200 years before Newton even defined what force was. He stated that: (1) the area in contact has no effect on friction, and (2) if the load of an object is doubled, its friction will also be doubled. However, Da Vinci did not publish his theories on friction.

Amontons (1663-1705) rediscovered the two basic laws of friction that first put forward by Da Vinci. Coulomb (1736-1806) verified the law rediscovered by Amonstons and introduced the concept of Coulomb friction (see Figure 3.1 (a)), where μ_C is the so-called kinetic friction coefficient, F_N is the normal force, and v_r is the relative velocity of motion). He suggested that the friction opposing the motion was constant and independent of the magnitude of the velocity. Coulomb friction is often called the dry friction because this friction is caused by pure contact.

Morin (1833) stated that there is a threshold friction that the applied force has to overcome before movement can occur. The friction opposing the motion before relative

motion starts, is called the static friction (see Figure 3.1 (b), where μ_s is the so-called static friction coefficient). The applied force required to overcome the static friction and start the relative motion is called the breakaway force. The combination of static friction model and Coulomb friction model is commonly referred to as the stick-slip friction model (or basic model of friction). It is shown in Figure 3.1 (c).

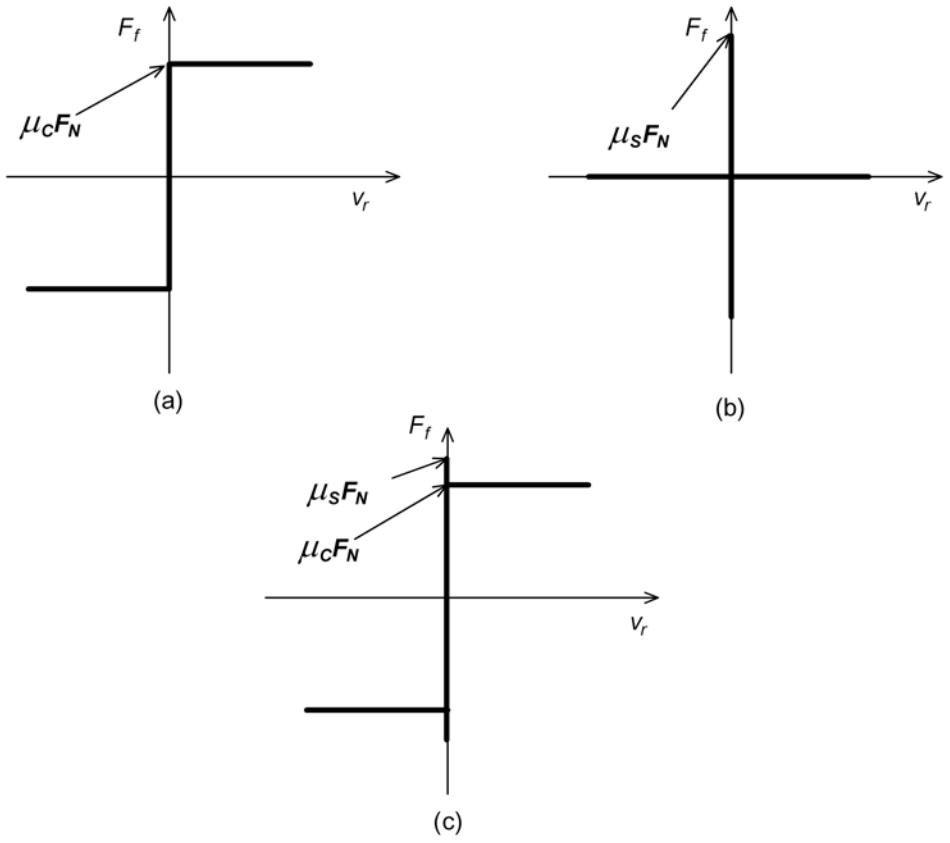

Figure 3.1 (a) Coulomb friction model, (b) static friction model, and (c) stick-slip (or basic) friction model.

One example is used to demonstrate the effect of stick-slip motion on linear spring actuated system. Assume the block m is at rest originally, a driving spring (with spring constant k) is uncompressed initially and the driving end commences to move with constant velocity v_d (see Figure 3.2 (a)). The spring is compressed until its compressive force reaches a value equal to the static friction F_s (see Figure 3.2 (b)). Then, the block starts to slip, and it is assumed that instantaneously the friction drops to the Coulomb friction F_c. The unbalanced force $(F_s - F_c)$ acts on the mass as acceleration $\dot{v}_m = \frac{F_s - F_c}{m}$,

so the slip velocity of the block increases until eventually the spring force drops sufficiently for deceleration to commence (see Figure 3.2 (c)). If the deceleration phase ends without the velocity falling to zero as for the case when the driving velocity is fast, then sticking does not reoccur, and the velocity of the block tends to the driving velocity v_d. If the velocity falls to zero during the deceleration phase then there are two possibilities for the next phase, either velocity reversal or sticking. The former should be excluded since it only occurs when $F_s > 3F_c$ [24]. If sticking occurs then again the driving spring is compressed until the block slips with the consequent drop in friction, and the system is then in the same state as at the beginning of the first slip phase. Thus the cycle is repeated.

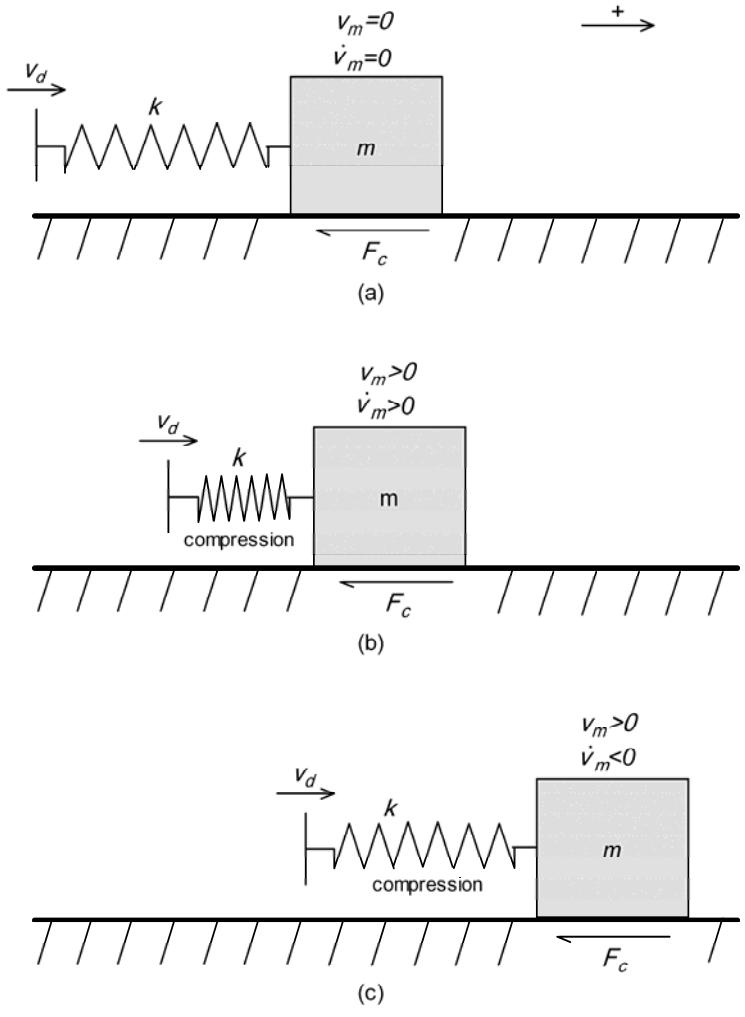

Figure 3.2 Stick-slip motion with constant driving velocity.

Lubricants such as grease and oils are often used in contacting surface to reduce wearing. These lubricants provide a fluid barrier between contacting surfaces and changes dry friction into a different type, the viscous friction. Reynolds (1842-1912) made a significant contribution to understanding viscosity in fluid, and he developed expressions for the friction caused by the viscosity of lubricants. Viscous friction is shown in Figure 3.3 (a). It has a linear relation with the relative velocity v_r (parameter b in Figure 3.3 is the viscous friction coefficient). Adding the viscous friction to the basic friction model, the so-called classical friction model is obtained (see Figure 3.3 (b)).

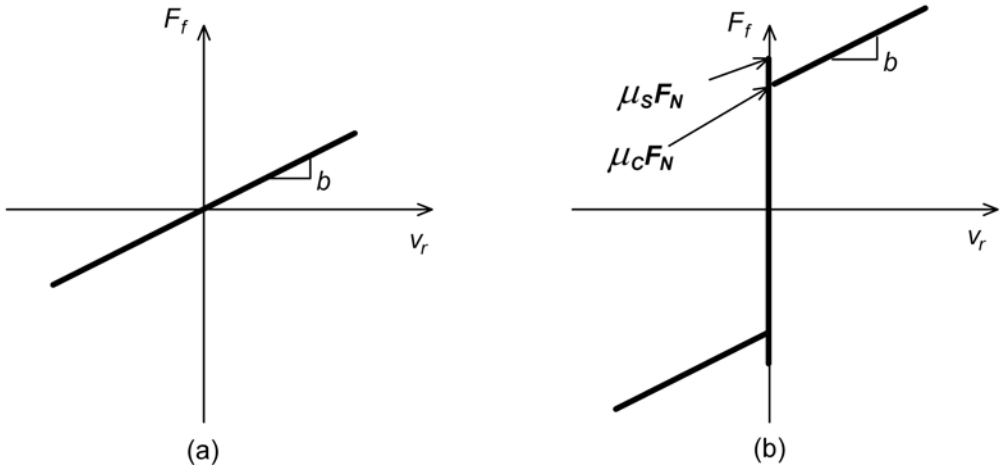

Figure 3.3 **(**a) Viscous friction model and (b) classical friction model.

Stribeck (1861-1950) made observations on friction when the contacting surface was moving at low velocity. He found that the friction was decreasing continuously with increasing velocity and claimed that the transition between stick and slip in friction was a continuous process. He named this phenomenon the Stribeck effect and the continuous transition, the Stribeck curve (see Figure 3.4 (a)). The Stribeck effect applies to lubricated surfaces. If the surface is dry and unlubricated, the transition from stick to slip can be considered essentially as discontinuous [1].

The classical friction model with Stribeck effect describes stick-slip motion under lubricated conditions, and the details of the stick-slip friction phenomena are captured by the experimental works from Tribology. The stick-slip motion can be categorized into four dynamic regimes (see Figure 3.4 (b)), each displaying the different characteristics of friction. These regimes are given as follows:

- Regime I : static friction
- Regime II: boundary layer lubrication
- Regime III: partial fluid lubrication
- Regime IV: full fluid lubrication

The four regimes each contribute to the dynamics that a driving force confronts as the driven object accelerates away from zero velocity.

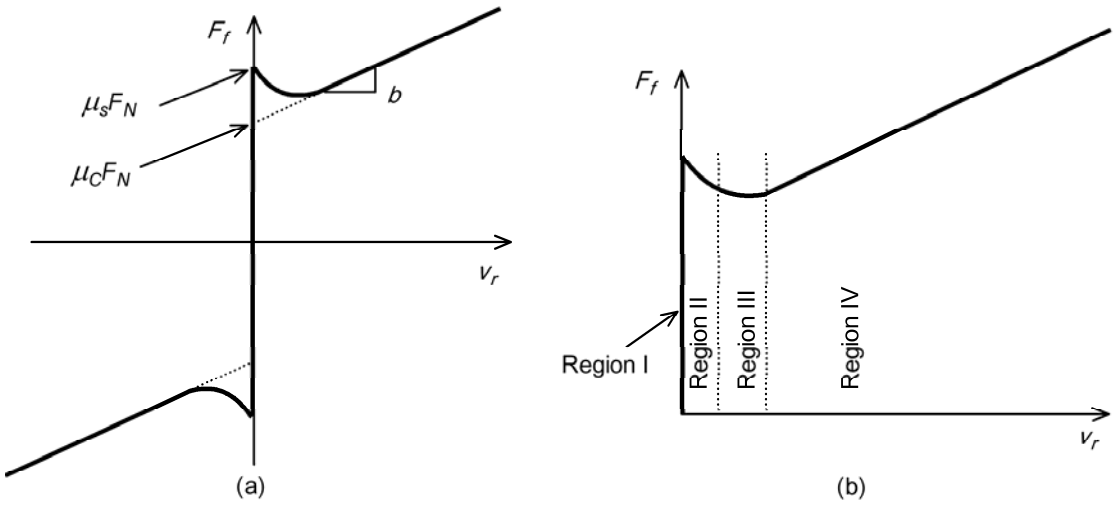

Figure 3.4 (a) Stribeck curve and (b) friction regimes of stick-slip motion.

3.2 Stick-slip Motion in Tribology

The word "tribology" is derived from the Greek word $TRIBOS$ meaning rubbing, so that a literal translation would be "the science of rubbing". Tribology was born in England in the 1930s. It is defined as the science and technology of interacting surfaces in relative motion and of related subjects and practices. It answers questions of wear mechanisms, true contact area, and relationships among friction, material properties and lubricating processes. Through tribology, physical understanding of friction can be obtained.

To understand the tribology of engineering surfaces, it is necessary to consider the surface topography. Early models of friction failed because the surface topography was misunderstood [25]. The true contact between engineering surfaces consists of conformal contact and nonconformal contact (see Figure 3.5). Conformal contacts are kinematically identified as area contacts, and nonconformal contacts are called point or line contact

when the radii of curvature of the surface do not match kinematically. The idealization of point or line contacts in nonconformal contacts is far from reality because the point or line contacts deform to create apparent areas of contacts, which increase with increasing load. The point or line contacts in noncoformal contacts are called asperities, and the true contact sites of asperities form the so-called contact junctions. The deformation of asperities at contact junctions is determined by the strength of the materials in study [2]. With the above interpretations of the true contact surface, friction behavior can be explained for each friction regimes in the stick-slip motion.

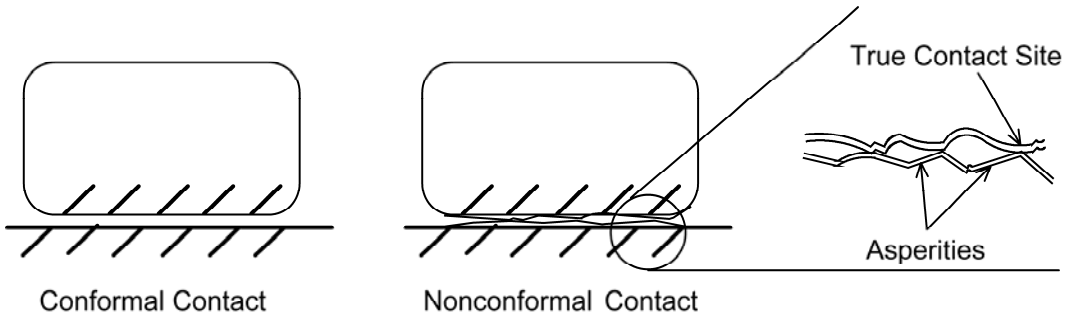

Figure 3.5 Surface topography.

Regime I: static friction

The first regime is the static friction or the presliding displacement. From the standpoint of control, asperities at contact junctions deform elastically, giving rise to presliding displacement; they also deform plastically, giving rise to the growing static friction. Dahl [4] studied experimental observations of presliding motion of friction and concluded that for small motions, a contact junction in static friction behaves like a spring (see Figure 3.6). This phenomenon is termed Dahl effect.

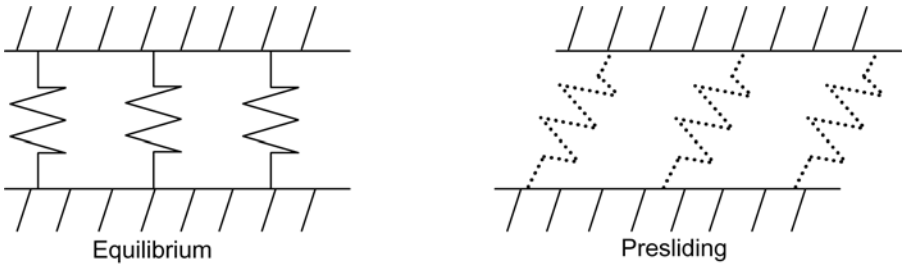

Figure 3.6 Dahl's spring model.

Regime II: boundary layer lubrication

This regime is called boundary lubrication regime, and it represents very low velocity sliding. The name comes from the fact that lubricants leave a deposit on the surface of the materials; nevertheless, they are unable to build a fluid film between the surfaces. This regime in the stick-slip motion is dominated by the solid to solid contact. Movement occurs when the applied force is greater than the static friction and the spring-like behavior of the asperities are sheared to rupture (see Figure 3.7). Because boundary lubrication is a process of shear in a solid, it is often assumed that friction in boundary lubrication is higher than fluid lubrication. This, however, is not always the case; it is not necessary for the shear strength of a solid to be greater than the viscous forces of a fluid [25].

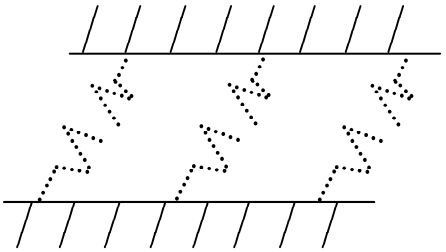

Figure 3.7 Rapture of spring-like behavior of asperities.

Regime III: partial fluid lubrication

In this regime, lubricant is brought into the nonconfromal contact region through motion. The greater viscosity or motion velocity, the thicker the fluid film will be. When the film is not thicker than the height of the asperities, some solid to solid contacts still occur. This is the reason why it is called the partial fluid lubrication. An analogy to the partial fluid lubrication is the water ski [2]. As the skier is elevated hydrodynamically by his increased velocity, his drag is reduced, allowing him or her to go even faster. With the increasing acceleration, the velocity increases and skier is elevated even higher. This is a positive feedback cycle. Hence, the dynamics of this regime is manifestly unstable. Partial fluid lubrication is the most difficult portions of modeling. It appears that the details of surface roughness, asperity size, and orientation, have significant effect on the behavior of friction in this regime. Of principal interest to the controls engineer is the

dynamics of partial fluid lubrication with changing velocity. Numerical investigations reveal a time lag between a change in velocity and a change in friction. Although the time lag may be small, its impact to stick-slip motion is substantial [25].

Regime IV: full fluid lubrication

In this regime, contacting surface is in full fluid lubrication. When full fluid lubrication occurs, all solid to solid contact has been eliminated and the surfaces are supported entirely by the lubricant. The relation between friction and velocity is near linear [1].

3.3 Modeling Friction

Engineers build model-based controllers and employ experimental data to adjust model parameters. To accurately design friction compensation in control system, a friction model must have a good representation of the real friction. The greatest challenge comes from the modeling of complex behaviors in friction for tiny motions and corresponding low velocities [25].

Simulation of stick-slip friction is difficult because of strongly nonlinear behavior in the vicinity of zero velocity. Karnopp [26] developed a friction model to overcome the problem with zero velocity detection and to avoid switching between different state equations for stick and slip. The model defines a zero velocity interval, $|v| < v^*$. Parameter v^* is used to delineate the region centered at zero velocity, inside which the velocity of the system is considered to be zero until the breakaway force applied to object is large enough to overcome the static friction. For velocities within this interval, the internal state of the system may change and be non-zero, but the output of the block is maintained at zero. The zero velocity interval however does not agree with real friction [6].

In Karnopp's model, the stick-slip friction is modeled as follows:

$$F_f = \begin{cases} F_a & \text{if } |F_a| \le F_s \text{ and } |v_r| \le v^* \\ F_s sign(F_a) & \text{if } |F_a| > F_s \text{ and } |v_r| \le v^* \\ F_C sign & \text{if } |v_r| > v^* \end{cases} \quad (3.1)$$

where F_a is the applied force (in servo pneumatic actuator, this force is the result of pressure differential P_Δ across the piston), F_s is the static friction, F_C is the Coulomb

friction. The particular value of v^* should be small enough to be considered negligible but large enough to avoid excessive stiffness in the numerical integration process [27].

One of the main problems with the simple classical stick-slip friction model is the discontinuity between static friction and Coulomb friction. The model does not provide a sufficient representation of friction, especially for a lubricated application because under lubrication the discontinuity is softened. In such conditions, behavior of friction depends on the changes of relative velocity [1].

Armstrong [25] presented theoretical treatment that predicted the critical velocity for termination of stick-slip friction as a function of system parameters. For control engineers these analyses provide an approach to the question of how slow a machine may be driven before the onset of stick-slip, and on what parameters this limit depends.

The friction model given in [9] consideres the behavior of friction as velocity varies. The model includes a combination of static friction, Coulomb friction, viscous friction, and the Stribeck effect. The friction is described as

$$F_f = F_N(\mu_C sign(v_r) + bv_r) - F_{stribeck}, \tag{3.2}$$

where

$$F_{stribeck} = F_N \frac{\mu_{stribeck} v_r}{1+\mu_{stribeck}|v_r|} \tag{3.3}$$

describes the Stribeck effect, $\mu_C > 0$ is the Coulomb friction coefficient, $b > 0$ is the viscous friction coefficient, $\mu_{stribeck}$ is a coefficient characterizing the modeling of the Stribeck effect, and F_N is the normal force. However, this model does not handle pre-sliding displacement. According to Amstrong [2], this can be done by describing the static behavior through a separate equation. Some mechanism must then give the switching between the modeling for sticking and the modeling for sliding.

The aforementioned friction model is a static mapping between the friction and the relative velocity, and it only describes a steady-state relationship. However, some friction phenomena cannot be captured by the static mappings, e.g., breakaway force variations and hysteretic behavior with varying velocity. Johannes et al. [28] experimentally found that the breakaway force depends on the increasing rate of the applied force. Hess et al.

[29] performed experiments with a periodic time varying velocity superimposed on a bias velocity, and the result of friction-velocity relation reveals hysteresis. The hysteresis is due to a time lag in the change of the friction following a change in the velocity. The time lag in the friction is called the frictional memory, and the time lag has been observed experimentally in a wide range of circumstances [2].

It has been argued that control strategies that attempt to compensate for the effect of friction without resorting to high gain control loops, inherently require a good friction model to predict and compensate for the friction [5]. Since control engineers are concerned with the dynamics of the friction, simple static mappings are not sufficient to address applications with high precision positioning requirement and low velocity tracking. There has been a significant interest in dynamic friction models. This has been driven by intellectual curiosity, demands for precision and advances in hardware that make it possible to implement friction compensators [6]. Thus, to obtain accurate friction compensation and best performance, friction model with dynamics behavior is necessary [2].

A dynamic model describing the spring-like behavior during sticking was introduced by Dahl [4]. The Dahl model is essentially Coulomb friction with a time lag in the change of friction when the direction of motions changes. Dahl's model accounts for the static friction and the Coulomb friction but does not describe the Stribeck effect [3].

The starting point for Dahl's model is the stress-strain curve in classical solid mechanics. When subject to stress the friction increases gradually until rupture occurs (refer back to Figure 3.7). Dahl modeled the stress-strain curve by a differential equation. Let x be the displacement, Dahl's model has the following form:

$$\frac{dF_f}{dx} = \sigma\left(1 - \frac{F_f}{F_c} sign(v_r)\right)^a \tag{3.4}$$

where σ is the equivalent spring constant and a is a parameter that determines the shape of the stress-strain curve. The friction F_f will never be larger than the Coulomb friction F_c if its initial value is such that $F_f(0) = F_c$ [3]. Notice that in this model the friction is only a function of the displacement and the sign of the relative velocity v_r. This implies that

the friction is only position dependent. A time domain Dahl friction model can be obtained by incorporating relative velocity term into equation (3.4):

$$\frac{dF_f}{dt} = \frac{dF_f}{dx} v_r = \frac{dF_f}{dx}\frac{dx}{dt} = \sigma\left(1 - \frac{F_f}{F_c} sign(v_r)\right) v_r. \tag{3.5}$$

where $a = 1$ is used and higher value will give a stress-strain curve with a sharper bend.

The LuGre model is another dynamic friction model presented in [5]. The model captures most of the friction characteristics, i.e., the Stribeck effect, hysteresis, spring-like characteristics for stiction, and varying breakaway force.

The modeling of presliding in LuGre friction model was inspired from Dahl's friction model. It visualizes the irregular asperities on contacting surfaces as elastic bristles (see Figure 3.8) and considers the average deflection of the bristles as a internal state z.

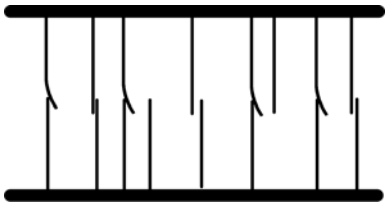

Figure 3.8 Bristles on contacting surface.

With reference to Dahl's spring model with equivalent spring constant σ, friction due to the average deflection of bristles is given as

$$F_f = \sigma z. \tag{3.6}$$

Substituting equation (3.6) into equation (3.5), the dynamics of internal state z is

$$\dot{z} = v_r - \sigma\left(\frac{|v_r|}{g}\right) z, \tag{3.7}$$

where the Coulomb friction F_C is replaced with a function g that models the Stribeck effect. A reasonable choice of g giving a good approximation of Stribeck effect is

$$g = F_c + (F_s - F_c) e^{\left(-\left(\frac{v_r}{v_s}\right)^2\right)}, \tag{3.8}$$

where v_s is the Stribeck velocity, or the threshold velocity, beyond which the average

bristle deflection becomes sufficiently large and rupture occurs. This corresponds to the sudden drop of friction in stick-slip motion.

Considering a combination of bending and damping of the bristle as well as viscous friction, the LuGre friction model has the final form given as

$$F_f = \sigma_0 z + \sigma_1 \dot{z} + \sigma_2 v_r, \tag{3.9}$$

where $\sigma_0 \equiv \sigma$ is equivalent spring constant of the bristles, σ_1 the equivalent damping coefficient for the rate of average bristle deflections, $\sigma_2 \equiv b$ is the viscous coefficient.

Given equations (3.7)-(3.9), the LuGre friction model is given as

$$\begin{aligned} F_f &= \sigma_0 z + \sigma_1 \dot{z} + \sigma_2 v_r \\ \dot{z} &= v_r - \left(\frac{|v_r|}{g}\right) z \\ \sigma_0 g &= F_c + (F_s - F_c) e^{\left(-\left(\frac{v_r}{v_s}\right)^2\right)} \end{aligned} \tag{3.10}$$

where σ_0 for the internal state dynamics $\dot{z}$ is rearranged into the Stribeck term g.

From the control perspective, parameter σ_0, σ_1, and σ_2 can be calibrated through systematic experimental identifications, which may involve considerable work [5]. These parameters may vary slowly but significantly in real applications due to temperature changes, material wear, lubrication conditions, and the normal acting forces between contact surfaces. The remaining parameters F_s, F_c, and v_s are normally estimated by the construction of the friction-velocity mapping measured during the steady state motions [30].

The LuGre friction model is used in the simulations of this study for two reasons: (i) the transition from static friction to kinetic friction needs to be modeled as a continuous process because lubricant is assumed to be present in the pneumatic cylinder, and (ii) the LuGre model provides a dynamic behavior of the friction internal state at low speed motion, which is desired for construction of the adaptive law incorporating the dynamic behaviors of friction.

3.4 Summary

In this chapter, a historical development of friction is reviewed, and the causes of friction

phenomena are explored through tribology. From control perspective, a good friction model can improve the performance of a control system. However, Friction is difficult to model. If the model does not reveal the true friction, then the control system can be unstable and reach a limit cycle. In the following chapter, stability analysis of system with friction is given to show the adverse effect of friction.

Chapter 4. Mathematical Preliminary for Stability Theory in Systems with Friction

This chapter is intended to investigate methods suitable in the analysis and control of systems with friction. In system analysis, it is quite often that the preliminary results of complex physical systems can be obtained from simplified models, e.g., a nonlinear system is locally unstable if its linear approximation is unstable. In the study of system with friction, the system is simplified into a non-smooth system model. Thereafter, an appropriate analysis can be carried out for the simplified system. In Section 4.1, the differences between a smooth system model and a non-smooth system model are clarified. A necessary condition to implement non-smooth system is the existence of solutions. Section 4.2 reviews Filippov's solution theory defined for the non-smooth system [7]. In advanced system analysis, one of the formalism for stability analysis is the Lyapunov stability theory. In Section 4.3 the theory is applied to non-smooth systems for stability analysis. Finally, the phase portrait of a system with persistent friction disturbance is used to verify the solution theory and the stability analysis.

4.1 Dynamical System Modeling

A dynamical system is a system whose states evolve with time. The adjective "dynamical" cannot be replaced by "dynamic" because the dynamic systems utilizing Newton's law of motion to describe the relationship between force and motion is a subset of dynamical systems, i.e., 2nd-order dynamical systems. The evolution of a dynamical system is governed by a set of rules and is usually put in the form of equations. Consider a dynamical system described by a set of ordinary differential equations:

$$\dot{\boldsymbol{x}}(t) = \boldsymbol{f}\big(t, \boldsymbol{x}(t)\big) \tag{4.1}$$

where $\boldsymbol{x}^{\boldsymbol{T}} = [x_1, x_2, \dots]$ is the state vector, $\boldsymbol{f} \in \boldsymbol{R} \times \boldsymbol{R}^{\boldsymbol{n}}$ is the differential equations whose variables are the states of the dynamical system, t is the time variable, and $\dot{\boldsymbol{x}} = d\boldsymbol{x}/dt$ is the time derivative of the state vector. Suppose that $\boldsymbol{f}\big(t, \boldsymbol{x}(t)\big)$ is continuous, and let

$(t_0, \boldsymbol{x}_0) \in \boldsymbol{R} \times \boldsymbol{R^n}$ be given. Then, if $\boldsymbol{f}\big(t, \boldsymbol{x}(t)\big)$ is linearly bounded, there exists one solution of system on $(-\infty, \infty)$ such that $\boldsymbol{x}(t_0) = \boldsymbol{x}_0$. Now add the hypothesis that $\boldsymbol{f}\big(t, \boldsymbol{x}(t)\big)$ is locally Lipschitz at $\boldsymbol{x}$, i.e., there exists constant $L(\boldsymbol{x}) > 0$ and $r > 0$ such that

$$\|\boldsymbol{f}(t, \boldsymbol{x_1}) - \boldsymbol{f}(t, \boldsymbol{x_2})\| \leq L(x)\|\boldsymbol{x_1} - \boldsymbol{x_2}\|, \forall x_1, x_2 \in B_r + \boldsymbol{x}, \tag{4.2}$$

where B is a ball with radius r in state space $\boldsymbol{R^n}$. Then there exists only one solution of the system on $(-\infty, \infty)$ such that $\boldsymbol{x}(t_0) = \boldsymbol{x}_0$ [9].

The difference between a smooth dynamical system and a non-smooth dynamical system is distinguished through an illustrating example. Consider a spring-mass assembly with one end of the spring attached to a stationary wall and the other end attached to a block (see Figure 4.1). Assuming that the block is subject to spring force and Coulomb friction,

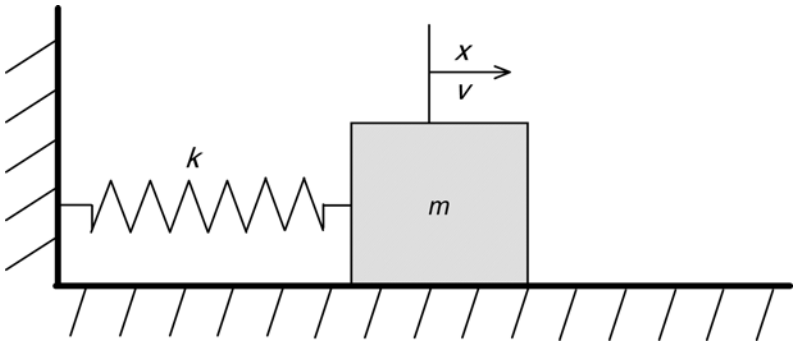

Figure 4.1 Mass-spring system with Coulomb friction.

the system can be represented by the following differential equation:

$$m\dot{v} = F_{spring} + F_C, \tag{4.3}$$

where F_{spring} is the force exerted on block by a linear spring, F_C is the Coulomb friction between block and the ground, m is the mass of the block, and v_r is the relative velocity of the block. Force laws are considered according to their energy potentials in the system. The energy potential of a linear spring is given as

$$U = \frac{1}{2}kx^2, \tag{4.4}$$

where x is the elongation of the spring and k is the spring constant. The force law of the spring can be expressed as

$$F_{spring} = f(x) = \frac{\partial U}{\partial x} = kx. \tag{4.5}$$

In contrast to the spring energy potential, the Coulomb friction has only energy pseudo-potential and it is given as

$$\phi = F_N \mu_C |v_r|. \tag{4.6}$$

where F_N is the normal force and μ_C is the Coulomb friction coefficient. The force law of Coulomb friction can be expressed as

$$F_C = f(v_r) = \frac{\partial \phi}{\partial v_r} = F_N \mu_C sign(v_r), \tag{4.7}$$

where the $sign(\cdot)$ function is defined as

$$sign(v_r) = \begin{cases} -1 & v_r < 0 \\ 0 & v_r = 0. \\ 1 & v_r > 0 \end{cases} \tag{4.8}$$

Both energy potential functions are absolute continuous (see Figure 4.2), but the energy potential for the spring force law is a smooth quadratic function (Figure 4.2 (a)) while the

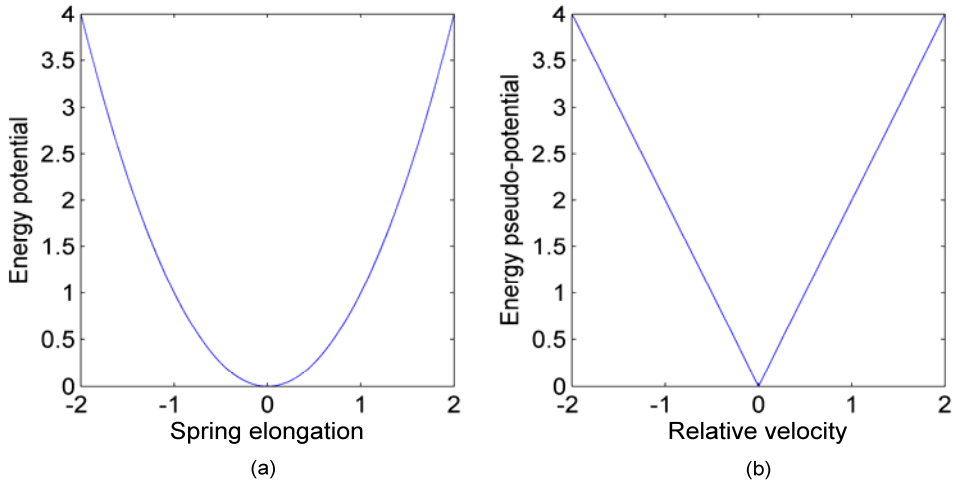

Figure 4.2 (a) Energy potential for spring force law and (b) Energy pseudo-potential for force law of Coulomb friction.

energy pseudo-potential for the force law of Coulomb friction is a non-smooth function (Figure 4.2 (b)). By non-smooth, it means there is a kink (non-smoothness) when the velocity passes the zero value. The definition of the existence and uniqueness of solution can be applied to the smooth potential function U. However, the non-smooth potential function ϕ does not satisfy the Lipschitz condition with a constant L everywhere, i.e., $L = \infty$ when relative velocity $v_r = 0$. Therefore, the definition of solution of non-smooth system is taken into consideration in a different domain, the Filippov's system.

4.2 Non-smooth Systems

In this section, the analysis of non-smooth systems is considered through an example of Coulomb friction in mechanical system. The classical derivative of a smooth continuous function is extended to the generalized derivative of Clarke for non-smooth continuous functions [9]. Considering the force law of Coulomb friction, where friction coefficient μ_C is assumed to be positive, the pseudo-potential ϕ and its partial derivative $\partial\phi/\partial v_r$ are shown in Figure 4.3 (a) and (b), respectively.

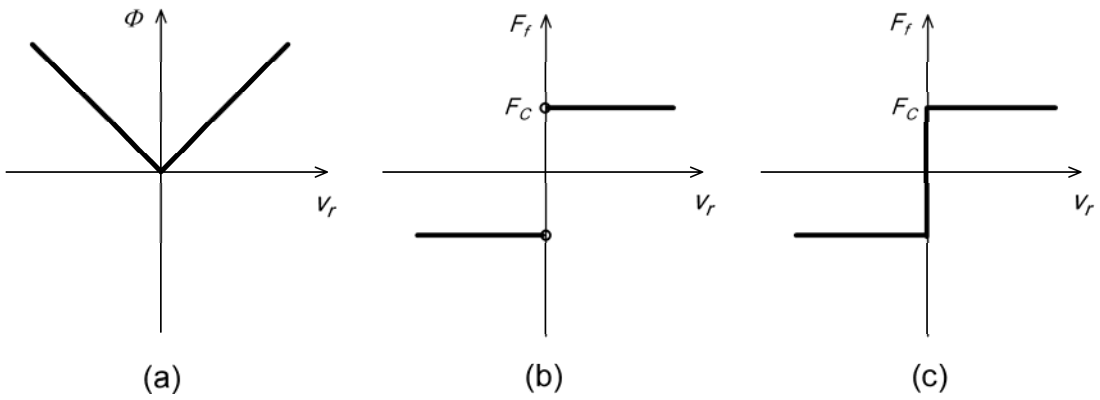

Figure 4.3 Potential, classical derivative, and generalized derivative.

The partial derivative $\partial\phi/\partial v_r$ is defined by the tangent line to the graph of ϕ when the graph is smooth at v_r. Although the function is not differentiable at everywhere in v_r, it possesses at each $v_r{}^*$a left and right derivatives defined as

$$\frac{\partial \phi}{\partial v_r}^{-} = \lim_{v_r \uparrow v_r^*} \frac{\phi(v_r)-\phi(v_r^*)}{v_r - v_r^*}$$
$$\frac{\partial \phi}{\partial v_r}^{+} = \lim_{v_r \downarrow v_r^*} \frac{\phi(v_r)-\phi(v_r^*)}{v_r - v_r^*}, \tag{4.9}$$

respectively. The generalized derivative of ϕ at $v_r = 0$ is declared as any value included between its left and right derivatives. Such an intermediate value can be expressed as a convex combination of the left and right derivatives:

$$\frac{\partial \phi}{\partial v_r} = (1-q)\frac{\partial \phi}{\partial v_r}^{-} + q\frac{\partial \phi}{\partial v_r}^{+}, \quad 0 \le q \le 1. \tag{4.10}$$

With reference to Figure 4.3 (c), the Coulomb friction has a map that associates with any v_r a set $F_C = F(v_r) = \partial\phi/\partial v_r$, and the Coulomb friction considered in such a fashion is a set-valued function of v_r. A set-valued function can therefore contain vertical segments on its graph. Coulomb friction F_C is a monotone set-valued function because its graph satisfies the following relation:

$$(F_C - {F_C}^*)^T(v_r - {v_r}^*) \ge 0, \ \forall({v_r}^*, {F_C}^*) \in graph(F_C), \ \forall(v_r, F_C) \in graph(F_C), \tag{4.11}$$

where $graph(F_C) = \{(v_r, F_C) |\ v_r \in R\}$.

The Coulomb friction F_C is called the maximal monotone function as well because there is no other monotone set-valued function whose graph strictly contains the graph of F_C (see Figure 4.3 (c)), and Coulomb friction can be described by set-valued $Sign(\cdot)$ function:

$$F(v_r) = Sign(v_r) = \frac{\partial \phi}{\partial v_r} = \begin{cases} -|F_c| & v_r < 0 \\ [-F_c, +F_c] & v_r = 0. \\ |F_c\,| & v_r > 0 \end{cases} \tag{4.12}$$

Consider a 1-D example, in which an under compensated block runs on a rough surface. As shown in Figure 4.4, assume that the block ($m = 1\ kg$) has an initial velocity v_0 and actuated by a constant force $F_a = 0.07\ N$. The Coulomb friction F_C always opposed the motion of the block and is modeled by the set-valued $Sign(\cdot)$ function.

The differential equation of the system given by Newton's 2nd law is

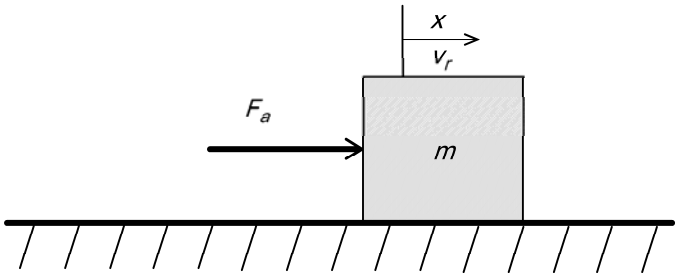

Figure 4.4 Mass move on rough surface.

$$m\dot{v}_r = F_a - F_c \tag{4.13}$$

Combining equation (4.13) with the set-valued function (4.12) representing the Coulomb friction,

$$m\dot{v}_r - F_a \in -F_C = -F(v_r) \tag{4.14}$$

Rearranging (4.14),

$$\dot{v}_r \in \frac{1}{m}\big(F_a - F(v_r)\big) = 0.07 - Sign(v_r) = \begin{cases} 1.07 & v_r < 0 \\ [-0.93, 1.07] & v_r = 0, \\ -0.93 & v_r > 0 \end{cases} \tag{4.15}$$

For a given initial condition, $v_0 \neq 0$, a solution of the initial value problem can be obtained as

$$v_r(t) = \begin{cases} 1.07t + C_1 & v < 0 \\ -0.93t + C_2 & v > 0 \end{cases} \tag{4.16}$$

with the constant C_1 and C_2 being determined by the initial conditions. Each solution reaches $v_r = 0$ in finite time. Once a solution arrives at $v_r = 0$, it cannot leave $v_r = 0$, because $\dot{v}_r > 0$ for $v_r < 0$ and $\dot{v}_r < 0$ for $v_r > 0$ [9]. The solution will therefore stay at $v_r = 0$, which implies that $\dot{v}_r$ belongs to the interval $[-0.93, 1.07]$ as defined in the generalized derivative. Hence, the existence of solution for the set-valued function is guaranteed by the linearly bounded derivative set $\dot{v}_r$. The system (4.15) having its solution defined in such a fashion is termed differential inclusion.

With reference to the general differential equation (4.1), it is natural for differential equations with discontinuous right-hand side to extend the notion of solution by replacing

the right-hand side $\boldsymbol{f}(\boldsymbol{x})$ with a set valued funciton $\boldsymbol{F}(\boldsymbol{x})$ such that $\boldsymbol{F}(\boldsymbol{x}) = \boldsymbol{f}(\boldsymbol{x})$ for all $\boldsymbol{x}$ for which $\boldsymbol{f}(\boldsymbol{x})$ is continuous in $\boldsymbol{x}$. At the point for which $\boldsymbol{f}(\boldsymbol{x})$ is discontinuous in $\boldsymbol{x}$ a suitable set for $\boldsymbol{F}(\boldsymbol{x})$ is required. Then an absolutely continuous function $\boldsymbol{x}(t)$ is said to be a solution of the differential inclusion if it fulfills

$$\dot{\boldsymbol{x}}(t) \in \boldsymbol{F}\big(t, \boldsymbol{x}(t)\big) \tag{4.17}$$

for almost everywhere except a set of Lebesgue measure zeros [9], where the Lebesgue measure on R assigns the value $d - c$ to the set $\{(c, d] |\, c \in R, d \in R\}$, i.e. $\mu\big((c, d]\big) = d - c$ for $d \geq c$, and Lebesgue measure of a single element is zero, i.e., Lebesgue measure zero.

The solution of differential equations with a discontinuous right-hand side obtained in such a fashion is based on Filippov's solution theory [7]. The solution $\boldsymbol{x}(t)$ in the sense of Filippov for a differential equation with a discontinuous right-hand side (also called Filippov's system) is absolutely continuous in time, i.e., there are no discontinuities in the solution.

4.3 Lyapunov Stability Theory

Given a control system, the first and most important question about its various properties is whether it is stable because an unstable control system is typically useless and potentially dangerous [13].

> *The English adjective "stable" originates from the Latin "stabilis", deriving itself from "stare", to stand. Its first acceptation is "standing firmly", "firmly established". A natural extension is "durable", not to mention the moral meaning "steady in purpose, constant"* [31].

Considering the differential equation (4.1), let $\boldsymbol{x}(t)$ be the unique solution for $t > t_0$, which depends continuously upon $(\boldsymbol{x}_0, t_0)$ and equals $\boldsymbol{x}_0$ at t_0. In addition, $\boldsymbol{x} = 0$ is assumed to be the equilibrium of (4.1). Graphically shown in Figure 4.5, for a 2nd-order system to be stable, the trajectory will initiate or terminate on the equilibrium point, where the distance from the equilibrium to any point on the trajectory is the magnitude of the state vector, $|\boldsymbol{x}|$.

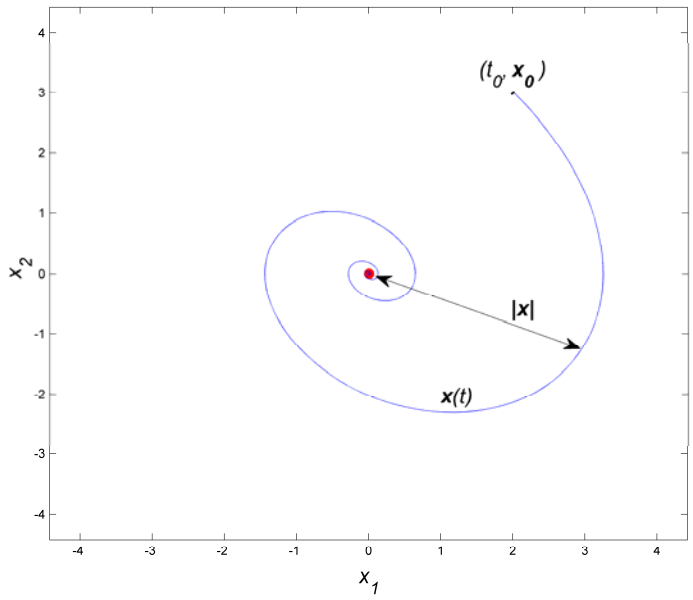

Figure 4.5 Phase plot of a stable 2nd-order system with equilibrium at the origin.

As far as control system engineers are concerned, stability means for a bounded input if the output is bounded, the system is stable [32]. Although many kinds of stability have been defined [33] only two are important to the control engineers. They are [32]: (1) the solution $\boldsymbol{x} = 0$ is said to be stable if for any $\varepsilon > 0$ and any t_0, there exists a $\sigma(\varepsilon, t_0)$ such that $|\boldsymbol{x}_0| < \sigma$ implies $|\boldsymbol{x}(t)| < \varepsilon$ for $t > t_0$; (2) the solution $\boldsymbol{x} = 0$ is said to be asymptotically stable if it is stable and in addition as $t \to \infty$, $|\boldsymbol{x}(t)| \to 0$.

The most useful and general approach for studying the stability of nonlinear system is the "General Problem of the Stability of Motion" developed by Russian mathematician Lyapunov in late 19th century. Lyapunov stability theory includes two methods for the stability analysis. One is the so-called linearization method and the other is the direct method. The linearization method draws conclusions about a nonlinear system's local stability around an equilibrium point from the stability properties of its linear approximation. The direct method is not restricted to local motion and determines the stability properties of a nonlinear system by constructing a scalar "energy-like" function $V(\boldsymbol{x})$ and analyzing the time derivative $\dot{V}(\boldsymbol{x}) = \Delta V^T \dot{\boldsymbol{x}}(t)$ along solution curves of the differential equation (4.1). Formally, such an "energy-like" function is called candidate Laypunov function. A real scalar function $V(\boldsymbol{x})$ is said to be a Lyapunov function for

equation (4.1) if it is positive definite and satisfies the Lipschitze condition (4.2) and $V(0) = 0$, such that $\Delta V^T \dot{\boldsymbol{x}}(t) \leq 0$ [32].

In 1892, Lyapunov proved the following theorems.

Theorem 4.1: If there exists a Lyapunov function $V(t, \boldsymbol{x})$ for the system (4.1), then $\boldsymbol{x} = 0$ is stable.

Theorem 4.2: If there exists a Lyapunov function $V(t, \boldsymbol{x})$ such that $\dot{V}(t, \boldsymbol{x})$ is negative definite, then $\boldsymbol{x} = 0$ is asymptotically stable.

The basic philosophy of Lyapunov's direct method is the mathematical extension of a fundamental physical observation: if the total energy of a mechanical or electrical system is continuously dissipated, the system must eventually settle down to an equilibrium point [32].

A solution $\boldsymbol{x}^*(t)$ of (4.1) is called stable at t_0, or more precisely, stable at $t = t_0$ in the sense of Lyapunov if for every $\varepsilon > 0$ there exists a $\delta(\varepsilon) > 0$ such that $\boldsymbol{x}(t)$ is any other solution with $\|\boldsymbol{x}(t_0) - \boldsymbol{x}^*(t_0)\| < \delta$, then $\|\boldsymbol{x}(t) - \boldsymbol{x}^*(t)\| < \varepsilon$ for all $t \geq t_0$. Thus, the concept of stability in the sense of Lyapunov, as shown in Figure 4.6, is nothing but continuous dependence of the solutions on $\boldsymbol{x}_0 = \boldsymbol{x}(t_0)$, uniformly with respect to $t \in [t_0, \infty)$ [9].

In general Lyapunov's theory is applied to systems with continuous right-hand side. In the following, the theory is extended to the system with discontinuous right-hand side.

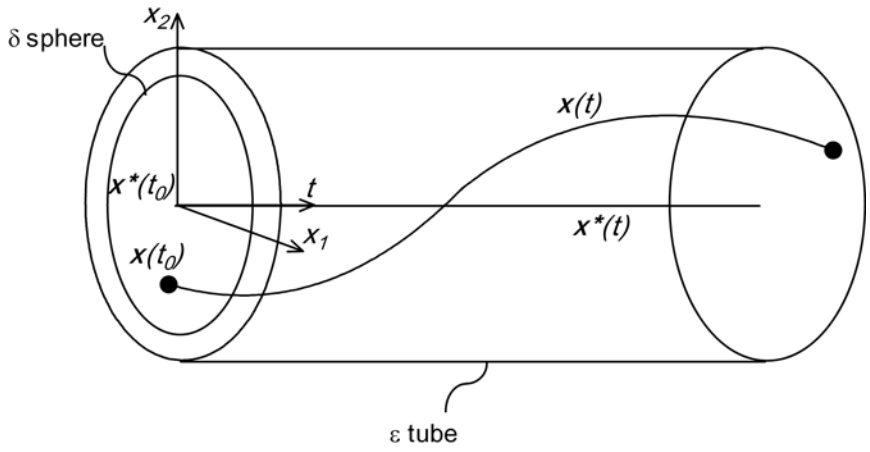

Figure 4.6 The concept of Lyapunov stability of an equilibrium point [28].

Denoting a solution of differential inclusion $\dot{\boldsymbol{x}} \in \boldsymbol{F}\big(t, \boldsymbol{x}(t)\big)$ starting from the initial condition $\boldsymbol{x}(t_0) = \boldsymbol{x}_0$ by $\boldsymbol{x}(t)$, the solution $\boldsymbol{x}(t)$ is in general non-unique [9]. A sufficient condition for uniqueness of solutions can be gained if $\boldsymbol{F}\big(t, \boldsymbol{x}(t)\big)$ possess the maximal monotone property.

The proof of the uniqueness is given by [9]. With reference to the differential inclusion $\dot{\boldsymbol{x}} \in -\boldsymbol{A}\big(\boldsymbol{x}(t)\big)$, define $S(-\boldsymbol{A}, t_0, \boldsymbol{x}_0)$ as the set of solution curves $\boldsymbol{x}(t)$, with $t \geq t_0$, starting from the initial condition $\boldsymbol{x}(t_0) = \boldsymbol{x}_0$, i.e.,

$$\boldsymbol{x}(t) \in S(-\boldsymbol{A}, t_0, \boldsymbol{x}_0). \tag{4.18}$$

Let $\boldsymbol{x}(t) \in S(-\boldsymbol{A}, t_0, \boldsymbol{x}_0)$ and $\boldsymbol{x}^*(t) \in S(-\boldsymbol{A}, t_0, \boldsymbol{x}_0)$ be solutions of the differential inclusion. Assume that the system does not have a unique solution. Then there exist $\boldsymbol{x}(t_0) = \boldsymbol{x}^*(t_0)$ such that $\boldsymbol{x}(t) \neq \boldsymbol{x}^*(t)$. Considering the Lyapunov function

$$V(t) = \frac{1}{2}\|\boldsymbol{x}(t) - \boldsymbol{x}^*(t)\|^2, \tag{4.19}$$

the time derivative of $V(t)$ yields

$$\begin{aligned}\dot{V}(t) &= \|\boldsymbol{x}(t) - \boldsymbol{x}^*(t)\| \frac{d}{dt}\|\boldsymbol{x}(t) - \boldsymbol{x}^*(t)\| \\ &= \big(\boldsymbol{x}(t) - \boldsymbol{x}^*(t)\big)^T \big(\dot{\boldsymbol{x}}(t) - \dot{\boldsymbol{x}}^*(t)\big) \\ &\in -\big(\boldsymbol{x}(t) - \boldsymbol{x}^*(t)\big)\big(\boldsymbol{A}\big(\boldsymbol{x}(t)\big) - \boldsymbol{A}(\boldsymbol{x}^*(t))\big) \leq 0\end{aligned} \tag{4.20}$$

Hence, the function $V(t)$ cannot increase meaning that the distance between $\boldsymbol{x}(t)$ and $\boldsymbol{x}^*(t)$ cannot increase with time, i.e.,

$$\|\boldsymbol{x}(t) - \boldsymbol{x}^*(t)\| \leq \|\boldsymbol{x}_0 - \boldsymbol{x}^*{}_0\|. \tag{4.21}$$

Taking $\boldsymbol{x}_0 = \boldsymbol{x}^*{}_0$, it follows that $\boldsymbol{x}(t) = \boldsymbol{x}^*(t)$, which is in contradiction with $\boldsymbol{x}(t) \neq \boldsymbol{x}^*(t)$. Consequently, the system has a unique solution.

Now consider a mass-spring system with persistent friction input (see Figure 4.7). The mass block is riding on a conveyer belt that is moving at a constant velocity v_d. Denote the horizontal position of the mass by x and its velocity by v. The relative velocity of the mass with respect to the belt is denoted by $v_r = v - v_d$. The static friction mapping (3.2)

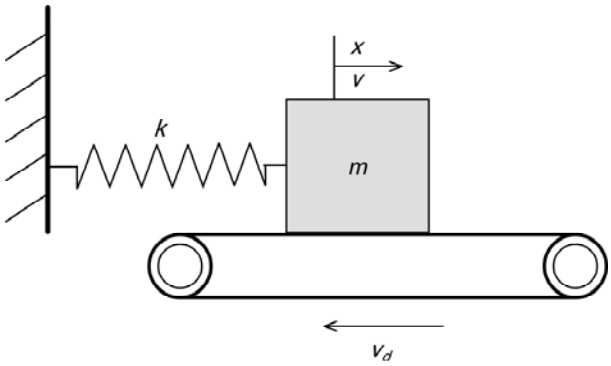

Figure 4.7 Mass-spring system with persistent friction disturbance.

is used in this example, and its plot is shown in Figure 3.4(a). The friction defined in the sense of differential inclusion is

$$\begin{aligned} F_f &\in F_N(\mu_C Sign(v_r) + bv_r) - F_{stribeck} \\ F_{stribeck} &= F_N \frac{\mu_{Stribeck} v_r}{1+\mu_{Stribeck}|v_r|}. \end{aligned} \tag{4.22}$$

From Newton's 2nd law, the equation of motion is

$$m\dot{v} + kx = F_f. \tag{4.23}$$

The equation of motion together with the set-valued friction law gives a 2nd-order differential inclusion,

$$\begin{aligned} \dot{v} &\in -\frac{k}{m}x + \frac{F_N}{m}(\mu_C Sign(v_r) + bv_r) - \frac{F_N}{m}\frac{\mu_{Stribeck} v_r}{1+\mu_{Stribeck}|v_r|}. \\ \dot{x} &= v \end{aligned} \tag{4.24}$$

The phase portrait of the system, which creates the stick-slip motion is given in Figure 4.8 for the parameter values $= 1\ kg$ $F_N = 10\ N$, $k = 1\ N/m$, $v_d = 0.3\ m/s$, $\mu_C = 0.2$, $b = 0.1$, and $\mu_{Stribeck} = 0.2$. The equilibrium is an unstable focus surrounded by a stable limit cycle, which alternates between the stick phase ($v = 0.3\ m/s$) and the backward slip phase (i.e., below the stick phase, $v < 0.3\ m/s$). It can be observed that the solution shows a kink in the phase portrait when the solution curves go from forward slip phase (i.e., above the stick phase, $v > 0.3\ m/s$) to the backward slip (or vice versa). At those time instance, the friction F_f jumps to another value. The acceleration $\dot{v}$ is not defined at those time instances for which such a change occurs. The resulting limit cycle is due to

the fact that the stick-slip friction (refer to Figure 3.4 (a)) is not a maximal monotone function; hence, there is the unstable equilibrium circled by the stable limit cycle. This example verifies the Filippov's solution theory for the existence of solution of non-smooth system and the Lyapunov stability theory for the uniqueness of solution to guarantee system stability.

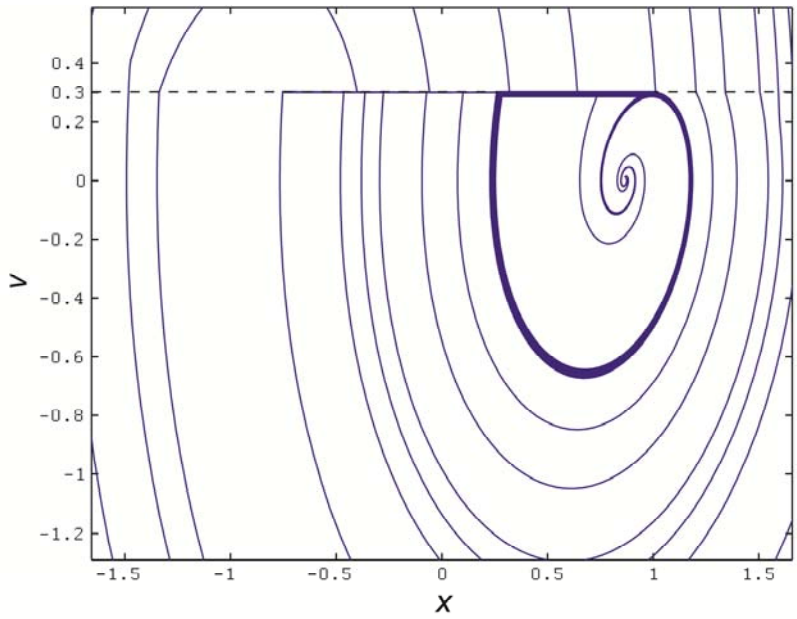

Figure 4.8 Phase portrait of mass-spring system with persistent friction disturbance.

4.4 Summary

In this chapter, systems with friction is simplified to non-smooth systems and analyzed through Lyapunov stability theory. The analysis result reveals that Stribect effect in the friction is the cause of the system instability and the limit cycle. The friction induced adverse effects can jeopardize the performance of control systems if friction compensation strategies are not considered properly. In the following chapter, Lyapunov-based control theory is used to develop nonlinear controllers, which give advanced control to pneumatic actuator system and adaptive friction compensation.

Chapter 5. Nonlinear Controller Design

In this Chapter, the Lyapunov-based control theory combined with adaptive-robust control is used to design a complete nonlinear controller for slow motion tracking control of a servo pneumatic actuator. The resulting nonlinear controller shows mathematical attempts to improve the performance of the system, including robust reference tracking, robust closed-loop stability, and on-line estimate of unknown parameters.

In nonlinear systems, the system responses cannot be determined systematically as linear systems do in either time domain or frequency domain. The behaviors of nonlinear system vary with different reference signals in time domain, and it is not possible to specify the system behavior in frequency domain [13]. In order to obtain qualitative specifications of the system behavior in the operating region of interest, computer simulation is an important analytical tool in determining whether design specifications are met, i.e., stability, accuracy and speed of response, and robustness.

In nonlinear controller design, model-based approach is an essential component. Once a mathematical model is constructed, the system parameters can be determined through experimental identifications. In the modeling of a system, the accuracy of the mathematical model is referred to as the degree of closeness to the actual system. From a control point of view, modeling inaccuracies can be classified into two major kinds: structured uncertainties and unstructured uncertainties. The first kind corresponds to inaccuracies on the terms actually included in the mathematical model, while the second kind corresponds to inaccuracies on the system order [13]. Modeling inaccuracies can have strong adverse effects on nonlinear control systems. Therefore, any practical design must address them explicitly. In pure model-based nonlinear control, the control law is designed from a nominal model of the physical system. How the control system will behave in the presence of model uncertainties is not clear at the design stage. The uncertainties depend on the precision of measurement systems, and the precision is the degree to which repeated measurements under unchanged conditions show the same results. Robust control is a nonlinear controller design approach based on the

consideration of both the nominal model and some characterization of the bounded model uncertainties. Robust control explicitly deals with uncertainties in its approach to controller design. Robust controls are designed to function properly so long as uncertain parameters or disturbances are within some known bounded modeling errors. Adaptive control is another nonlinear controller design approach that deals with uncertain systems or time-varying systems. Adaptive approach is in general more advanced than robust approach because the algorithm of adaptive control does not require the known bounded modeling errors as a priori.

In this chapter, a straightforward approach to provide robustness of nonlinear system through sliding mode control is given in Section 5.1. Section 5.2 introduces the traditional Lyapunov-based design via a technique called cascade control. The application of traditional Lyapunov-based controller design is limited to lower-order dynamical systems. In Section 5.3, backstepping design technique is applied systematically to higher-order dynamical systems so as to break through the barrier that limits the applications of the traditional Lyapunov-based control algorithm. Section 5.4 adapts a dynamical adaptive backstepping-sliding mode control algorithm to develop a nonlinear controller for servo pneumatic actuator. The novel controller is able to accomplish tracking control of nonlinear servo pneumatic actuator with robustness to parameter uncertainties as well as estimating the unknown parameters in the friction.

The control system for servo pneumatic actuator is shown in Figure 5.1. A feedback scheme of typical servo pneumatic actuator is given as follows: (i) the servo control valve receives the control input from the controller and determines the amount of air flows into and out of the corresponding cylinder chambers; (ii) a force is created by the pressure

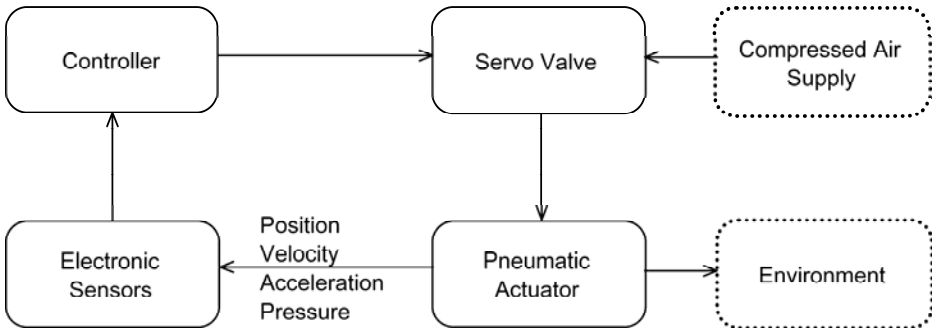

Figure 5.1 Servo pneumatic actuator closed-loop control.

differential across the piston, and this force acting as the actuating force moves the piston and piston rod; (iii) electronic sensors sense the actuator state values, including position, velocity, acceleration, and chamber pressures of the actuator; (iv) the state values are fed back to the controller, where the control algorithm use the feedback values to calculate the future control inputs.

The mathematical model of the pneumatic system is derived in Chapter 2 and is rewritten as follows:

$$\dot{x}_v = -\frac{x_v}{\tau} + \frac{k_v u_v}{\tau} \tag{5.1}$$

$$A_v = w x_v \tag{5.2}$$

$$\psi_i(P_u,\ P_d) = \begin{cases} \psi(P_s,\ P_i) & \text{for } A_v \geq 0 \\ \psi(P_i,\ P_{atm}) & \text{for } A_v < 0 \end{cases} \qquad i = 1, 2 \tag{5.3}$$

$$\psi_i(P_u, P_d) = \begin{cases} \frac{C_d P_u}{\sqrt{T}} \sqrt{\frac{r}{R}\left(\frac{2}{(r+1)}\right)^{(r+1)/(r-1)}} & \frac{P_d}{P_u} \leq P_{cr} \\ \frac{C_d P_u}{\sqrt{T}} \sqrt{\left(\frac{2r}{R(r+1)}\right)\left(\left(\frac{P_u}{P_d}\right)^{2/r} - \left(\frac{P_u}{P_d}\right)^{(r+1)/r}\right)} & \frac{P_d}{P_u} > P_{cr} \end{cases} \tag{5.4}$$

$$\begin{aligned} \dot{m}_1 &= A_v \psi_i(P_u, P_d) \\ \dot{m}_2 &= -A_v \psi_i(P_u, P_d) \end{aligned} \tag{5.5}$$

$$\begin{aligned} \dot{P}_1 &= \frac{rRT}{V_{o1} + A\left(\frac{L}{2} + x_p\right)} \dot{m}_1 - \frac{rP_1 A}{V_{o1} + A\left(\frac{L}{2} + x_p\right)}\ v_p \\ \dot{P}_2 &= \frac{rRT}{V_{o2} + A\left(\frac{L}{2} - x_p\right)} \dot{m}_2 + \frac{rP_2 A}{V_{o2} + A\left(\frac{L}{2} - x_p\right)}\ v_p. \end{aligned} \tag{5.6}$$

$$\dot{v}_p = \frac{1}{M}\left(P_\Delta A - F_f\right) \tag{5.7}$$

$$\dot{x}_p = v_p \tag{5.8}$$

For the controller design, simplifications are made to the mathematical model of servo pneumatic actuator. According to [22], the relationship between the control input u_v and the valve spool position x_v can be treated as a simple proportional gain, i.e.,

$$x_v = k_v u_v. \tag{5.9}$$

In other words, the controller derived from the above simplification does not consider the time lag. This suggests that the physical servo valve should have considerably small time lag (or the response of the servo valve should be very fast with respect to the actuator dynamics) in order to implement the developed controller. Otherwise, the developed controller from the assumption of simple control gain should not be implemented.

Substituting equation (5.9) into equation (5.2), the relationship between orifice area A_v and control input u_v is

$$A_v = w k_v u_v. \tag{5.10}$$

Given equation (5.10), the control input can be obtained from the following equation:

$$u_v = A_v / w k_v. \tag{5.11}$$

According to [11], the pressure differential dynamics $\dot{P}_\Delta = \dot{P}_1 - \dot{P}_2$ can be obtained from equation (5.6):

$$\dot{P}_\Delta = \frac{rRT}{V_{o1}+A\left(\frac{L}{2}+x_p\right)}\dot{m}_1 - \frac{rP_1A}{V_{o1}+A\left(\frac{L}{2}+x_p\right)}\, v_p - \frac{rRT}{V_{o2}+A\left(\frac{L}{2}-x_p\right)}\dot{m}_2 - \frac{rP_2A}{V_{o2}+A\left(\frac{L}{2}-x_p\right)}\, v_p\,. \tag{5.12}$$

Equation (5.12) can be separated into terms affected by the flow dynamics $\dot{m}_i$ and terms which are functions of piston position and velocity, i.e.,

$$c = \gamma RT\left(\frac{\dot{m}_1}{V_{o1}+A\left(\frac{L}{2}+x_p\right)} - \frac{\dot{m}_2}{V_{o2}+A\left(\frac{L}{2}-x_p\right)}\right) \tag{5.13}$$

$$p = -\gamma A v_p\left(\frac{P_1}{V_{o1}+A\left(\frac{L}{2}+x_p\right)} + \frac{P_2}{V_{o1}+A\left(\frac{L}{2}-x_p\right)}\right). \tag{5.14}$$

Substituting equation (5.5) into equation (5.13),

$$c = rRT\left(\frac{\psi_1(P_u,P_d)}{V_{o1}+A\left(\frac{L}{2}+x_p\right)} + \frac{\psi_2(P_u,P_d)}{V_{o2}+A\left(\frac{L}{2}-x_p\right)}\right)A_v. \tag{5.15}$$

where P_u and P_d are assigned according to the pressure switching rule (5.3).

Given equation (5.15), c can be simplified as

$$c = bA_v, \tag{5.16}$$

where

$$b = rRT\left(\frac{\psi_1(P_u,P_d)}{V_{o1}+A\left(\frac{L}{2}+x_p\right)} + \frac{\psi_2(P_u,P_d)}{V_{o2}+A\left(\frac{L}{2}-x_p\right)}\right). \tag{5.17}$$

According to equations (5.12) and (5.14)-(5.16), the pressure differential dynamics $\dot{P}_\Delta$ can be simplified into

$$\dot{P}_\Delta = p + bA_v. \tag{5.18}$$

Combining equations (5.1), (5.2), (5.6)-(5.8), and (5.18), the nonlinear system equations of servo pneumatic actuator can be written as follows:

$$\begin{aligned}
\dot{P}_\Delta &= p + bA_v \\
\dot{P}_1 &= \frac{rRT}{V_{o1}+A\left(\frac{L}{2}+x_p\right)}\dot{m}_1 - \frac{rP_1A}{V_{o1}+A\left(\frac{L}{2}+x_p\right)}\, v_p \\
\dot{P}_2 &= \frac{rRT}{V_{o2}+A\left(\frac{L}{2}-x_p\right)}\dot{m}_2 + \frac{rP_2A}{V_{o2}+A\left(\frac{L}{2}-x_p\right)}\, v_p. \\
\dot{v}_p &= \frac{1}{M}\left(P_\Delta A - F_f\right) \\
\dot{x}_p &= v_p
\end{aligned} \tag{5.19}$$

The complete system dynamics of the servo pneumatic actuator are therefore characterized by the state vector $\boldsymbol{x^T} = [\, P_\Delta\ P_1\ P_2\ v_p\ x_p]$ and the single control input u_v.

According to equation (5.19), the servo pneumatic actuator can be analyzed under the general differential equation form:

$$\dot{\boldsymbol{x}} = \boldsymbol{f}(\boldsymbol{x}) + b(\boldsymbol{x})u. \tag{5.20}$$

where $\boldsymbol{x^T} = [x\ \dot{x}\ \ldots\ x^{(n-1)}]$ is the state vector, x is the output of interest, $\boldsymbol{f}(\boldsymbol{x})$ and $b(\boldsymbol{x})$ are functions whose parameters are not known exactly and time varying, and u is the general control input. In the following, the general differential equation form is used to demonstrate the development of various control laws for nonlinear system, and then the control algorithms are implemented on the servo pneumatic actuator to obtain the control law.

5.1 Sliding Mode Control

Robustness is the sensitivity to parameter changes which are not considered in the design, such as disturbances, measurement noise, unmodeled dynamics, etc. A system should be able to withstand these effects when performing the tasks of interest. In nonlinear system, however, stability does not imply the ability to withstand persistent disturbances of even small magnitudes [13].

A standard robust design approach to tackle the parametric and modeling uncertainties of nonlinear systems is the sliding mode control methodology. The sliding mode control actually is the Lyapunov stability theory applied to a 1st-order system. It employs the intuitive feedback control strategy for 1st-order systems- "if the error is negative, push hard enough in the positive direction (and conversely)". A notational simplification is required to convert the n^{th}-order system into a 1st-order system, and the control input is obtained from the time derivative of the resulting 1st-order system. For the transformed problems, the "perfect" performance can be achieved in the presence of arbitrary parameter uncertainties. Such performance, however, is obtained at the price of extremely high control activities. For the class of systems to which it applies, sliding mode control approach provides a systematic way to solve the problem of maintaining the stability and the consistent performance in the face of modeling inaccuracies.

With reference to the differential equation (5.20), an n^{th}-order system is converted to a 1st-order system by a notational simplification:

$$s(\boldsymbol{x}, t) = \left(\frac{d}{dt} + \lambda\right)^{n-1} e, \tag{5.21}$$

where $e = x - x_d$ is the tracking error of interest, x_d is the desired output of interest, $\frac{d}{dt}$ is the differential operator, λ is a term that relates to the convergence rate (or eigenevalue) of the output of interest, and s is the sliding surface defined in the state space $\boldsymbol{R}^n$ and represents a true measure of tracking performance.

Furthermore, the bound φ on s can be directly translated into bound ε on the tracking error vector,

$$\boldsymbol{e} = \boldsymbol{x} - \boldsymbol{x}_d, \tag{5.22}$$

where $\boldsymbol{e^T} = [e\ \dot{e}\ \ddot{e}\ ...]$ and $\boldsymbol{x}_d{}^T = [x_d\ \dot{x}_d\ \ddot{x}_d\ ...]$ is the desired state vector.

The corresponding transformation of performance measures assuming $e(0) = 0$ is

$$\forall\, t \geq 0, |s| \leq \varphi \Rightarrow\ \forall t \geq 0, \left|x^i\right| \leq (2\lambda)^i \varepsilon, i = 0, \dots, n-1, \tag{5.23}$$

where $\varepsilon = \ \varphi/\lambda^{n-1}$ [13]. In this way, an n^{th}-order tracking problem can be replaced by a 1^{st}-order stabilization problem. The simplified 1^{st}-order tracking problem of keeping the scalar s at zero can be achieved by choosing the control law u such that outside the sliding surface,

$$\frac{1}{2}\frac{d}{dt}s^2 \leq -\eta|s|, \tag{5.24}$$

where η is a strickly positive constant. Condition (5.24) states that the squared "distance" to the surface, as measured by s^2, decreases along all system trajectories. Thus, it constrains trajectories to point towards the surface s. In particular, once on the surface, the system trajectories remain on the surface [13].

The sliding mode controller design consists of two steps. First, a feedback control law u is selected to verify sliding condition (5.24). However, in order to account for the presence of modeling imprecision and of disturbance, the control law has to be discontinuous across the sliding surface s. Since the implementation of the associated control switching is imperfect, this leads to chattering. Chattering is undesirable in practice since it involves high control activity and may excite high frequency dynamics neglected in the course of modeling. Thus, in a second step, the discontinuous control input u is suitably smoothed by a sliding layer to achieve an optimal trade-off between control bandwidth and tracking precision.

Considering the servo pneumatic actuator model given in equation (5.19), F_f and p are nonlinear and time varying; They can be estimated by $\hat{F}_f$ and $\hat{p}$, respectively. The estimated errors on F_f and p are assumed to be bounded by some known function F and P, respectively, i.e.,

$$\left|\hat{F}_f - F_f\right| \leq F \tag{5.25}$$

$$|\hat{p} - p| \leq P \tag{5.26}$$

Define a sliding surface according to equation (5.21),

$$s = \left(\frac{d}{dt} + \lambda\right)^{n-1} e. \tag{5.27}$$

Given $n = 3$ and $e = x_p - x_d$, equationn (5.27) becomes

$$s = \left(\frac{d}{dt} + \lambda\right)^2 (x_p - x_d) = \left(\dot{v}_p - \ddot{x}_d\right) + 2\lambda\left(v_p - \dot{x}_d\right) + \lambda^2\left(x_p - x_d\right). \tag{5.28}$$

Substituting equation (5.7) into equation (5.28),

$$s = \frac{1}{M}\left(P_\Delta A - F_f\right) - \ddot{x}_d + 2\lambda\left(v_p - \dot{x}_d\right) + \lambda^2\left(x_p - x_d\right). \tag{5.29}$$

Differentiate equation (5.29) with respect to time, the time derivative of the sliding surface incorporating equation (5.7) and (5.8) is

$$\dot{s} = \frac{1}{M}\left(\dot{P}_\Delta A - \dot{F}_f\right) - \dddot{x}_d + 2\lambda\left(\frac{1}{M}\left(P_\Delta A - F_f\right) - \ddot{x}_d\right) + \lambda^2\left(v_p - \dot{x}_d\right). \tag{5.30}$$

Substituting equation (5.18) into equation (5.30),

$$\dot{s} = \frac{1}{M}\left((p + bA_v)A - \dot{F}_f\right) - \dddot{x}_d + 2\lambda\left(\frac{1}{M}\left(P_\Delta A - F_f\right) - \ddot{x}_d\right) + \lambda^2\left(v_p - \dot{x}_d\right). \tag{5.31}$$

Then, the control law bA_v to achieve $\dot{s} = 0$ is

$$bA_v = \left(\frac{M}{A}\left(\dddot{x}_d - 2\lambda\left(\frac{1}{M}\left(P_\Delta A - \hat{F}_f\right) - \ddot{x}_d\right) - \lambda^2\left(v_p - \dot{x}_d\right)\right) - \hat{p} + \frac{1}{A}\dot{\hat{F}}_f\right). \tag{5.32}$$

Given that the nonlinear control gain b is bounded as

$$0 \leq b_{min} \leq |b| \leq b_{max}, \tag{5.33}$$

the geometric mean of the lower and upper bound of the gain is a reasonable estimate [13]:

$$\hat{b} = sign(A_v)\sqrt{b_{min}b_{max}} \tag{5.34}$$

Bound can then be written in the form of

$$\beta^{-1} \leq \hat{b}/b \leq \beta, \tag{5.35}$$

$$\text{where } \beta = \left(\frac{b_{max}}{b_{min}}\right)^{1/2} \tag{5.36}$$

is the gain margin of the control design.

To account for the uncertainty in F_f and $p(\boldsymbol{x})$ while satisfying the sliding condition (5.24), control law is given as

$$\hat{A}_v = \left(\hat{b}^{-1}\left(bA_v - \eta sign(s)\right)\right), \tag{5.37}$$

where η is a positive constant. By choosing η large enough, such that

$$\eta \geq \beta(F + P) + (\beta - 1)|bA_v|, \tag{5.38}$$

ensures the satisfaction of condition (5.24).

In the second step, a boundary layer is created to reduce the chattering due to the discontinuity in the variable structure control, i.e.,

$$\hat{A}_v = \begin{cases} \hat{b}^{-1}\left(bA_v - \eta\left(\frac{s}{\varphi}\right)\right) & |s| \leq \varphi \\ \hat{b}^{-1}(bA_v - \eta sign(s)) & |s| > \varphi \end{cases}, \tag{5.39}$$

where φ is the bound of the sliding layer.

Consequently, the approximate control input $\hat{u}_v$ is obtained from equation (5.11). The same approach was used by Gulati et al. [12] to construct a sliding mode controller for the tracking control of servo pneumatic actuator.

5.2 Cascade Control

In this section, an extension of the Lyapunov function concept, called the control Lyapunov function (CLF) [15] is considered to develop a closed-loop system with the desirable stability and performance. The controller design in this section is different from the controller described earlier because it is the starting point of a systematic approach to construct nonlinear controllers based on the Lyapunov stability theory.

Suppose that the problem for the system (5.20) is to design a feedback control law such that the equilibrium $\boldsymbol{x^T} = 0$ of the closed-loop system is globally asymptotically stable. A function $V(\boldsymbol{x})$ is chosen as a candidate Lyapunov function, whose derivative along the solutions of system (5.20) need to satisfy $\dot{V}(\boldsymbol{x}) \leq -W(\boldsymbol{x})$, i.e.,

$$\frac{\partial V}{\partial \boldsymbol{x}}(\boldsymbol{x})(f(\boldsymbol{x}) + b(\boldsymbol{x})u) \leq -W(\boldsymbol{x}), \tag{5.40}$$

where $W(\boldsymbol{x})$ is a positive definite function. A stabilizing control law for system (5.20) may exist but may fail to satisfy condition (5.40) because of a poor choice of $V(\boldsymbol{x})$ and $W(\boldsymbol{x})$. A system for which a good choice of $V(\boldsymbol{x})$ and $W(\boldsymbol{x})$ exists is said to possess a CLF.

For a 1st-order scalar nonlinear system

$$\dot{x} = -x^3 + u, \tag{5.41}$$

the control input u is derived base on the CLF concept in the following. Taking

$$V(x) = \frac{1}{2}x^2 \tag{5.42}$$

as a CLF for system (5.41), the control input u that satisfies (5.40) with $W(x) = x^2$ is

$$u = x^3 - x, \tag{5.43}$$

such that

$$\frac{\partial V}{\partial x}(x)(f(x) + u) \leq -x^2. \tag{5.44}$$

Depending on the experience of the designers, the control input u can take different forms to satisfy condition (5.40), but a suitable control law requires less control efforts than others.

The applications of traditional CLF are limited to systems with relative degree one or two. The cascade control strategy is based on the methodology of order reduction described by Utkin [14]. Similar to the notational simplification used in sliding mode control, cascade control converts the higher-order system into lower-order cascaded subsystems; then implements CLF concept to guarantee that the cascaded subsystems

achieve the desired system behavior [11].

The cascade control strategy views the servo pneumatic system as cascaded subsystems: a mechanical subsystem driven by the force generated by a pneumatic subsystem (see Figure 5.2) [11].

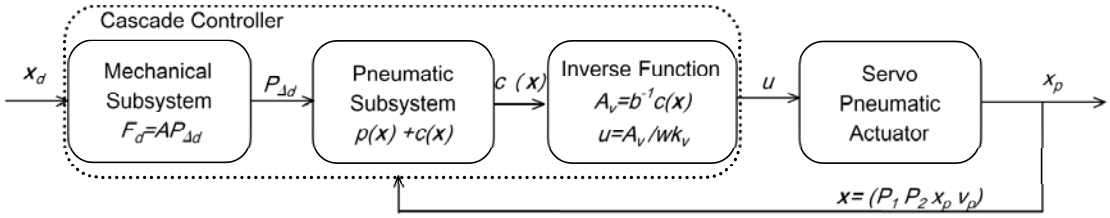

Figure 5.2 Cascade control for servo pneumatic actuator.

To rewrite the pneumatic model in a cascaded form appropriate for the cascade controller design, define the following relation:

$$M\dot{v}_p + F_f = F_a, \tag{5.45}$$

where M is the mass of piston and piston rod assembly, $\dot{v}_p$ is the piston acceleration, F_f is the friction, and F_a is the actuating force. Equation (5.45) represents the mechanical subsystem driven by a pneumatic force, i.e.,

$$F_a = AP_\Delta, \tag{5.46}$$

where P_Δ is the pressure differential across the piston and A is the piston annulus area.

The cascade control design for the servo pneumatic actuator is described as follows: (i) compute a control law F_d for the mechanical subsystem, such that the tracking is achievable; (ii) compute a control input u_v, such that the pneumatic subsystem applies the desired pneumatic pressure differential $P_{\Delta d}$.

To perform this task, the pressure differential tracking error $\tilde{P}_\Delta$ is defined as

$$\tilde{P}_\Delta = P_\Delta - P_{\Delta d}. \tag{5.47}$$

The control law F_d for the mechanical subsystem is developed from sliding mode algorithm discussed in the previous section. The following control law to obtain trajectory tracking in the mechanical subsystem is obtained from [11]:

$$F_d = \left(M\ddot{x}_r - K_D s + F_f\right) \tag{5.48}$$

where K_D is a positive constant, x_r is a reference displacement, s is the sliding surface, and F_f is the friction. According to the notational simplification in sliding mode control algorithm, the reference velocity $\dot{x}_r$ can be obtained by modifying the desired velocity $\dot{x}_d$ as follows:

$$\begin{aligned} &\dot{x}_r = \dot{x}_d - \lambda e \\ &e = x_p - x_d \\ &s = v_p - \dot{x}_r = \dot{e} + \lambda e\,. \end{aligned} \tag{5.49}$$

where λ is positive convergent rate factor and $e = x_p - x_d$ is the position tracking error between actual piston displacement x_p and desired piston displacement x_d. Substituting the control law (5.48) into the differential equation of the mechanical subsystem (5.45), the time derivative of sliding surface is given as

$$M\dot{s} + K_D s - F = A\tilde{P}_\Delta, \tag{5.50}$$

where F is the bound of friction estimate defined according to equation (5.25).

At this point, the differential equations for both error variables, namely s and $\tilde{P}_\Delta$, can be used to consider the CLF,

$$V = \frac{1}{2}Ms^2 + \frac{1}{2}\tilde{P}_\Delta{}^2. \tag{5.51}$$

Given equations (5.47) and (5.50), the time derivative of equation (5.51) is

$$\dot{V} = s\left(A\tilde{P}_\Delta - K_D s - F\right) + \tilde{P}_\Delta\left(\dot{P}_\Delta - \dot{P}_{\Delta d}\right). \tag{5.52}$$

Substituting $\dot{P}_\Delta$ of equation (5.18) into equation (5.52),

$$\dot{V} = s\left(A\tilde{P}_\Delta - K_D s - F\right) + \tilde{P}_\Delta\left(p + bA_v - \dot{P}_{\Delta d}\right). \tag{5.53}$$

Assume error due to estimate $\hat{F}_f$ is very small; then, to guarantee $\dot{V} \leq 0$, the control law is

$$\hat{A}_v = \frac{1}{\hat{b}}\left(\dot{P}_{\Delta d} - As - p - k_p\tilde{P}_\Delta\right), \tag{5.54}$$

such that

$$\dot{V} = -K_D s^2 - k_p \tilde{P}_\Delta{}^2 \tag{5.55}$$

Consequently, the approximate control input $\hat{u}_v$ is obtained from the relation (5.11). This method was applied to the servo pneumatic actuator by Guenther et al. [11] to design the cascade controller for stabilization and tracking control.

5.3 Backstepping Control

The limitation associated with the aforementioned CLF approach to control system is that the applications are only available to systems with relative degree one or two. The backstepping controller design approach breaks through the barrier that limits the traditional CLF design and provides a systematic way to construct the nonlinear controllers. The backstepping design methodology was first popularized by Krstic et al. [15] and has been successfully applied to problems including servo hydraulic control system [30]. The control input produced by this methodology depends on the system model and the equations chosen for the virtual control laws.

The backstepping design concept is illustrated with a simple 2nd-order dynamical system:

$$\begin{aligned} \dot{x} &= f(x) + g(x)\varepsilon \\ \dot{\varepsilon} &= u \end{aligned} \tag{5.56}$$

where x and ε are the system states, u is the control input. Assume that there is a continuously differentiable feedback control law $\varepsilon = \alpha(x)$, such that

$$V = \frac{1}{2}x^2 \tag{5.57}$$

is positive definite and radially unbounded function, and its time derivative satisfies

$$\frac{dV}{dx}\big(f + g\alpha(x)\big) \leq -W(x), \tag{5.58}$$

where $\alpha(x)$ is a virtual control law and $W(x)$ is a positive definite function.

Then, the control error variable is introduced as

$$e = \varepsilon - \alpha(x). \tag{5.59}$$

Equation (5.57) can be transformed by the control error variable (5.59) into the following system equations:

$$\begin{aligned} \dot{x} &= f(x) + g(x)(\alpha(x) + e) \\ \dot{e} &= u - \frac{d\alpha}{dx}\big(f(x) + g(x)(\alpha(x) + e)\big) \end{aligned} \tag{5.60}$$

Defining the CLF as

$$V_1 = V + \tfrac{1}{2}\big(\varepsilon - \alpha(x)\big)^2, \tag{5.61}$$

the resulting time derivative of V_1 is

$$\dot{V}_1 = -W(x) + e\left(u - \tfrac{d\alpha}{dx}\big(f(x) + g(x)(\alpha(x) + e)\big)\right). \tag{5.62}$$

The simplest way to make $\dot{V}_1$ negative definite is to set

$$u - \tfrac{d\alpha}{dx}\big(f(x) + g(x)(\alpha(x) + e)\big) = -ke, \tag{5.63}$$

where k is a positive constant. Hence, the resulting control input from equation (5.63) is

$$u = \tfrac{d\alpha}{dx}\big(f(x) + g(x)(\alpha(x) + e)\big) - ke. \tag{5.64}$$

The backstepping concept can be applied to higher-order dynamical systems. For the servo pneumatic actuator in specific, the state variables are defined according the system equation (5.19), and the backstepping design begins by defining the position tracking error:

$$e_1 = x_p - x_d. \tag{5.65}$$

where x_p is the actual piston displacement and x_d is the desired displacement. The time derivative of equation (5.65) taking into account of equation (5.8) is

$$\dot{e}_1 = v_p - \dot{x}_d. \tag{5.66}$$

The first CLF is constructed with the error variable e_1:

$$V_1 = \tfrac{1}{2}{e_1}^2. \tag{5.67}$$

According to the aforementioned 2nd-order dynamical system example (5.56), equation (5.67) inspires a suitable virtual control law:

$$\alpha_1 = \dot{x}_d - k_1 e_1, \tag{5.68}$$

where k_1 is a positive constant.

Then, the second error variable can be defined as

$$e_2 = v_p - \alpha_1. \tag{5.69}$$

Given equations (5.66), (5.68), and (5.69), the time derivative of V_1 is

$$\dot{V}_1 = -k{e_1}^2 + e_2 e_1. \tag{5.70}$$

Given equations (5.7) and (5.68), the time derivative of e_2 is

$$\dot{e}_2 = \frac{1}{M}\left(P_\Delta A - F_f\right) - \ddot{x}_d + k_1 \dot{e}_1 \tag{5.71}$$

Now the second CLF can be constructed with the error variables $e_1$and e_2 as

$$V_2 = V_1 + \tfrac{1}{2}{e_2}^2. \tag{5.72}$$

Given equations (5.70) and (5.71), the time derivative of V_2 is

$$\dot{V}_2 = -k_1{e_1}^2 + e_2 e_1 + e_2\left(\tfrac{1}{M}\left(P_\Delta A - F_f\right) - \ddot{x}_d - k\dot{e}_1\right). \tag{5.73}$$

In order to have $\dot{V}_2 \leq 0$, the second virtual control law is chosen as

$$\alpha_2 = \tfrac{1}{A}\left(F_f + M(\ddot{x}_d - k_2 e_2 - k\dot{e}_1 - e_1)\right). \tag{5.74}$$

Then, the third error variable can be defined as

$$e_3 = P_\Delta - \alpha_2. \tag{5.75}$$

Given equations (5.74) and (5.75), equation (5.73) becomes

$$\dot{V}_2 = -k_1{e_1}^2 - k_2{e_2}^2 + \frac{A}{M} e_3 e_2. \tag{5.76}$$

With reference to $\dot{P}_\Delta$ of equation (5.18) and equation (5.74), the time derivative of e_3 is

$$\dot{e}_3 = p + bA_v - \frac{1}{A}\left(\dot{F}_f + M\left(-k_2\dot{e}_2 + \ddot{x}_{pd} - k\ddot{e}_1 - \dot{e}_1\right)\right). \tag{5.77}$$

The third CLF can be constructed with the error variables e_1, e_2, and $e_3$as

$$V_3 = V_2 + \frac{1}{2}{e_3}^2. \tag{5.78}$$

Given equations (5.76) and (5.77), the time derivative of V_3 is

$$\dot{V}_3 = -k_1{e_1}^2 - k_2{e_2}^2 + \frac{A}{M}e_3e_2 + e_3\left(p + bA_v - \frac{1}{A}\left(\dot{F}_f + M\left(-k_2\dot{e}_2 + \ddot{x}_{pd} - k\ddot{e}_1 - \dot{e}_1\right)\right)\right). \tag{5.79}$$

To have $\dot{V}_3 \leq 0$, the approximation of control law is

$$\hat{A}_v = \frac{1}{\hat{b}}\left(-k_3e_3 - \hat{p} - \frac{A}{M}e_2 + \frac{M}{A}(-k_2\dot{e}_2 + \ddot{x}_d - k_1\ddot{e}_1 - \dot{e}_1) + \frac{\dot{F}_f}{\mathrm{A}}\right), \tag{5.80}$$

where errors due to friction estimated $\hat{F}_f$ and its time derivative $\hat{\dot{F}}_f$ are assumed to be very small. Thereafter, the approximate control input $\hat{u}_v$ is obtained from the relation (5.11).

A similar approach to design backstepping controller for servo pneumatic actuator was introduced by Rao et al.[10].

5.4 Dynamical Adaptive Backstepping-Sliding Mode Control

Adaptive controllers that are capable of controlling unknown plants and adapting to unpredictable changes in the environment have a long and rich history [15]. Lyapunov-based adaptive control is classified as one of the traditional adaptive schemes. It involves parameter identification with “parameter estimators.” The vital part of the estimators is the parameter adaptation algorithm, commonly referred to as the “parameter update law”. The Lyapunov-based adaptive control is used in this study for two reasons: (i) all controllers in this chapter are designed according to Lyapunov-based approach, so incorporating a Lyapunov-based adaptive law provides a uniform approach to tackle nonlinear system with parameter uncertainties; (ii) the controller and adaptive law derived from Lyapunov-based design has the desired properties for control system, i.e., stability and convergence [15].

In order to understand some issues related to the adaptive control in general and the Lyapunov-based adaptive control in particular, consider a simple 1st-order system with unknown parameter θ:

$$\dot{x} = u + \theta x \tag{5.81}$$

where u is the control input, x is the output of interest. Given $\hat{\theta}$ as the estimate of θ along with a control law u, the goal is to make the time derivative of CLF,

$$V(x, \hat{\theta}) = \frac{1}{2}x^2 + \frac{1}{2}(\theta - \hat{\theta})^2, \tag{5.82}$$

a decreading function of time.

Given the time derivative of equation (5.82),

$$\dot{V} = \frac{dV}{dx}\dot{x} + \frac{dV}{d\hat{\theta}}\dot{\hat{\theta}}, \tag{5.83}$$

the control input u and parameter update law $\dot{\hat{\theta}}$ are to be determined to guarantee that $\dot{V} \leq -kx^2$ with k being a positive constant, namely

$$\dot{V} = x(u + \theta x) + (\theta - \hat{\theta})\dot{\hat{\theta}} \leq -kx^2. \tag{5.84}$$

Rearranging terms of equation (5.84),

$$xu + \hat{\theta}\dot{\hat{\theta}} + \theta\left(x^2 - \dot{\hat{\theta}}\right) \leq -kx^2. \tag{5.85}$$

Since neither u nor $\dot{\hat{\theta}}$ is allowed to depend on the unknown θ [15], the only choice for the update law $\dot{\hat{\theta}}$ is

$$\dot{\hat{\theta}} = x^2. \tag{5.86}$$

The remaining condition

$$xu + \hat{\theta}\dot{\hat{\theta}} \leq -kx^2 \tag{5.87}$$

allows the selection of control input to be

$$u = -\left(\left(k + \hat{\theta}\right)x\right). \tag{5.88}$$

As expected, this example shows that the Lyapunov-based adaptive control uses control law and parameter update law to guarantee the output and the parameter convergence simultaneously, i.e., $x \to 0$ and $\left(\theta - \hat{\theta}\right) \to 0$ [15]. The estimate in the control law is static while update law itself is dynamical. In other words, the dynamic part of the controller is designed as a parameter update law with which the static part is continuously adapted to the new parameter estimate. This is why this type of control law is called dynamical adaptive control law. In the presence of unknown constant parameters dynamical adaptive control is able to achieve both convergence of the closed-loop state and convergence of the tracking error to zero.

The dynamical adaptive backstepping (DAB) control algorithm, which combines the dynamical adaptive law and backstepping control, was proposed by Rios-Bolivar et al. [16], and the control algorithm has been implemented in the dynamical adaptive regulation of uncertain nonlinear chemical processes. In order to provide robustness in the presence of undesirable disturbances, a combined dynamical adaptive backstepping-sliding mode control (DAB-SMC) design algorithm was proposed by Rios-Bolivar [17]. The application of this approach in adaptive-robust regulation of two nonlinear continuous chemical processes with uncertainty and its validity was demonstrated via computer simulations [18]. In the following of this section the DAB-SMC control algorithm is adapted to develop an adaptive-robust controller to track the desired trajectory in the servo pneumatic actuator moving at low speed.

As mentioned before, the control input produced from the backstepping concept depends on the system model and the equations chosen for the virtual control laws. The difference between the controller developed in this section and controllers from previous sections is that the parameters in the friction is assumed to be unknown to the controller; therefore, the adaptive law is used to estimate the friction parameters. Given friction differential equations (3.10) and servo pneumatic actuator differential equations (5.19), the complete system equations can be written as

$$
\begin{aligned}
\dot{P}_{\Delta} &= p + bA_v \\
\dot{P}_1 &= \frac{rRT}{V_{o1}+A\left(\frac{L}{2}+x_p\right)}\dot{m}_1 - \frac{rP_1A}{V_{o1}+A\left(\frac{L}{2}+x_p\right)}\ v_p \\
\dot{P}_2 &= \frac{rRT}{V_{o2}+A\left(\frac{L}{2}-x_p\right)}\dot{m}_2 + \frac{rP_2A}{V_{o2}+A\left(\frac{L}{2}-x_p\right)}\ v_p \\
\dot{v}_p &= \frac{1}{M}\left(P_{\Delta}A - \sigma_0 z - \sigma_1 \dot{z} - \sigma_2 v_p\right) \\
\dot{z} &= v_p - \frac{|v_p|}{g} z \\
\dot{x}_p &= v_p\ ,
\end{aligned}
\tag{5.89}
$$

where the new state vector for the dynamical system is $\boldsymbol{x^T} = [\ P_{\Delta}\ P_1\ P_2\ v_p\ z\ x_p]$.

The DAB-SMC derivation begins with second error variable e_2 of the backstepping design described in the previous section. In equation (5.89), the dynamics of acceleration $\dot{v}_p$ has unknown parameters (σ_0, σ_0, and σ_2) and state (z); hence, the adaptive law and the state observer need to be constructed according to the Lyapunov-based adaptive law. Substituting $\dot{v}_p$ and $\dot{z}$ of equation (5.89) into the time derivative of equation (5.69),

$$
\dot{e}_2 = \frac{1}{M}\left(P_{\Delta}A - \left(\sigma_0 z - \sigma_1 \frac{|v_p|}{g} z + (\sigma_1 + \sigma_2)v_p\right)\right) - \ddot{x}_{pd} + k_1\dot{e}_1. \tag{5.90}
$$

Using σ_{12} to represent $(\sigma_1 + \sigma_2)$ and z_0 and z_1 to represent the internal state z associated with σ_0 and σ_1, respectively, equation (5.90) becomes

$$
\dot{e}_2 = \frac{1}{M}\left(P_{\Delta}A - \left(\sigma_0 z_0 - \sigma_1 \frac{|v_p|}{g} z_1 + \sigma_{12} v_p\right)\right) - \ddot{x}_{pd} + k_1\dot{e}_1. \tag{5.91}
$$

Given the parameter estimates $\hat{\sigma}_0$, $\hat{\sigma}_1$, and $\hat{\sigma}_{12}$ for σ_0, σ_1, and σ_{12}, respectively and state observer $\hat{z}_0$ and $\hat{z}_1$ for z_0 and z_1, respectively, equation (5.91) becomes

$$
\begin{aligned}
\dot{e}_2 = \frac{1}{M}\left(P_{\Delta}A - \left(\hat{\sigma}_0\hat{z}_0 - \hat{\sigma}_1 \frac{|v_p|}{g}\hat{z}_1 + \hat{\sigma}_{12} v_p\right)\right) - \ddot{x}_{pd} + k_1\dot{e}_1 - \frac{1}{M}\Big(\sigma_0(z_0 - \hat{z}_0) - \\
\sigma_1 \frac{|v_p|}{g}(z_1 - \hat{z}_1)\Big) - \frac{1}{M}\left(\hat{z}_0(\sigma_0 - \hat{\sigma}_0) - \hat{z}_1 \frac{|v_p|}{g}(\sigma_1 - \hat{\sigma}_1) + v_p(\sigma_{12} - \hat{\sigma}_{12})\right).
\end{aligned}
\tag{5.92}
$$

By utilizing this estimation arrangement, two unknown parameters associated with the internal state z, namely, σ_0 and σ_1, can be estimated individually. This arrangement allows a good estimation of the friction instead of combining the two unknown

parameters and estimating them as one linearized parameter.

Then, define the estimation error variables as

$$\begin{aligned}
\tilde{z}_0 &= z_0 - \hat{z}_0 \\
\tilde{z}_1 &= z_1 - \hat{z}_1 \\
\tilde{\sigma}_0 &= \sigma_0 - \hat{\sigma}_0 \\
\tilde{\sigma}_1 &= \sigma_1 - \hat{\sigma}_1 \\
\tilde{\sigma}_{12} &= \sigma_{12} - \hat{\sigma}_{12}.
\end{aligned} \tag{5.93}$$

Substituting equation (5.93) into equation (5.92),

$$\begin{aligned}
\dot{e}_2 = \frac{1}{M}\left(P_\Delta A - \left(\hat{\sigma}_0\hat{z}_0 - \hat{\sigma}_1\frac{|v_p|}{g}\hat{z}_1 + \hat{\sigma}_{12}v_p\right)\right) - \ddot{x}_{pd} + k_1\dot{e}_1 - \frac{1}{M}\Big(\sigma_0\tilde{z}_0 - \\
\sigma_1\frac{|v_p|}{g}\tilde{z}_1\Big) - \frac{1}{M}\Big(\hat{z}_0\tilde{\sigma}_0 - \hat{z}_1\frac{|v_p|}{g}\tilde{\sigma}_1 + v_p\tilde{\sigma}_{12}\Big).
\end{aligned} \tag{5.94}$$

Constructing the CLF with respect to error variable e_2, the estimation error variables of unknown states (z_0 and z_1), and parameters estimation error variables (σ_0, σ_1, and σ_{12}),

$$V_2 = V_1 + \frac{1}{2}{e_2}^2 + \frac{1}{2}\sigma_0{\tilde{z}_0}^2 + \frac{1}{2}\sigma_1{\tilde{z}_1}^2 + \frac{1}{2}\gamma_0{\tilde{\sigma}_0}^2 + \frac{1}{2}\gamma_1{\tilde{\sigma}_1}^2 + \frac{1}{2}\gamma_{12}{\tilde{\sigma}_{12}}^2. \tag{5.95}$$

The time derivative of equation (5.95) is

$$\begin{aligned}
\dot{V}_2 = \dot{V}_1 + e_2\dot{e}_2 + \sigma_0\tilde{z}_0\big(\dot{z}_0 - \dot{\hat{z}}_0\big) + \sigma_1\tilde{z}_1\big(\dot{z}_1 - \dot{\hat{z}}_1\big) + \gamma_0\tilde{\sigma}_0\dot{\tilde{\sigma}}_0 + \gamma_1\tilde{\sigma}_1\dot{\tilde{\sigma}}_1 + \\
\gamma_{12}\tilde{\sigma}_{12}\dot{\tilde{\sigma}}_{12}.
\end{aligned} \tag{5.96}$$

Substituting equations (5.70) and (5.94) into equation (5.96), $\dot{V}_2$ becomes,

$$\begin{aligned}
\dot{V}_2 = -k_1{e_1}^2 + e_1e_2 + e_2\left(\frac{1}{M}\left(P_\Delta A - \left(\hat{\sigma}_0\hat{z}_0 - \hat{\sigma}_1\frac{|v_p|}{g}\hat{z}_1 + \hat{\sigma}_{12}v_p\right)\right) - \ddot{x}_{pd} + \right. \\
\left. k_1\big(v_p - \dot{x}_d\big)\right) + e_2\left(-\frac{1}{M}\Big(\sigma_0\tilde{z}_0 - \sigma_1\frac{|v_p|}{g}\tilde{z}_1\Big) - \frac{1}{M}\Big(\hat{z}_0\tilde{\sigma}_0 - \hat{z}_1\frac{|v_p|}{g}\tilde{\sigma}_1 + v_p\tilde{\sigma}_{12}\Big)\right) + \\
\sigma_0\tilde{z}_0\big(\dot{z}_0 - \dot{\hat{z}}_0\big) + \sigma_1\tilde{z}_1\big(\dot{z}_1 - \dot{\hat{z}}_1\big) + \gamma_0\tilde{\sigma}_0\dot{\tilde{\sigma}}_0 + \gamma_1\tilde{\sigma}_1\dot{\tilde{\sigma}}_1 + \gamma_{12}\tilde{\sigma}_{12}\dot{\tilde{\sigma}}_{12}.
\end{aligned} \tag{5.97}$$

Replacing $\hat{\sigma}_0\hat{z}_0 - \hat{\sigma}_1\frac{|v_p|}{g(v_p)}\hat{z}_1 + \hat{\sigma}_{12}v_p$ of equation (5.97) with $\hat{F}_f$, and rearranging,

$$\dot{V}_2 = -k_1 {e_1}^2 + e_2\left(\frac{1}{M}\left(P_\Delta A - \hat{F}_f\right) + e_1 - \ddot{x}_d + k_1\left(v_p - \dot{x}_d\right)\right) + \tilde{z}_0\left(-\frac{1}{M}\sigma\sigma_0 + \sigma_0\left(\dot{z}_0 - \dot{\hat{z}}_0\right)\right) + \tilde{z}_1\left(\frac{1}{M}\frac{|v_p|}{g}\sigma\sigma_1 + \sigma_1\left(\dot{z}_1 - \dot{\hat{z}}_1\right)\right) + \tilde{\sigma}_0\left(-\frac{1}{M}\sigma\hat{z}_0 + \gamma_0\dot{\hat{\sigma}}_0\right) + \tilde{\sigma}_1\left(\frac{1}{M}\frac{|v_p|}{g}\sigma\hat{z}_1 + \gamma_1\dot{\hat{\sigma}}_1\right) + \tilde{\sigma}_{12}\left(-\frac{1}{M}\sigma v_p + \gamma_{12}\dot{\hat{\sigma}}_{12}\right). \quad (5.98)$$

To achieve

$$\dot{V}_2 = -k_1 {e_1}^2 - k_2 {e_2}^2 - \sigma_0\frac{|v_p|}{g}{\tilde{z}_0}^2 - \sigma_1\frac{|v_p|}{g}{\tilde{z}_1}^2, \quad (5.99)$$

it is desired to have

$$\frac{1}{M}\left(P_\Delta A - \hat{F}_f\right) + e_1 - \ddot{x}_d + k_1\left(v_p - \dot{x}_d\right) = -k_2 e_2 \quad (5.100)$$

$$-\frac{1}{M}e_2\sigma_0 + \sigma_0\left(\dot{z}_0 - \dot{\hat{z}}_0\right) = -\sigma_0\frac{|v_p|}{g}\tilde{z}_0 \quad (5.101)$$

$$\frac{1}{M}\frac{|v_p|}{g}e_2\sigma_1 + \sigma_1\left(\dot{z}_1 - \dot{\hat{z}}_1\right) = -\sigma_1\frac{|v_p|}{g}\tilde{z}_1 \quad (5.102)$$

$$-\frac{1}{M}e_2\hat{z}_0 + \gamma_0\dot{\hat{\sigma}}_0 = 0 \quad (5.103)$$

$$\frac{1}{M}\frac{|v_p|}{g}e_2\hat{z}_1 + \gamma_1\dot{\hat{\sigma}}_1 = 0 \quad (5.104)$$

$$-\frac{1}{M}e_2 v_p + \gamma_{12}\dot{\hat{\sigma}}_{12} = 0 \quad (5.105)$$

Inspired from equation (5.100), the virtual control law is given as

$$\alpha_2 = \frac{1}{A}\left(M\left(\ddot{x}_d - e_1 - k_1\left(v_p - \dot{x}_d\right) - k_2 e_2\right) + \hat{F}_f\right) \quad (5.106)$$

Substituting $\tilde{z}_0 = z_0 - \hat{z}_0$ and $\dot{z}_0 = v_p - \frac{|v_p|}{g}z_0$ into equation (5.101),

$$\dot{\hat{z}}_0 = v_p - \frac{e_2}{M} - \frac{|v_p|}{g}\hat{z}_0. \quad (5.107)$$

Substituting $\tilde{z}_1 = z_1 - \hat{z}_1$ and $\dot{z}_1 = v_p - \frac{|v_p|}{g}z_1$ in equation (5.102),

$$\dot{\hat{z}}_1 = v_p + \frac{e_2}{M}\frac{|v_p|}{g} - \frac{|v_p|}{g}\hat{z}_1. \tag{5.108}$$

Rearranging terms in equations (5.103)-(5.105),

$$\dot{\hat{\sigma}}_0 = \frac{1}{\gamma_0}\frac{e_2}{M}\hat{z}_0 \tag{5.109}$$

$$\dot{\hat{\sigma}}_1 = -\frac{1}{\gamma_1}\frac{e_2}{M}\frac{|v_p|}{g}\hat{z}_1 \tag{5.110}$$

$$\dot{\hat{\sigma}}_{12} = \frac{1}{\gamma_{12}}\frac{e_2}{M}v_p. \tag{5.111}$$

Now, the third error variable is defined as

$$e_3 = P_\Delta - \alpha_2. \tag{5.112}$$

Substituting equation (5.106) into equation (5.112),

$$e_3 = P_\Delta - \frac{1}{A}\left(M\left(\ddot{x}_d - e_1 - k_1\left(v_p - \dot{x}_d\right) - k_2 e_2\right) + \hat{F}_f\right). \tag{5.113}$$

Given equations (5.106)-(5.113), equation (5.98) becomes

$$\dot{V}_2 = -k_1 {e_1}^2 - k_2 {e_2}^2 + \frac{A}{M}e_2 e_3 - \sigma_0\frac{|v_p|}{g}{\tilde{z}_0}^2 - \sigma_1\frac{|v_p|}{g}{\tilde{z}_1}^2. \tag{5.114}$$

The time derivative of equation (5.113) is

$$\dot{e}_3 = \dot{P}_\Delta - \frac{1}{A}\left(M\left(\dddot{x}_d - k_1\left(\dot{v}_p - \ddot{x}_d\right) - k_2\dot{e}_2 - \dot{e}_1\right) + \dot{\hat{F}}_f\right). \tag{5.115}$$

Assume that the time derivative of the estimation $\dot{\hat{F}}_f$ in (5.115) can be ignored,

$$\dot{e}_3 = \dot{P}_\Delta - \frac{1}{A}\left(M\left(\dddot{x}_d - k_1\left(\dot{v}_p - \ddot{x}_d\right) - k_2\dot{e}_2 - \dot{e}_1\right)\right). \tag{5.116}$$

Constructing the third CLF,

$$V_3 = V_2 + \frac{1}{2}s^2 \tag{5.117}$$

with the sliding surface given as

$$s = \Gamma_1 e_1 + \Gamma_2 e_2 + e_3, \tag{5.118}$$

where Γ_1 and Γ_2 are positive constant.

Given equation (5.114) and time derivative of equation (5.118), the time derivative of V_3 is

$$\dot{V}_3 = -k_1 {e_1}^2 - k_2 {e_2}^2 + \frac{A}{M} e_2 e_3 - \sigma_0 \frac{|v_p|}{g} {\tilde{z}_0}^2 - \sigma_1 \frac{|v_p|}{g} {\tilde{z}_1}^2 + s(\Gamma_1 \dot{e}_1 + \Gamma_2 \dot{e}_2 + \dot{e}_3). \tag{5.119}$$

Substituting equations (5.66), time derivative of (5.69), and (5.117) into equation (5.119),

$$\begin{aligned} \dot{V}_3 = {} & -k_1 {e_1}^2 - k_2 {e_2}^2 + \frac{A}{M} e_2 e_3 - \sigma_0 \frac{|v_p|}{g} {\tilde{z}_0}^2 - \sigma_1 \frac{|v_p|}{g} {\tilde{z}_1}^2 + s \Big(\Gamma_1 \dot{e}_1 + \\ & \Gamma_2 \big(\dot{v}_p - \ddot{x}_d + k_1 \dot{e}_1 \big) + \dot{P}_\Delta - \frac{1}{A} \Big(M \big(\dddot{x}_d - k_1 \big(\dot{v}_p - \ddot{x}_d \big) - k_2 \big(\dot{v}_p - \ddot{x}_d + k_1 \dot{e}_1 \big) - \dot{e}_1 \big) \Big) \Big). \end{aligned} \tag{5.120}$$

Separate term associate with $\dot{v}_p$ in equation (5.120),

$$\begin{aligned} \dot{V}_3 = {} & -k_1 {e_1}^2 - k_2 {e_2}^2 + \frac{A}{M} e_2 e_3 - \sigma_0 \frac{|v_p|}{g(v_p)} {\tilde{z}_0}^2 - \sigma_1 \frac{|v_p|}{g} {\tilde{z}_1}^2 + s \Big(\Gamma_1 \dot{e}_1 + \\ & \Big(\Gamma_2 + \frac{M}{A} k_2 \Big) (k_1 \dot{e}_1 - \ddot{x}_d) + \dot{P}_\Delta - \frac{M}{A} (\dddot{x}_d + k_1 \ddot{x}_d - \dot{e}_1) + \Big(\Gamma_2 + \frac{M}{A} k_1 + \frac{M}{A} k_2 \Big) \dot{v}_p \Big). \end{aligned} \tag{5.121}$$

Given the parameter convergence of friction estimate $\hat{F}_f$, the estimation error $\dot{\tilde{v}}_p = \big(\dot{v}_p - \dot{\hat{v}}_p \big)$ will converge on the sliding surface s, i.e.,

$$-\Gamma_3 s = \Big(\Gamma_2 + \frac{M}{A} k_1 + \frac{M}{A} k_2 \Big) \big(\dot{v}_p - \dot{\hat{v}}_p \big) \tag{5.122}$$

Substitute $\dot{v}_p = P_\Delta A - \hat{F}_f$ into equation (5.122), and rearranging,

$$\dot{\hat{v}}_p = \frac{1}{M} (P_\Delta A - \hat{F}_f) + \frac{\Gamma_3}{\Gamma_2 + \frac{M}{A} k_1 + \frac{M}{A} k_2} s \tag{5.123}$$

With reference to [18], to obtain

$$\dot{V}_3 = -k_1 {e_1}^2 - k_2 {e_2}^2 + \frac{A}{M} e_2 e_3 - k_3 s^2 - \eta |s| - \sigma_0 \frac{|v_p|}{g(v_p)} {\tilde{z}_0}^2 - \sigma_1 \frac{|v_p|}{g(v_p)} {\tilde{z}_1}^2, \tag{5.124}$$

it is necessary to have

$$\Gamma_1\dot{e}_1 + (\Gamma_2 - k_2)\left(k_1\dot{e}_1 - \ddot{x}_{pd}\right) + \dot{P}_\Delta - \frac{M}{A}(\ddot{x}_d + k_1\ddot{x}_d - \dot{e}_1) + \left(\Gamma_2 + \frac{M}{A}k_1 + \frac{M}{A}k_2\right)\hat{\dot{v}}_p = -k_3 s - \eta sign(s). \tag{5.125}$$

Rearranging equation (5.125),

$$\dot{P}_\Delta = \frac{M}{A}(\ddot{x}_d + k_1\ddot{x}_d - \dot{e}_1) - \left(\Gamma_2 + \frac{M}{A}k_1 + \frac{M}{A}k_2\right)\hat{\dot{v}}_p - \Gamma_1\dot{e}_1 - (\Gamma_2 - k_2)\left(k_1\dot{e}_1 - \ddot{x}_{pd}\right) - k_3 s - \eta sign(s). \tag{5.126}$$

Substituting $\dot{P}_\Delta$ of equation (5.18) into equation (5.126), the control law is

$$\hat{A}_v = \frac{1}{\hat{b}}\left(\frac{M}{A}(\ddot{x}_d + k_1\ddot{x}_d - \dot{e}_1) - \left(\Gamma_2 + \frac{M}{A}k_1 + \frac{M}{A}k_2\right)\hat{\dot{v}}_p - \Gamma_1\dot{e}_1 - (\Gamma_2 - k_2)(k_1\dot{e}_1 - \ddot{x}_d) - k_3 s - \eta sign(s) - \hat{p}\right). \tag{5.127}$$

Consequently, the approximate control input $\hat{u}_v$ is obtained from the relation (5.11).

According to [18], equation (5.124) can be rewritten as

$$\dot{V}_3 = -\boldsymbol{e}^T Q\boldsymbol{e} - \eta|s| - \sigma_0\frac{|v_p|}{g(v_p)}\tilde{z}_0{}^2 - \sigma_1\frac{|v_p|}{g(v_p)}\tilde{z}_1{}^2, \tag{5.128}$$

where Q is a symmetric matrix with the following form

$$Q = \begin{bmatrix} k_1 + k_3\Gamma_1{}^2 & 2k_3\Gamma_1\Gamma_2 & 2k_3\Gamma_1 \\ 2k_3\Gamma_1\Gamma_2 & k_2 + k_3\Gamma_2{}^2 & -\frac{A}{M} + 2k_3\Gamma_2 \\ 2k_3\Gamma_1 & -\frac{A}{M} + 2k_3\Gamma_2 & k_3 \end{bmatrix}, \tag{5.129}$$

and $\boldsymbol{e^T} = [e_1\ e_2\ e_3]$ is the error vector.

Given Sylvester's theorem, a necessary and sufficient condition for Q to be a positive definite matrix is that all the principal minors should be strictly positive, i.e.,

$$
\begin{aligned}
&k_1 + k_3{\Gamma_1}^2 > 0 \\
&\begin{vmatrix} k_1 + k_3{\Gamma_1}^2 & 2k_3\Gamma_1\Gamma_2 \\ 2k_3\Gamma_1\Gamma_2 & k_2 + k_3{\Gamma_2}^2 \end{vmatrix} > 0 \\
&\begin{vmatrix} k_1 + k_3{\Gamma_1}^2 & 2k_3\Gamma_1\Gamma_2 & 2k_3\Gamma_1 \\ 2k_3\Gamma_1\Gamma_2 & k_2 + k_3{\Gamma_2}^2 & -\frac{A}{M} + 2k_3\Gamma_2 \\ 2k_3\Gamma_1 & -\frac{A}{M} + 2k_3\Gamma_2 & k_3 \end{vmatrix} > 0.
\end{aligned}
\tag{5.130}
$$

Such a Q satisfies the condition $\dot{V}_3 \leq 0$.

5.5 Summary

In this chapter, the dynamical adaptive backsteping-sliding mode control developed for the servo pneumatic actuator is adapted from the theoretical work proposed by Rios-Bilivar[17]. The synthesis of the controller is a process of manufacturing the three nonlinear controllers in previous works, i.e., the sliding mode controller, the cascade controller, and the backstepping controller. The control law and adaptive laws of the controller are summarized in the following.

Control law:

$$
\begin{aligned}
&\hat{u}_v = \frac{1}{wk_v\hat{b}}\Big(\frac{M}{A}(\dddot{x}_d + k_1\ddot{x}_d - \dot{e}_1) - \Big(\Gamma_2 + \frac{M}{A}k_1 + \frac{M}{A}k_2\Big)\hat{v}_p - \Gamma_1\dot{e}_1 - (\Gamma_2 - \\
&k_2)(k_1\dot{e}_1 - \ddot{x}_d) - k_3 s - \eta sign(s) - \hat{p}\Big) \\
&e_1 = x_p - x_d \\
&e_2 = v_p - \dot{x}_d + k_1 e_1 \\
&e_3 = P_\Delta - \frac{1}{A}\big(M\big(\ddot{x}_d - e_1 - k_1\big(v_p - \dot{x}_d\big) - k_2 e_2\big) + \hat{F}_f\big) \\
&s = \Gamma_1 e_1 + \Gamma_2 e_2 + e_3
\end{aligned}
\tag{5.131}
$$

Adaptive laws:

$$
\begin{aligned}
&\dot{\hat{\sigma}}_0 = \frac{1}{\gamma_0}\frac{e_2}{M}\hat{z}_0 \\
&\dot{\hat{\sigma}}_1 = -\frac{1}{\gamma_1}\frac{e_2}{M}\frac{|v_p|}{g}\hat{z}_1 \\
&\dot{\hat{\sigma}}_{12} = \frac{1}{\gamma_{12}}\frac{e_2}{M}v_p
\end{aligned}
\tag{5.132}
$$

Friction internal state observers:

$$\dot{\hat{z}}_0 = v_p - \frac{e_2}{M} - \frac{|v_p|}{g}\hat{z}_0$$
$$\dot{\hat{z}}_1 = v_p + \frac{e_2}{M}\frac{|v_p|}{g} - \frac{|v_p|}{g}\hat{z}_1 \quad (5.133)$$

Acceleration observer:

$$\dot{\hat{v}}_p = \frac{1}{M}\left(P_\Delta A - \hat{F}_f\right) + \frac{\Gamma_3}{\Gamma_2 + \frac{M}{A}k_1 + \frac{M}{A}k_2}s \quad (5.134)$$

The controller requires the following states feedback, i.e., the piston displacement x_p, the piston velocity v_p, and the pressures P_1 and P_2. The control gains k_1, k_2, k_3, Γ_1, Γ_2, and Γ_3 has to be tuned so as to provide satisfactory performance along with its stability and convergence characteristics inherited from the Lyapunov-based design approach.

Chapter 6. Simulation Results

In this chapter, computer simulations are implemented to analyze the novel nonlinear controller developed for the servo pneumatic actuator. The simulation code is programmed with Matlab 7.4.0 (R2007a) programming language. An IBM PC operating at 1.8 GHz of CPU clock rate (Intel Core2 Duo) with 2GB of RAM was used for running the simulation program. Section 6.1 carries out a set of open-loop simulations to verify the validity of the mathematical model for servo pneumatic actuator, which is assembled from the actuator differential equations (2.23) and the LuGre friction differential equations (3.10). For comparison purposes, three nonlinear controllers from previous work, i.e., the sliding mode controller, the cascade controller, and the backstepping controller, are simulated with respect to reference trajectories in Section 6.2. Section 6.3 presents the simulations of the dynamical adaptive backstepping-sliding mode controller (DAB-SMC). The chapter closes with an integration of the tuned DAB-SMC controller and a Lyapunov-based pressure observer that has the potential to reduce the number of feedbacks.

To implement a numerical simulation of the servo pneumatic actuator, knowledge of the appropriate system parameters is required. The reference servo pneumatic actuator consists of a FESTO MPYE-5 series 5-port three-position solenoid driven proportional directional flow control valve and a FESTO DNC series double-rod type pneumatic actuator. Where possible, the system parameters were either obtained directly from previous works [22, 34], or estimated from available manufacturer (FESTO Canada)'s catalogs. Table 6.1 lists the system parameters for the servo pneumatic actuator simulator. The friction model nominal parameters are obtained from relevant literatures [11, 22]. The exact value of friction parameters (σ_0, σ_1, and σ_2) are not needed because the DAB-SMC controller estimates those parameters on-line through the dynamical adaptive laws. The nominal parameters of LuGre friction model are listed in Table 6.2.

Table 6.1 Servo pneumatic actuator nominal parameters.

Parameter	Symbol	Nominal Value
supply pressure	P_s	50985.81 Pa
atmospheric pressure	P_{atm}	10197.16 Pa
total mass of piston, rods	M	1.91kg
actuator stroke	L	500 mm
piston annulus area	A	10.6 cm^2
cylinder fixed volume	V_{o1},V_{o2}	5 mm^3
ideal gas constant	R	287 $J/kg \cdot K$
temperature of air source	T	300K
ratio of specific heats	r	1.4
thermal expansion coefficient	α	1-1.4
valve coefficient of discharge	C_d	0.7
valve orifice area gradient	w	22.6 mm^2/mm
max / min valve spool displacement	$x_{v,max}$ / $x_{v,min}$	$+/-$ 1.25 mm
valve idle zone	$-$	$-0.05 < u_v < 0.05$ V
valve spool position gain	k_v	0.25 mm/V
valve critical pressure ratio	P_{cr}	0.2

Table 6.2 LuGre friction model nominal parameters.

Parameter	Symbols	Nominal Value
spring constant	σ_0	4500 N/m
damping coefficient	σ_1	93.13 N/m/s
viscous coefficient	σ_2	89.86 N/m/s
Stribeck velocity	v_s	0.02 m/s
static friction	F_s	38.5 N
Coulomb friction	F_C	32.9 N

6.1 Model Verification

In this section, the mathematical model of servo pneumatic actuator is verified. A systematic way to verify a mathematical model can be accomplished through the observation of the computer simulation results and the experimental results of the system under study. Thereafter, the parameters of the mathematical model can be adjusted according to the discrepancies in the comparison between simulation and experiment. In [22], the system parameter identifications and validation works of the mathematical model of the servo pneumatic actuator are documented comprehensively. A good agreement has been observed between the experimental and simulation results. However, unlubricated condition for the pneumatic cylinder is assumed in [22]; hence, the Karnopp's friction model is implemented in the simulation program. Relevant literatures [3, 11] has suggested that it is valid to use LuGre friction model in servo pneumatic actuators if the lubricants are assumed to present in the actuator to reduce wear.

The integration of simulation program was accomplished through the fourth-order Runge-Kutta scheme with a fixed integration time step of 1 msec. The initial conditions were set such that the system started from rest with the actuator located at the middle of the full stroke. The supply and atmosphere pressures for the simulation are set to 509851.1 Pa and 101971.6 Pa respectively. The initial pressure in each of the actuator chambers were set to the middle of the full pressure range (305914.8 Pa) during the simulation.

Open loop control input signals are created to carry out the servo pneumatic actuator response test for the mathematical model validation, and they consists of a sinusoidal function with 1.2 V amplitude and a frequency of 2π rad/s,

$$u = 1.2\sin(2\pi t), \tag{6.1}$$

and a decreasing sinusoidal function with a decay rate of 0.16,

$$u = 1.2\sin(2\pi t)e^{-0.16t}. \tag{6.2}$$

Both testing control signals begin from 0 V, and they are shown in Figure 6.1 and Figure 6.3, respectively. In Figure 6.1, a sinusoidal testing signal is used in the validation

because the system response can be observed and compared between fast motion and slow motion of the simulated model of pneumatic actuator. The position and velocity plot in Figure 6.1 shows that the actuator has zero velocity after each plateau value of the control signal. This is due to the fact that the actuator force created from the control signal is smaller than the friction force, and the actuator comes to a rest. In Figure 6.2, the pressures in both chambers fluctuate between 200 kPa and 400 kPa to generate the actuation force during the simulation. The friction plot in Figure 6.2 shows that as the velocity of the actuator increases, the friction also increases. This relationship between friction and relative velocity is corresponding to the changes in viscous friction. During the rest, the friction is nonzero and is in the static friction range. As the actuator force reaches the breakaway force, the friction changes from static friction to dynamic friction. In Figure 6.3, the decreasing sinusoidal signal is used to demonstrate the effect of deadband in servo valve to the actuator motion. As the control input signal u_v is reduced to the deadband range (i.e., $-0.55\ V$ to $0.55\ V$), the motion of the actuator stops. During these instances, the valve spool does not move; hence, the pressures in actuator chambers, as shown in Figure 6.4, do not change, and the friction force reduces to zero due to the fact that the actuation force, which induces the static friction, is reduced to zero. Outside the deadband the control input signal u_v is recalculated in the servo valve model through a shift function $u_v = sign(u_v)(|u_v| - 0.55)$. Despite discrepancies due to the friction modeling, results of the open-loop simulation in this study have a good agreement with the simulation results from previous works [22].

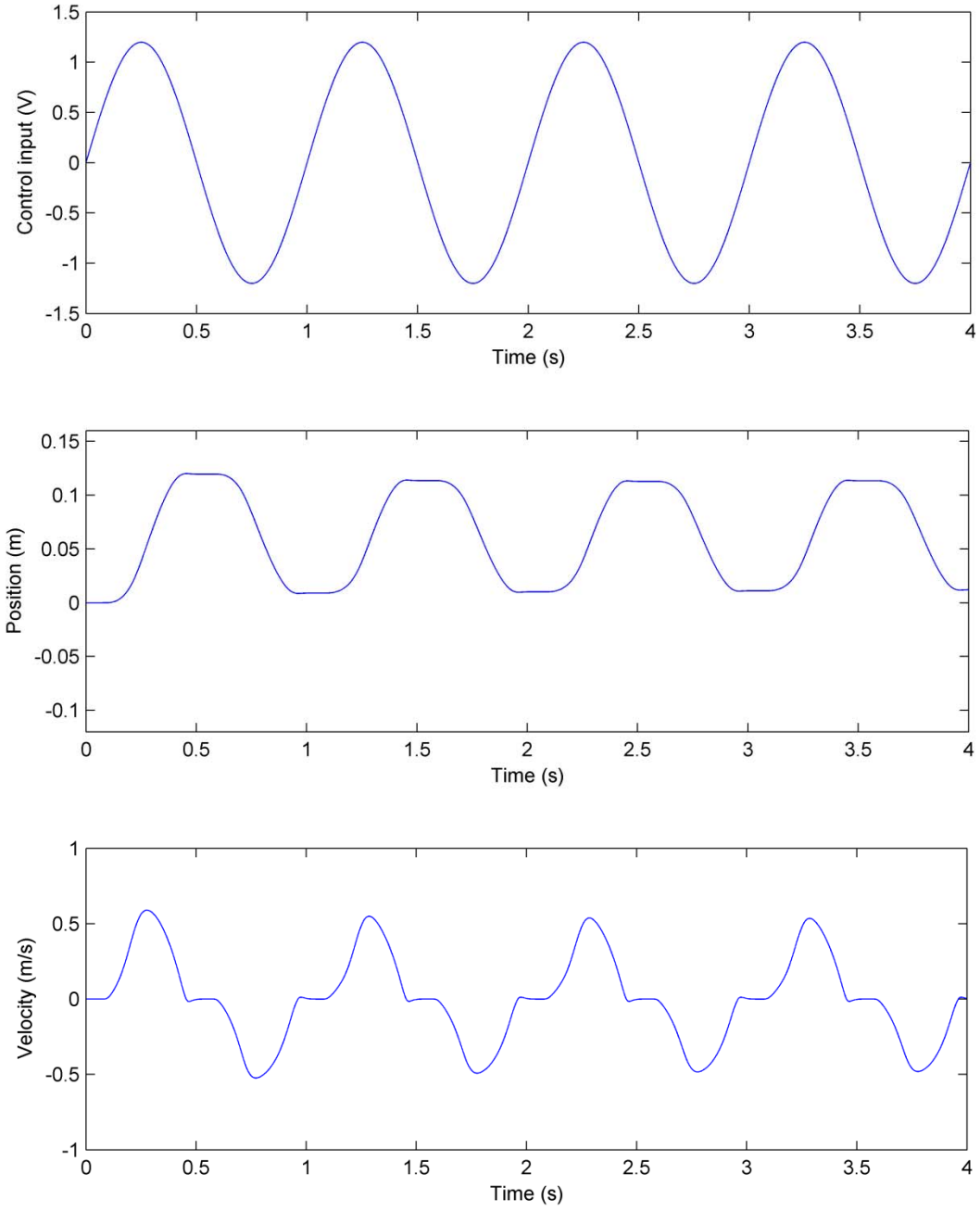

Figure 6.1 Simulated open-loop responses for a sinusoidal control signal.

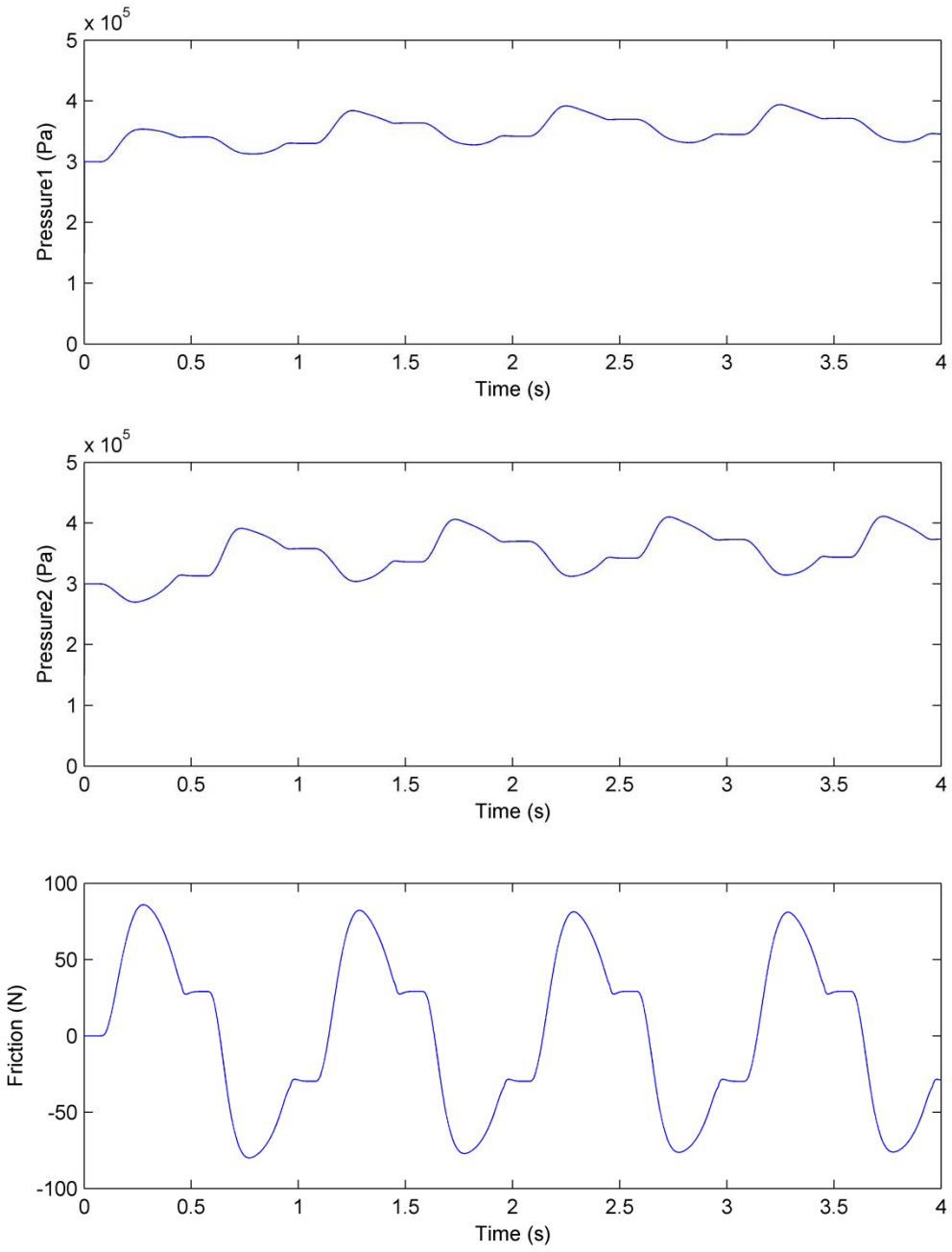

Figure 6.2 Simulated open-loop responses for a sinusoidal control signal (continued).

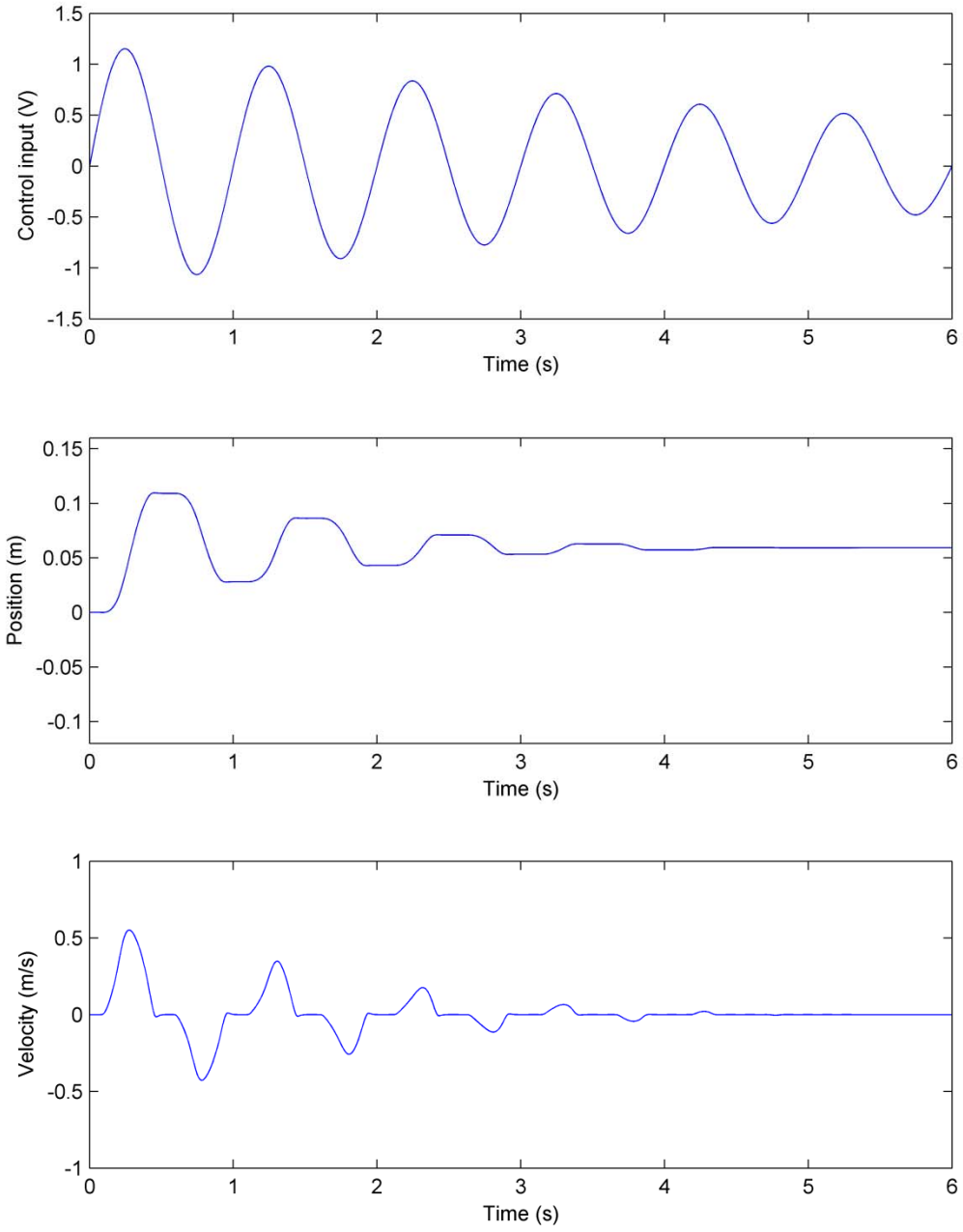

Figure 6.3 Simulated open-loop responses for a decreasing sinusoidal control signal.

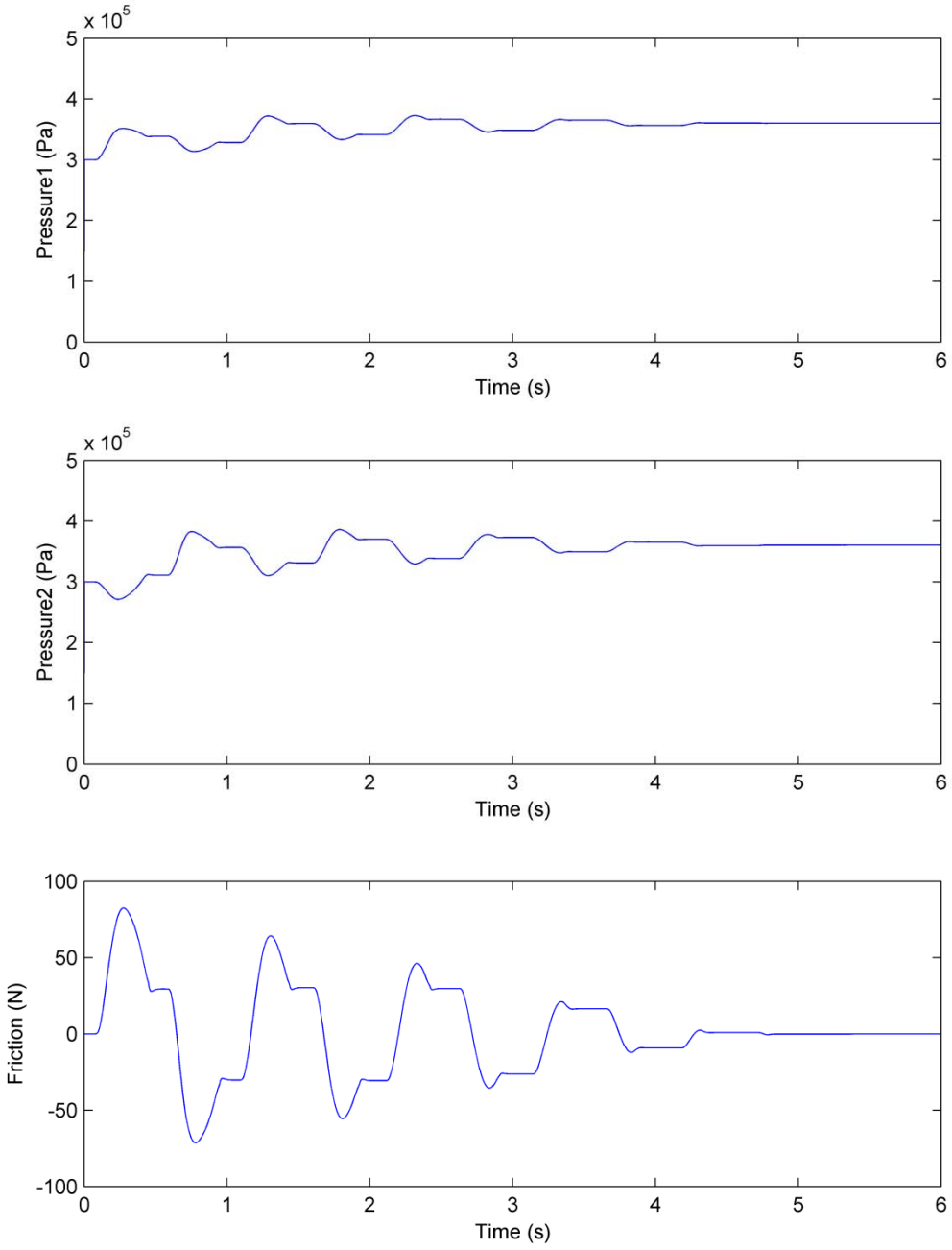

Figure 6.4 Simulated open-loop responses for a decreasing sinusoidal control signal (continued).

6.2 Nonlinear Controller Simulations from Previous Works

With the mathematical model of the servo pneumatic actuator verified in the previous section, the simulation of nonlinear control system are performed using a decreasing sinusoidal desired trajectory

$$x_d = 0.2\sin(0.5t)\,e^{-0.16t}, \tag{6.3}$$

and a ramp desired trajectory. The smooth transition in the ramp desired trajectory is created from a 7th-order polynomial function [11],

$$x_p = -2(\tfrac{t}{2})^7 + 7(\tfrac{t}{2})^6 - 8.4(\tfrac{t}{2})^5 + 3.5(\tfrac{t}{2})^3. \tag{6.4}$$

In previous work [11], this polynomial function was suggested to test the pneumatic actuator model. There are significant variations in velocity and acceleration during the smooth transition of the ramp reference trajectory. These variations in higher order states of the system allows to test the performance of the controller.

The transition starts with the position at $0\ m$ measured from the middle of the full stroke of the actuator cylinder, and reaches a steady-state at $x_d = 0.1\ m$.

The magnitude of the ramp transition function can be altered through a scale factor L, and the time of the transition can be changed with a shift factor τ which represents the starting time of each transition. Incorporating both factors, the resulting transition function is

$$x_{poly} = L\left(-2\left(\tfrac{t-\tau}{2}\right)^7 + 7\left(\tfrac{t-\tau}{2}\right)^6 - 8.4\left(\tfrac{t-\tau}{2}\right)^5 + 3.5\left(\tfrac{t-\tau}{2}\right)^3\right) \tag{6.5}$$

The time function of ramp trajectory is constructed as follows:

$$
\begin{aligned}
x_d &= -2\left(\tfrac{t}{2}\right)^7 + 7\left(\tfrac{t}{2}\right)^6 - 8.4\left(\tfrac{t}{2}\right)^5 + 3.5\left(\tfrac{t}{2}\right)^3 && t < 2 \\
x_d &= 0.1 && 2 \geq t < 4 \\
x_d &= 0.1 - 0.5\left(-2\left(\tfrac{t-4}{2}\right)^7 + 7\left(\tfrac{t-4}{2}\right)^6 - 8.4\left(\tfrac{t-4}{2}\right)^5 + 3.5\left(\tfrac{t-4}{2}\right)^3\right) && 4 \geq t < 6 \\
x_d &= 0.05 && 6 \geq t < 8 \\
x_d &= 0.05 - 0.25(-2\left(\tfrac{t-8}{2}\right)^7 + 7\left(\tfrac{t-8}{2}\right)^6 - 8.4\left(\tfrac{t-8}{2}\right)^5 + 3.5\left(\tfrac{t-8}{2}\right)^3) && 8 \geq t < 10 \\
x_d &= 0.025 && 10 \geq t < 12 \\
x_d &= 0.025 - 0.125(-2\left(\tfrac{t-12}{2}\right)^7 + 7\left(\tfrac{t-12}{2}\right)^6 - 8.4\left(\tfrac{t-12}{2}\right)^5 + 3.5\left(\tfrac{t-12}{2}\right)^3) && 12 \geq t < 14 \\
x_d &= 0.0125 && 14 \geq t < 16 \\
x_d &= 0.0125 - 0.125(-2\left(\tfrac{t-16}{2}\right)^7 + 7\left(\tfrac{t-16}{2}\right)^6 - 8.4\left(\tfrac{t-16}{2}\right)^5 + 3.5\left(\tfrac{t-16}{2}\right)^3) && 16 \geq t < 18 \\
x_d &= 0 && t \geq 18
\end{aligned}
\tag{6.6}
$$

The ramp trajectory and decreasing sine trajectory are plotted in Figure 6.5 and Figure 6.6, respectively, along with the corresponding velocity and acceleration obtained from the 1st and 2nd time derivative of the position trajectory function, respectively.

The decreasing sinusoidal trajectory is selected as the reference trajectory because comparisons of system responses can be established between fast relative motion (approximately 0.1 m/s) and slow relative motion. As the reference velocity reduces, the simulation results can be used to reveal the effect of friction to the actuator system on site of the Stribeck velocity (0.02 m/s). The ramp reference signal is selected for testing the actuator system response because it establishes comparisons between tracking performance and regulation performance of the actuator. Meanwhile, the transition of the two tasks can be evaluated during the simulation as well.

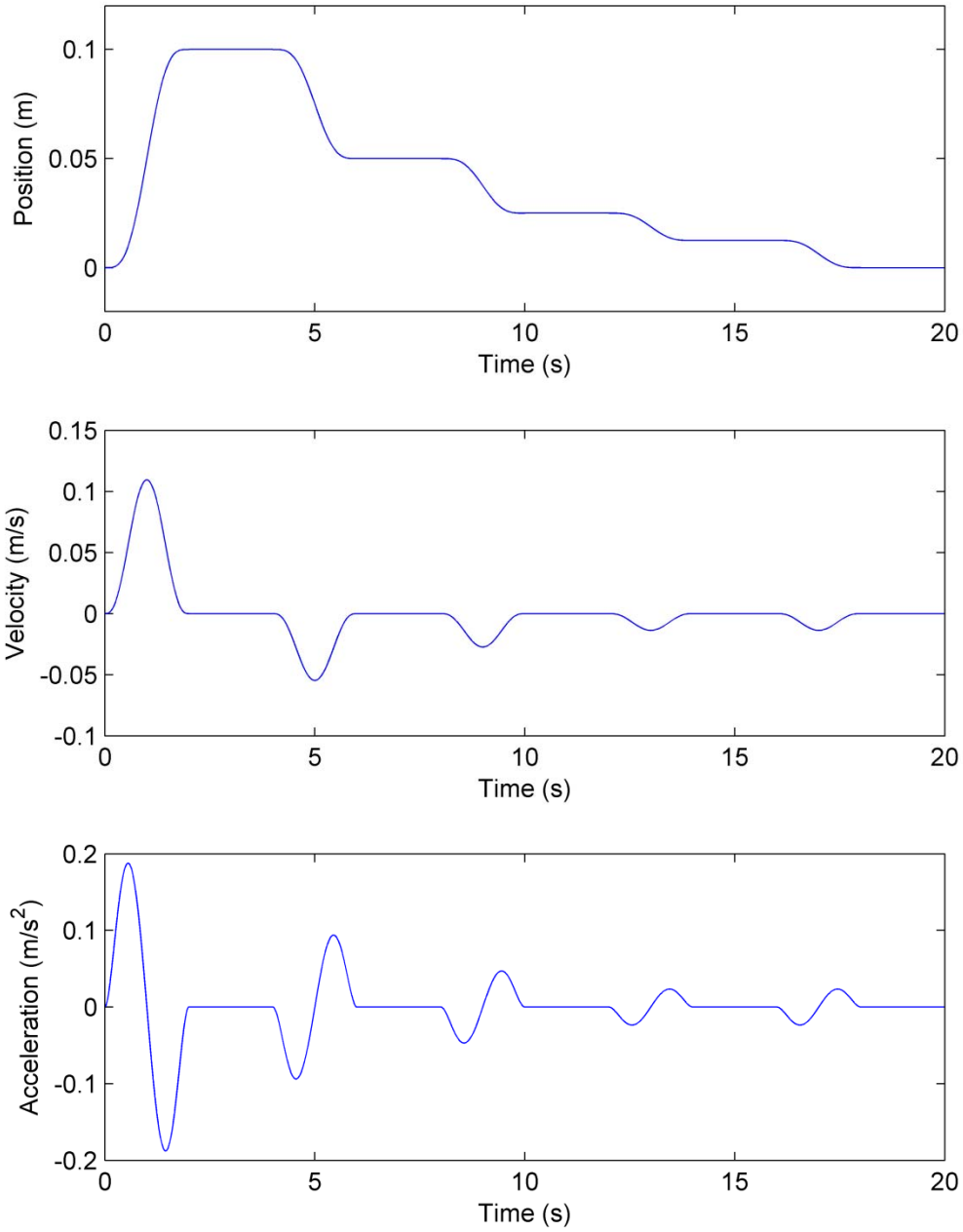

Figure 6.5 Ramp test signal and associated velocity and acceleration profile for the evaluation of the controller's performance.

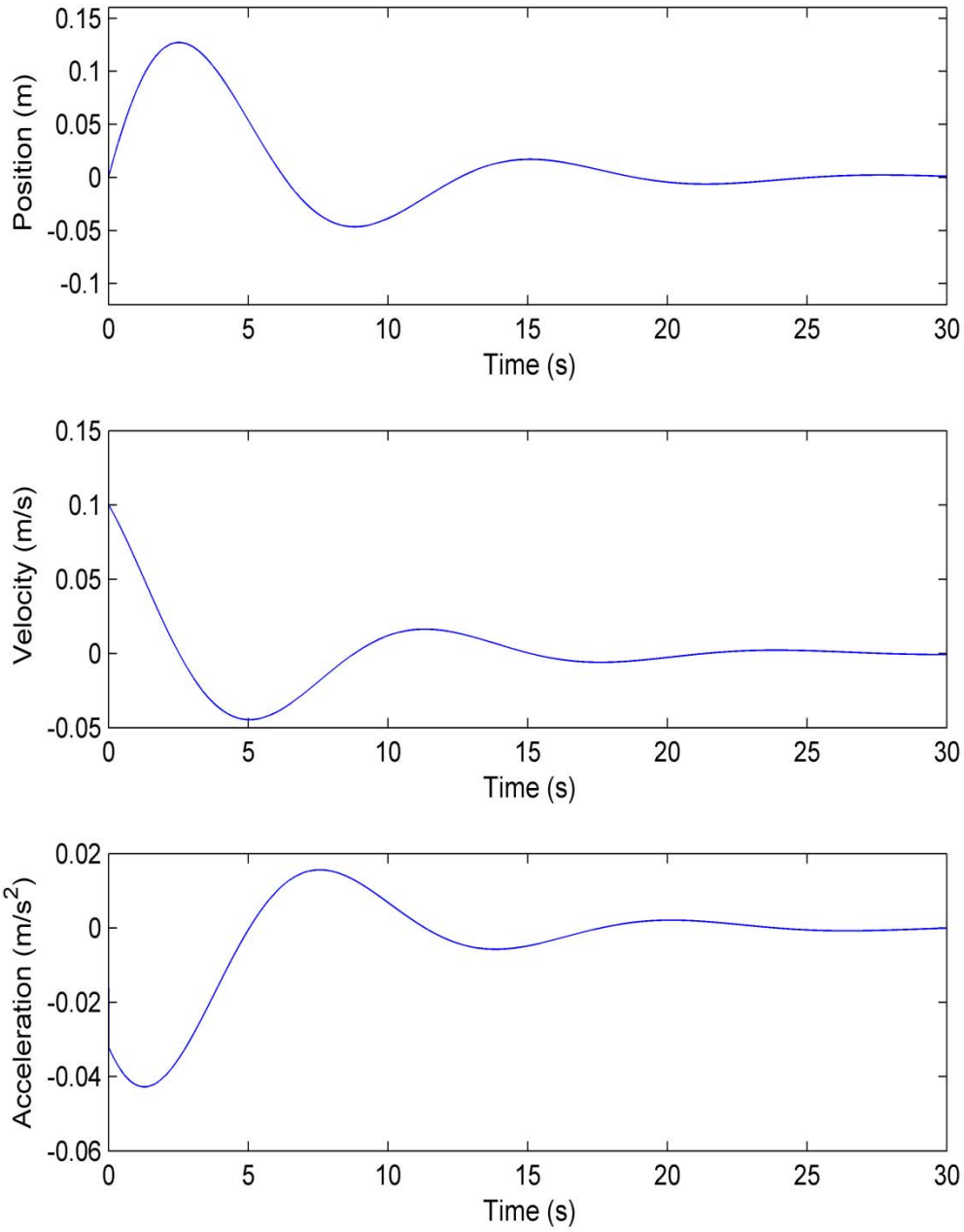

Figure 6.6 Decreasing sinusoidal test signal and associated velocity and acceleration profile for the evaluation of the controller's performance.

For each nonlinear controller, three sets of simulation scenarios are carried out, i.e., no friction in the servo pneumatic actuator, no friction compensation for the servo pneumatic actuator with friction, and friction compensation for the servo pneumatic actuator with friction.

The friction in this section is compensated through the feedforward model-based friction compensation. For these controllers, the control input to the actuator requires the time derivative of friction. Therefore, the friction model requires a slight modification to be used in the simulations. The modification is required because theoretically $\frac{d}{dt}|v_p|$ in the time derivative of friction is not defined. During the implementation, a smooth function $sm(v_r)$ is used when v_r change the sign. According to [11], the smooth function is given as

$$sm(v_p) = \frac{2}{\pi} v_p \arctan(k_{sm} v_p), \tag{6.7}$$

where k_{sm} is a positive constant and a large value of k_{sm} gives good approximation of the original function $|v_p|$. Hence, the time derivative of friction $\dot{F}_f$ exist everywhere. The derivative of the smooth function is given as

$$\frac{d}{dt} sm(v_p) = \left(\frac{2}{\pi} \arctan(k_{sm} v_p) + \frac{2}{\pi} \frac{k_{sm} v_p}{1 + (k_{sm} v_p)^2} \right) \dot{v}_p \tag{6.8}$$

With this modification, the derivative of the model-based friction compensation is able to contribute its control effort to the controllers, and $k_{sm} = 10000$ is used for the simulation.

The sliding mode controller is simulated with the given sets of simulation criteria. In Figure 6.7, the position error plot for sliding mode control shows oscillation at the beginning of the ramp reference tracking motion, and the result of oscillation has contributions from controller hasting the actuator to track the reference signal. Eventually, the controller is able to establish a stable tracking error with respect to the reference trajectory. In the position error plot of Figure 6.7, the tracking error switches sign, and this switch represents that the actuator always follows the reference trajectory during the tracking task. The pressure plot in Figure 6.8 shows that the pressures in the

two actuator chambers have very small pressure differential, and this is due to the fact that the actuation force is the only force acting on the piston and the friction is set to zero (see friction plot in Figure 6.8). The velocity plot in Figure 6.8 also shows initial oscillation, and this confirms that controller tries to establish a steady state tracking with the reference velocity. Figure 6.9 shows the system response to the decreasing sinusoidal reference trajectory. In comparison with the ramp tracking response, the same sliding mode controller takes fewer efforts to establish a steady state tracking with the sinusoidal reference trajectory. With reference to Figure 6.9, the position error does not decrease as the amplitude of reference trajectory decreases, and this suggests that the velocity and acceleration of the reference trajectory have no significant influence on the tracking errors.

With reference to Figure 6.10, the tracking error increases due to the addition of friction to the system model. The initial oscillation is reduced on the same sliding mode controller, and this is due to the damping effect added to the system by viscous friction. Despite the relative large tracking errors, the controller is able to manage the tracking task in a stable manner, which is demonstrated by the control signal in Figure 6.10. In Figure 6.11, system response for sinusoidal reference tracking with friction also shows large tracking errors, and the controller take reasonable effort to keep tracking the reference trajectory.

With respect to Figure 6.12, the sliding mode controller with the friction compensation almost halves the tracking error for ramp reference trajectory in comparison to tracking without friction compensation, and the controller takes few efforts to establish a steady state tracking. The pressures plot in Figure 6.13 shows a pressure differential during tracking and regulation, and this is due to the fact that the additional actuation force is required to counteract the opposing friction. The friction plot in Figure 6.13 shows that friction exists all the time during the tracking and regulation. With reference to Figure 6.14, the tracking errors for sinusoidal reference is also reduced to half of those in the reference tracking without friction compensation, and control signal plot shows that control signal is very smooth for sinusoidal reference tracking.

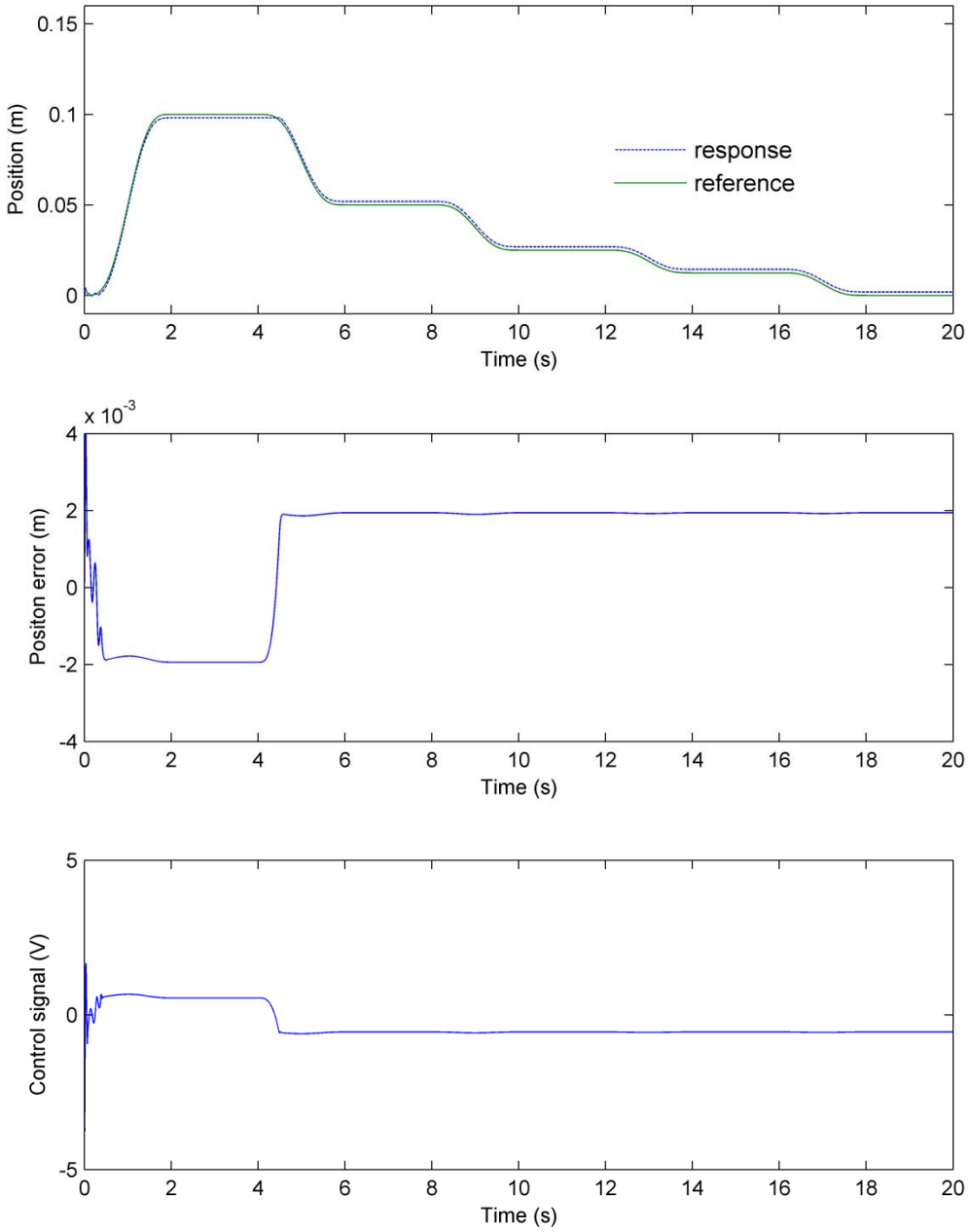

Figure 6.7 Simulated ramp trajectory for sliding mode control responses with the assumption of no friction in the servo pneumatic actuator.

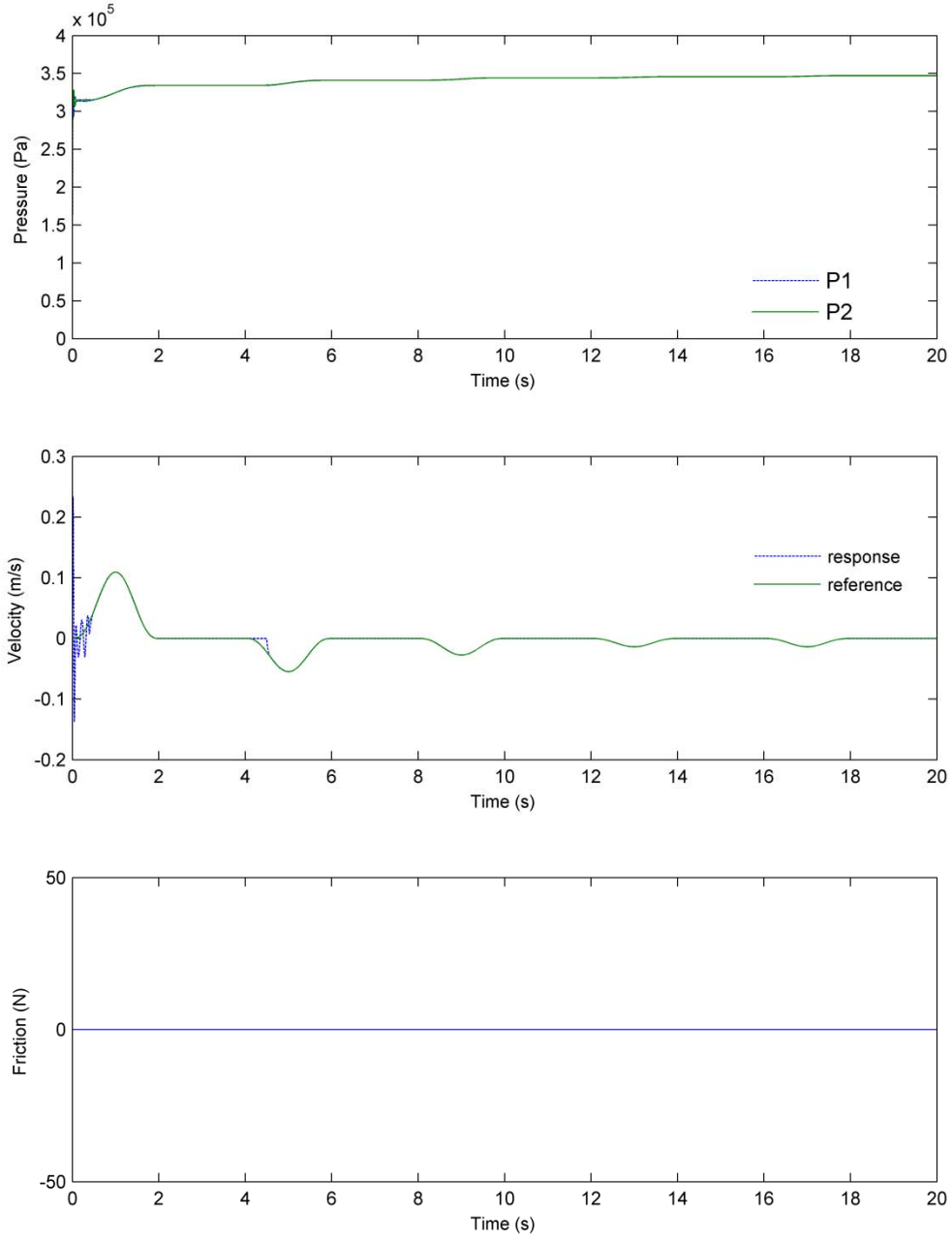

Figure 6.8 Simulated ramp trajectory for the sliding mode control responses with the assumption of no friction in the servo pneumatic actuator (continued).

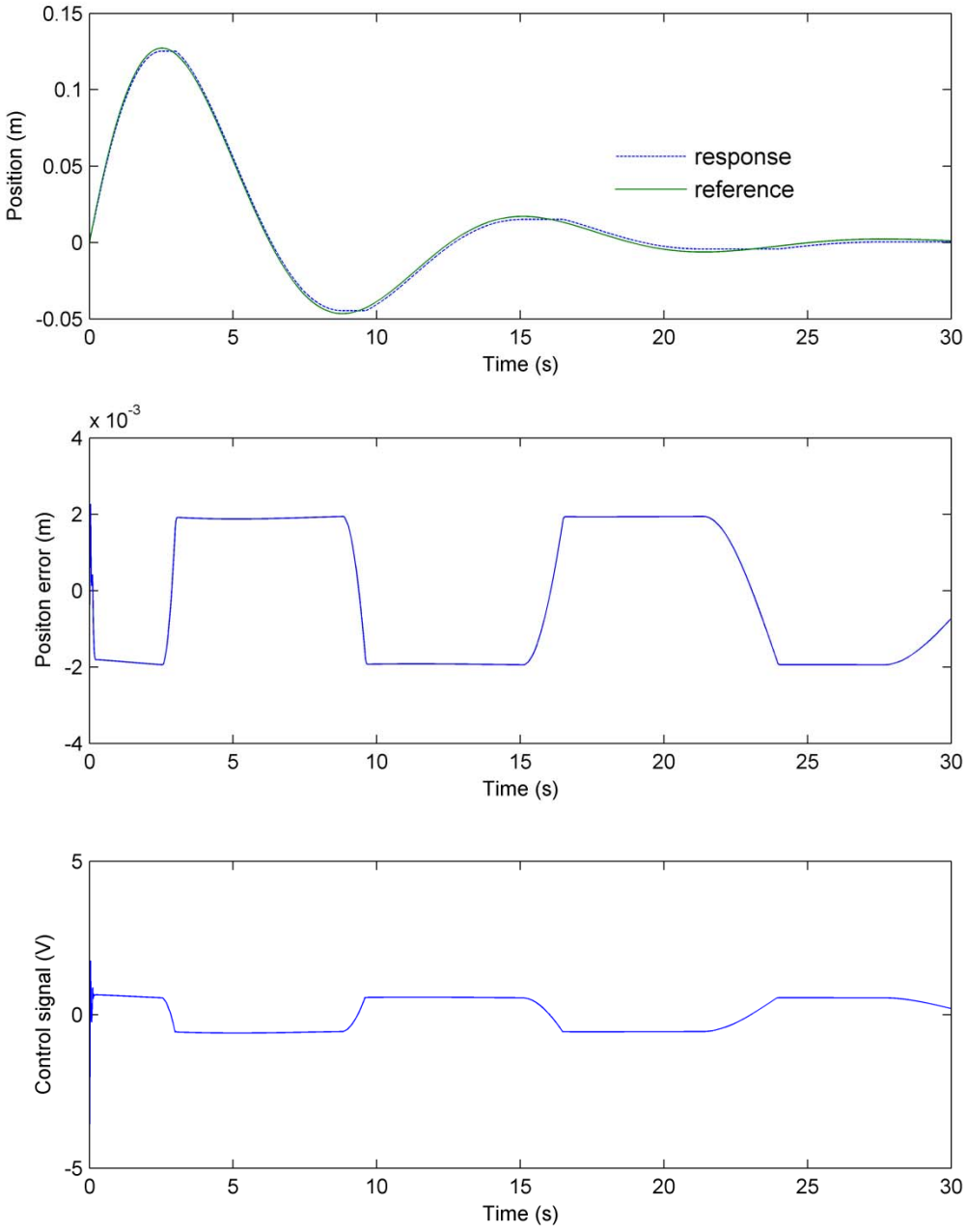

Figure 6.9 Simulated decreasing sine trajectory for the sliding mode control responses with the assumption of no friction in the servo pneumatic actuator.

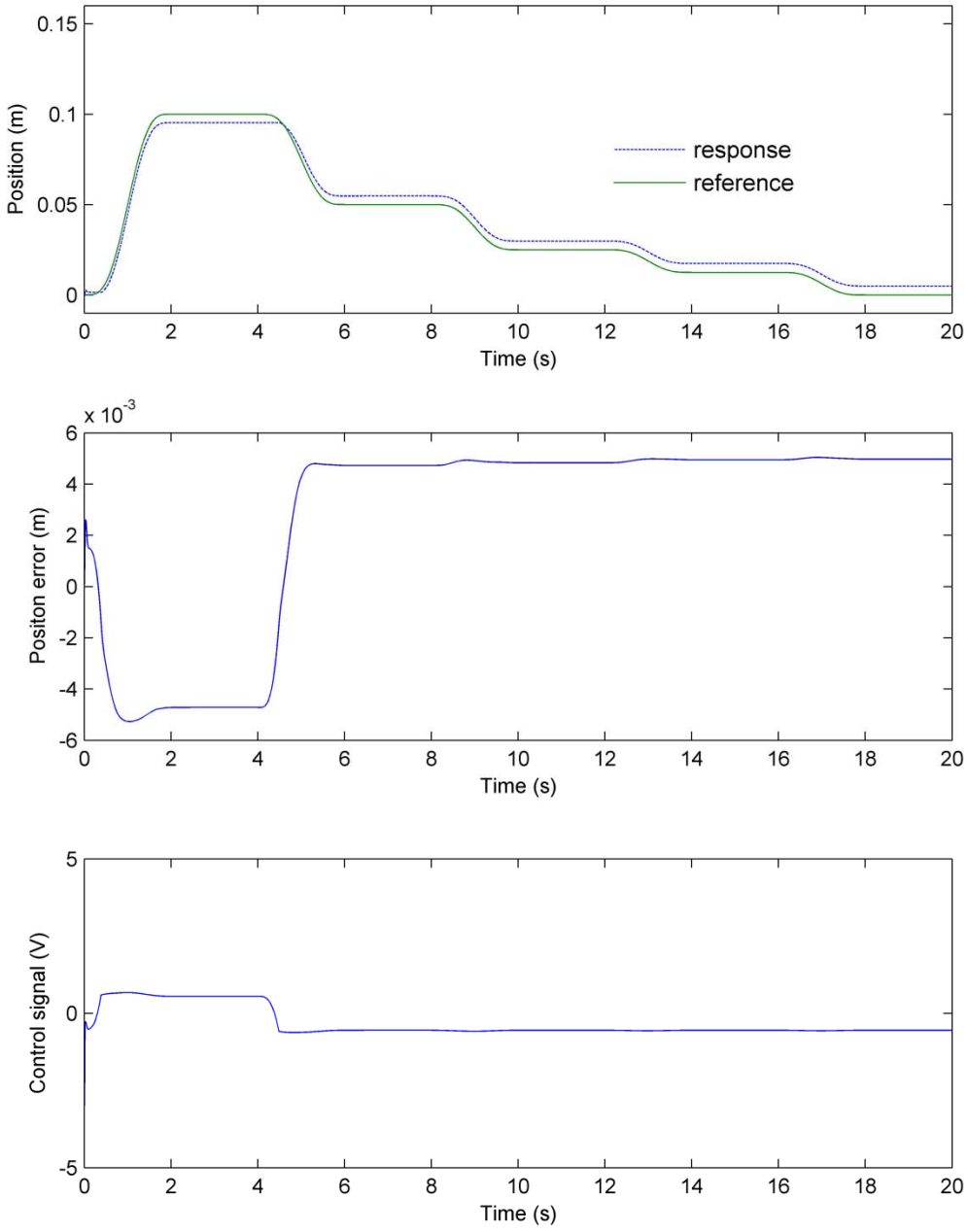

Figure 6.10 Simulated ramp trajectory for the sliding mode control responses without friction compensation in the servo pneumatic actuator with friction.

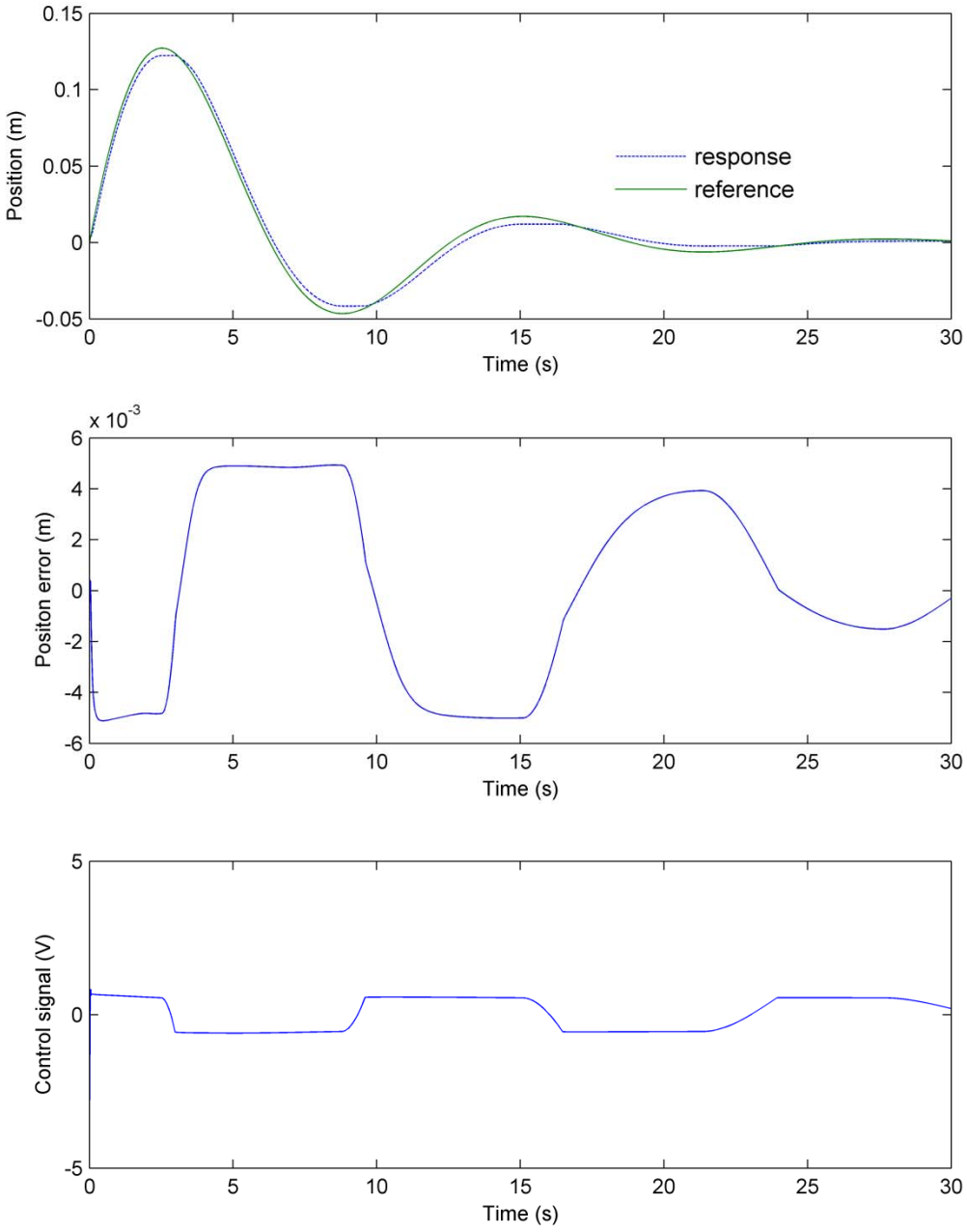

Figure 6.11 Simulated decreasing sine trajectory for the sliding mode control responses without friction compensation in the servo pneumatic actuator with friction.

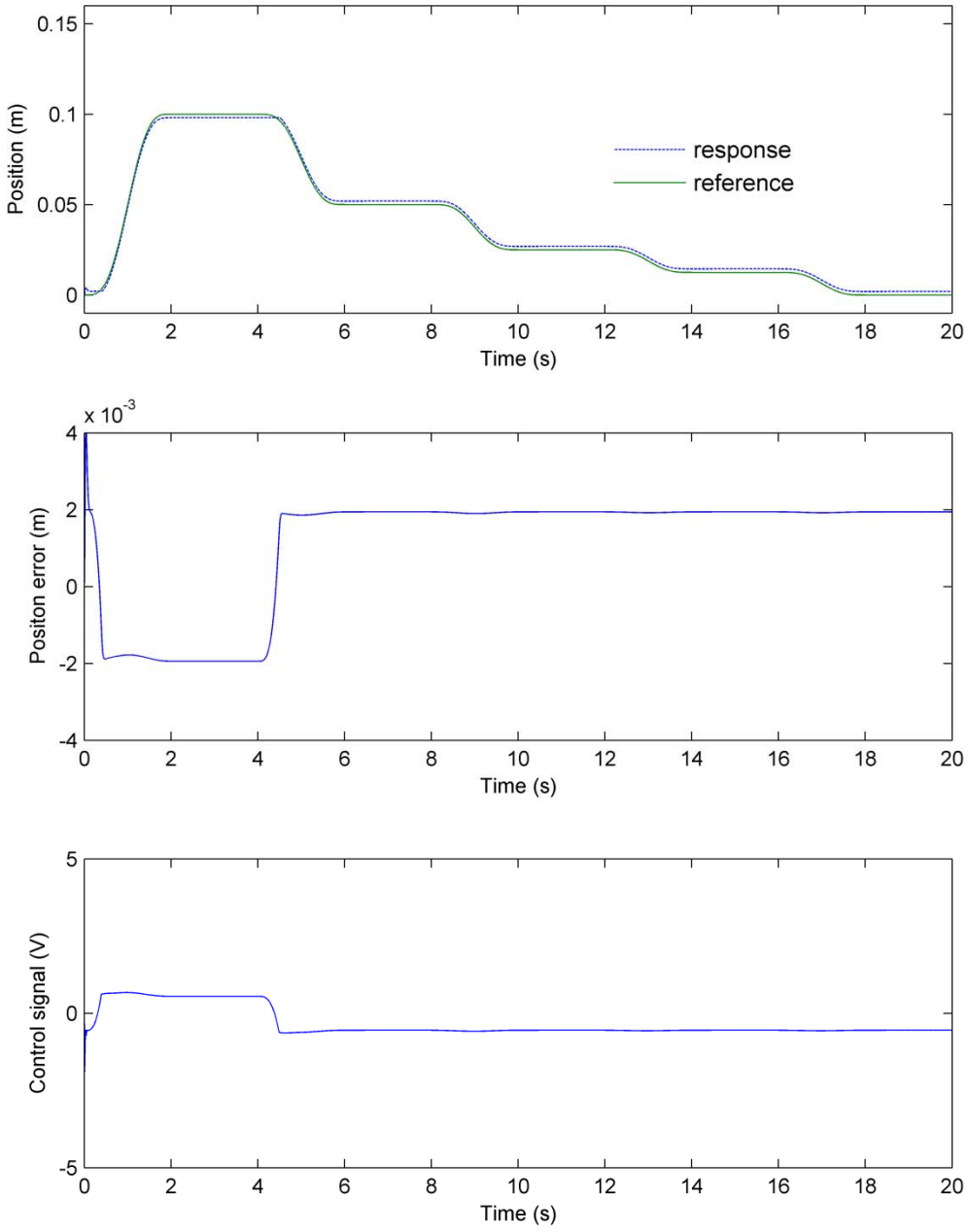

Figure 6.12 Simulated ramp trajectory for the sliding mode control responses with friction compensation in the servo pneumatic actuator with friction.

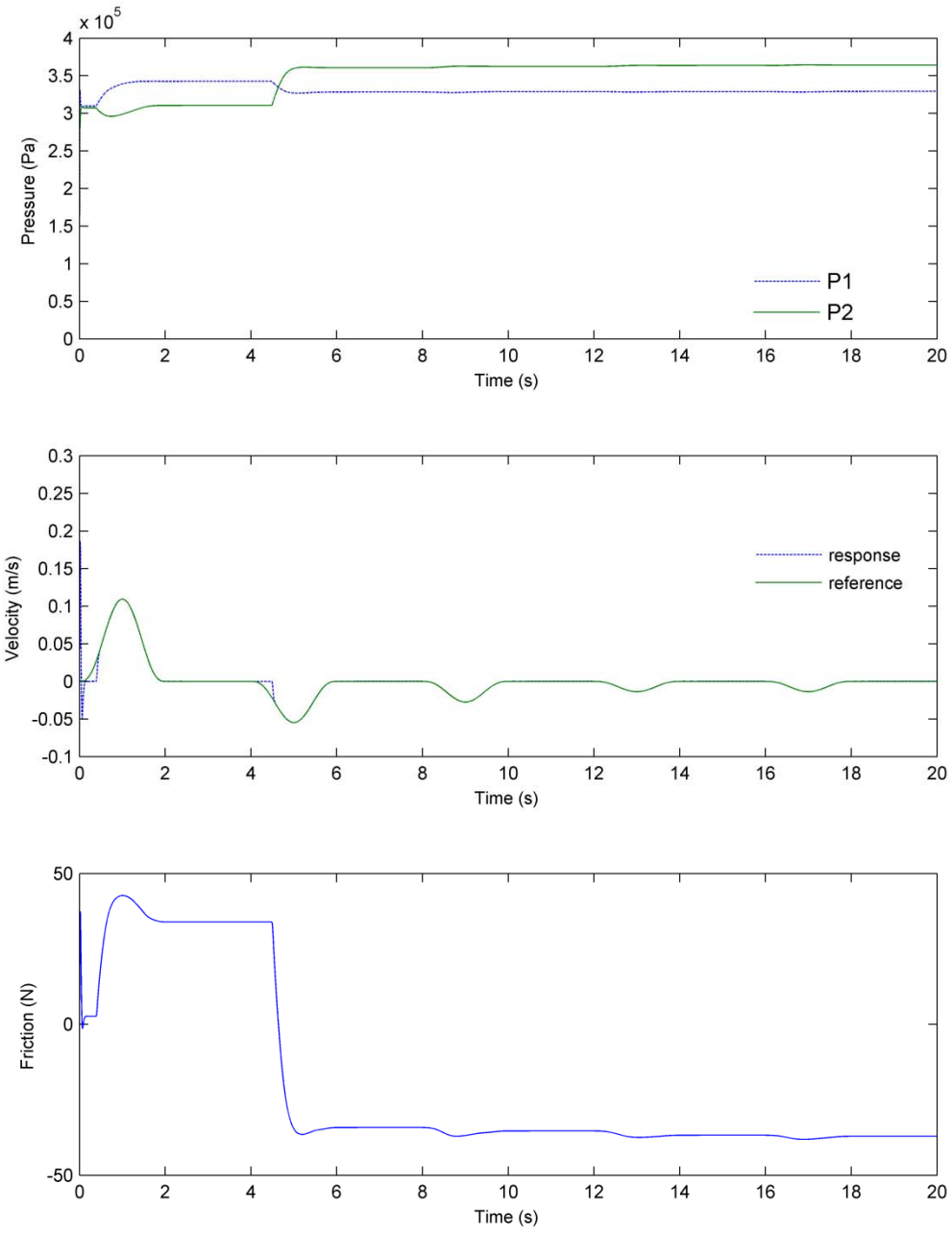

Figure 6.13 Simulated ramp trajectory for the sliding mode control responses with friction compensation in the servo pneumatic actuator with friction (continued).

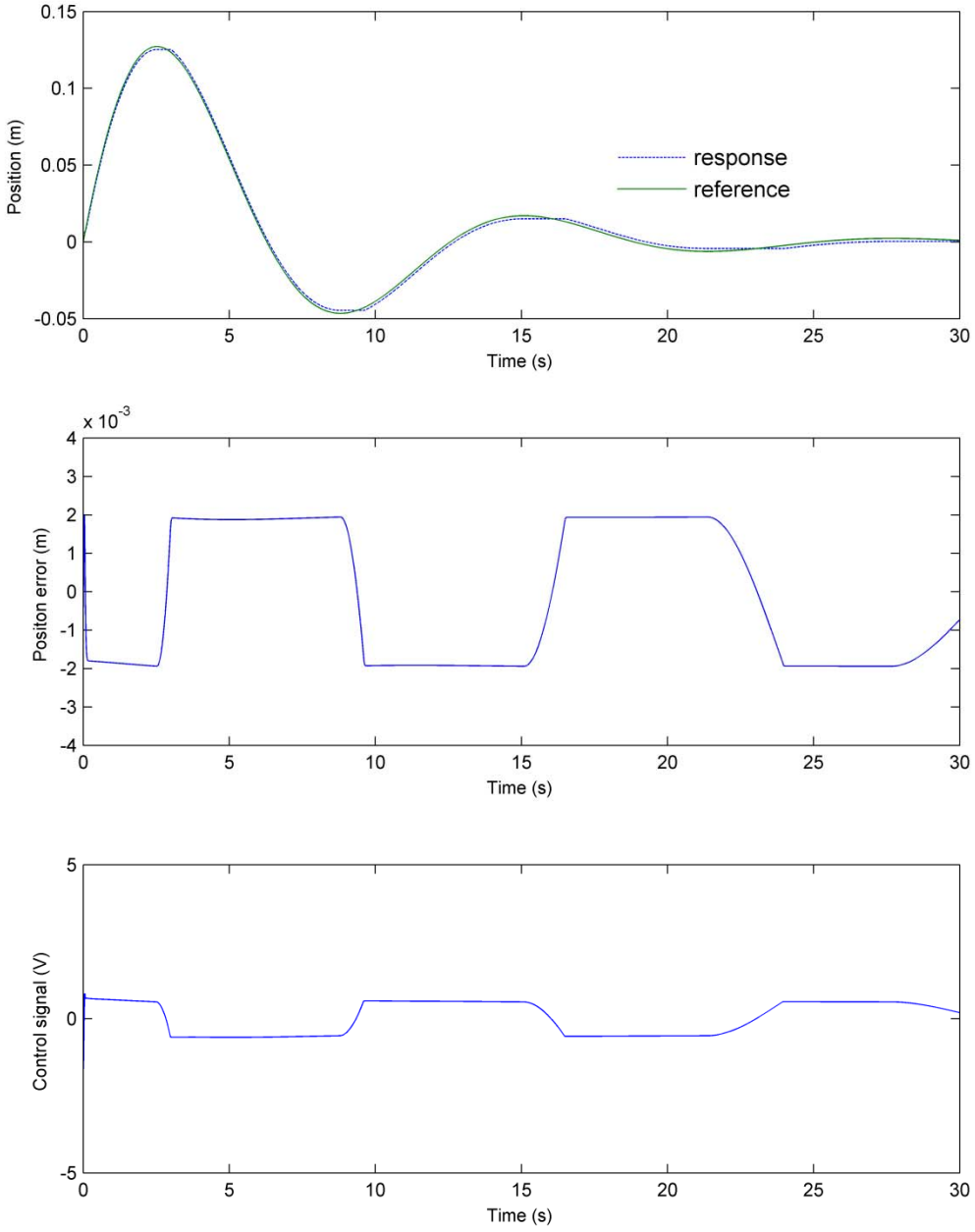

Figure 6.14 Simulated decreasing sine trajectory for the sliding mode control responses with friction compensation in the servo pneumatic actuator with friction.

The same reference trajectories are used to exam the performance of cascade controller. In the first set of simulation, the friction is not considered in the model. In Figure 6.15, the ramp reference tracking for the system model without friction shows the same tracking pattern as that of sliding mode control: initial oscillation and stable tracking afterwards. The values of the tracking error are close to those of previous controller. With reference to Figure 6.16, similar behaviours of pressure and velocity to those of sliding mode control are observed. With respect to Figure 6.17, the tracking behaviour for sinusoidal reference trajectory shows the same pattern as that in the sliding mode control, and the values of tracking error for both controllers are close to each other.

In the second set of simulation test, friction is introduced to the model. With reference to the simulation results of ramp reference tracking in Figure 6.18, large tracking errors are observed from position error plot in comparison with those of sliding mode control without friction compensation. With respect to the simulation results of sinusoidal reference tracking in Figure 6.19, tracking pattern is the same as that shown in Figure 6.11 of sliding mode control except larger tracking errors given by the cascade control. Both reference tracking results suggests that sliding mode control performs better than cascade control in the case of tracking without friction compensation.

In the third set of simulation test, friction compensation is introduced to the cascade control. In Figure 6.20, significant reduction of tracking errors in the position plot is observed. Due to the friction, the pressure differential appears in the pressure plot of Figure 6.21. The additional actuation force created by the pressure differential is used to counteract the friction force (see friction plot in Figure 6.21). With reference to Figure 6.22, the tracking error for sinusoidal reference tracking also has significant reduction due to the addition of friction compensation, and control signal plot shows that control signal is very smooth for sinusoidal reference tracking.

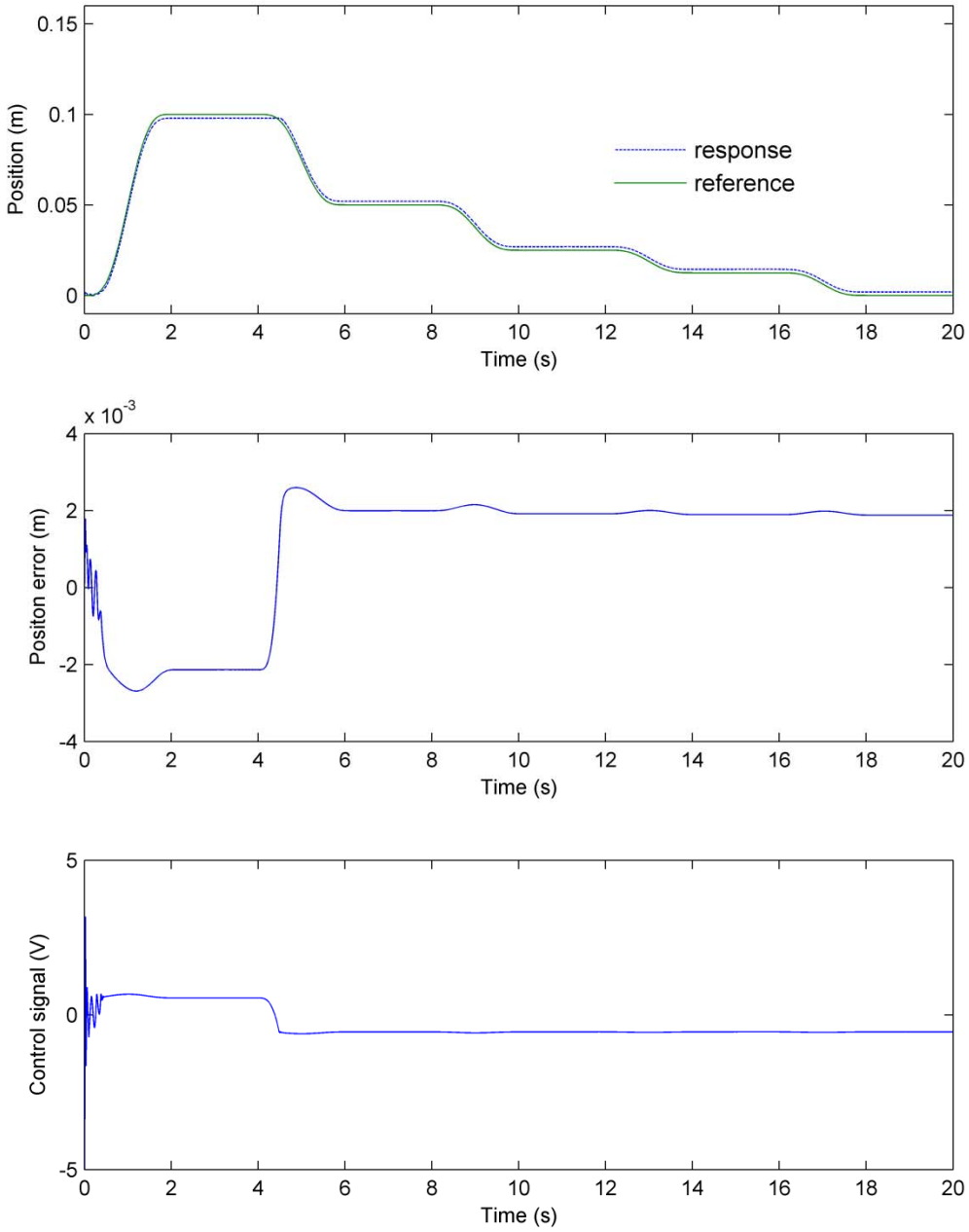

Figure 6.15 Simulated ramp trajectory for cascade control responses with the assumption of no friction in the servo pneumatic actuator.

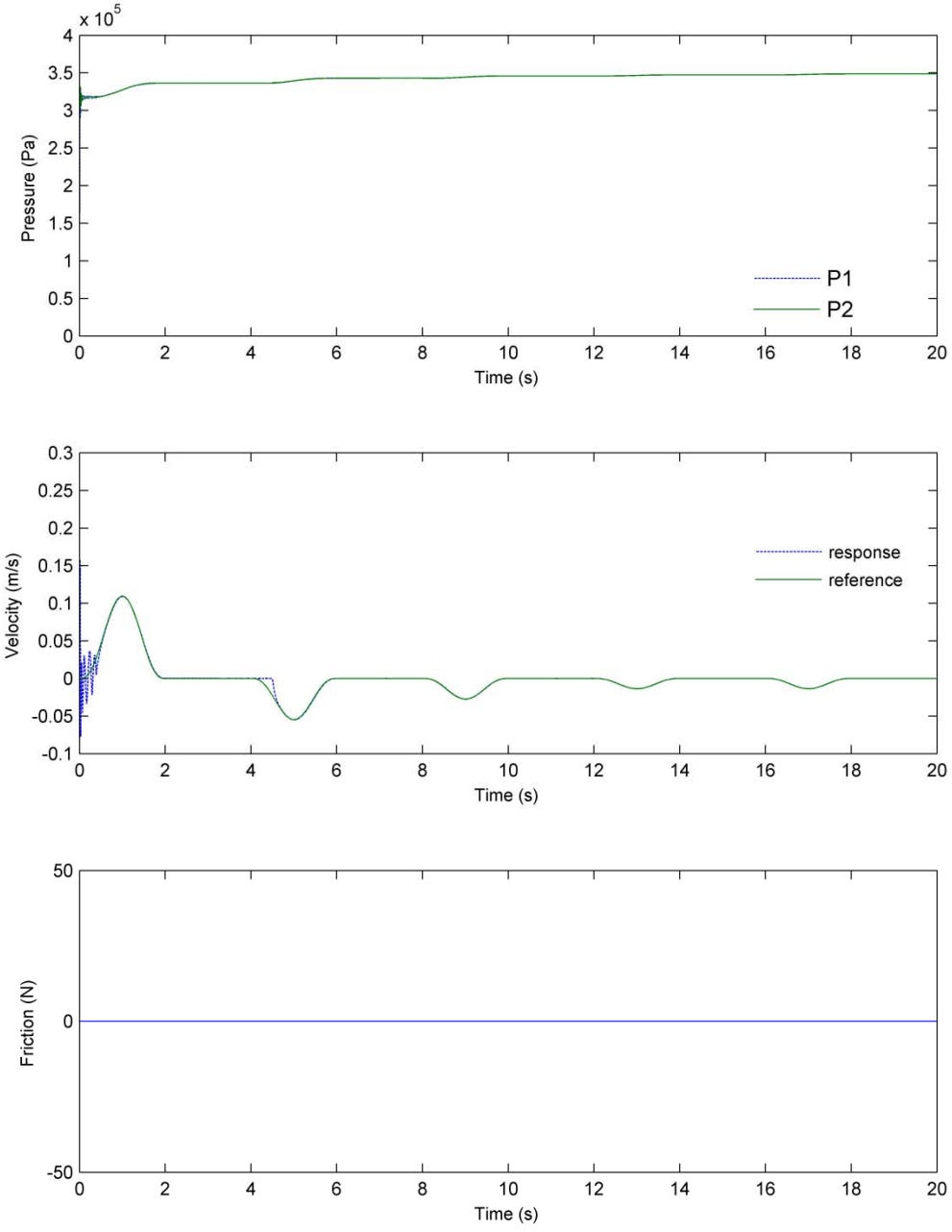

Figure 6.16 Simulated ramp trajectory for cascade control responses with the assumption of no friction in the servo pneumatic actuator (continued).

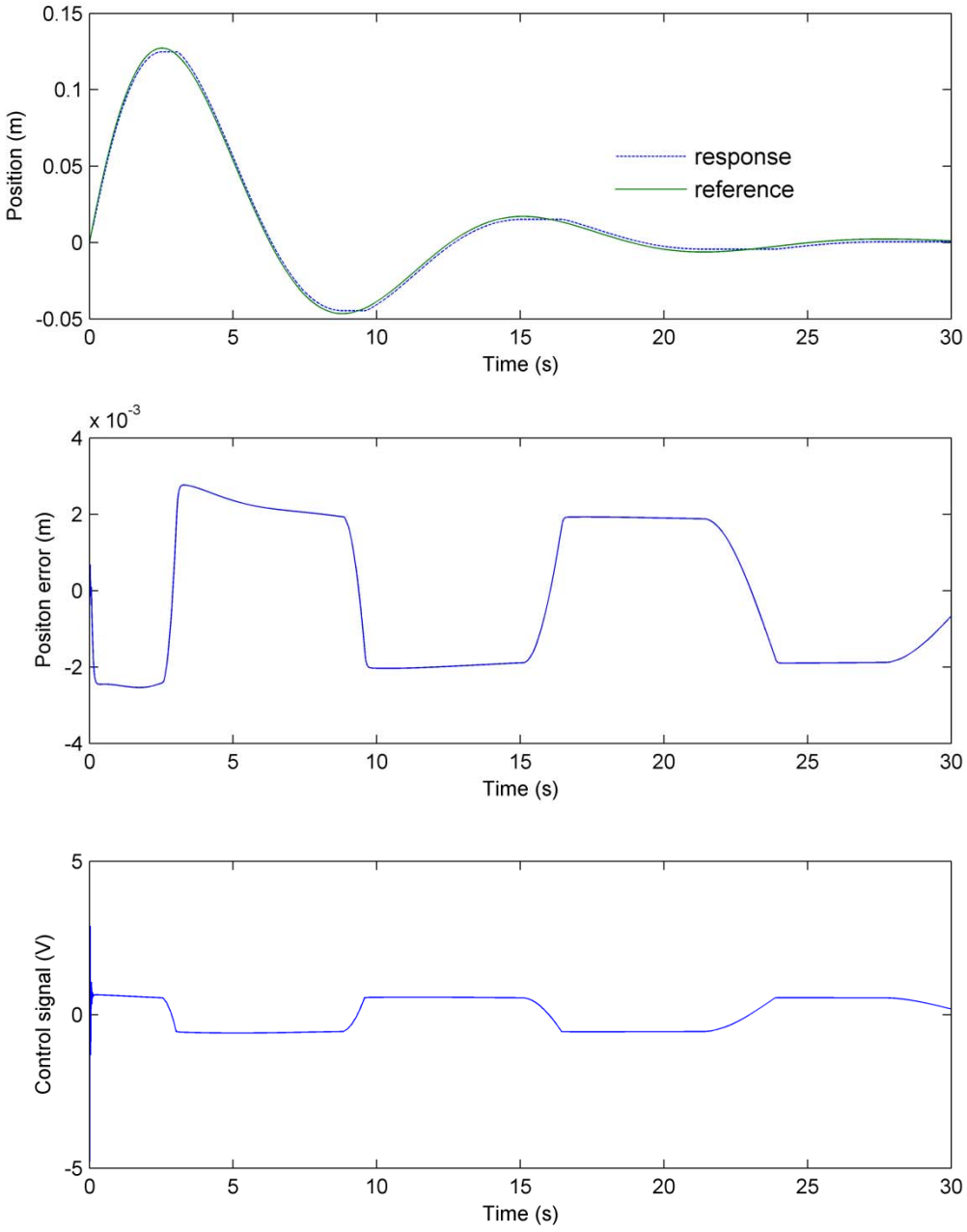

Figure 6.17 Simulated decreasing sine trajectory for cascade control responses with the assumption of no friction in the servo pneumatic actuator.

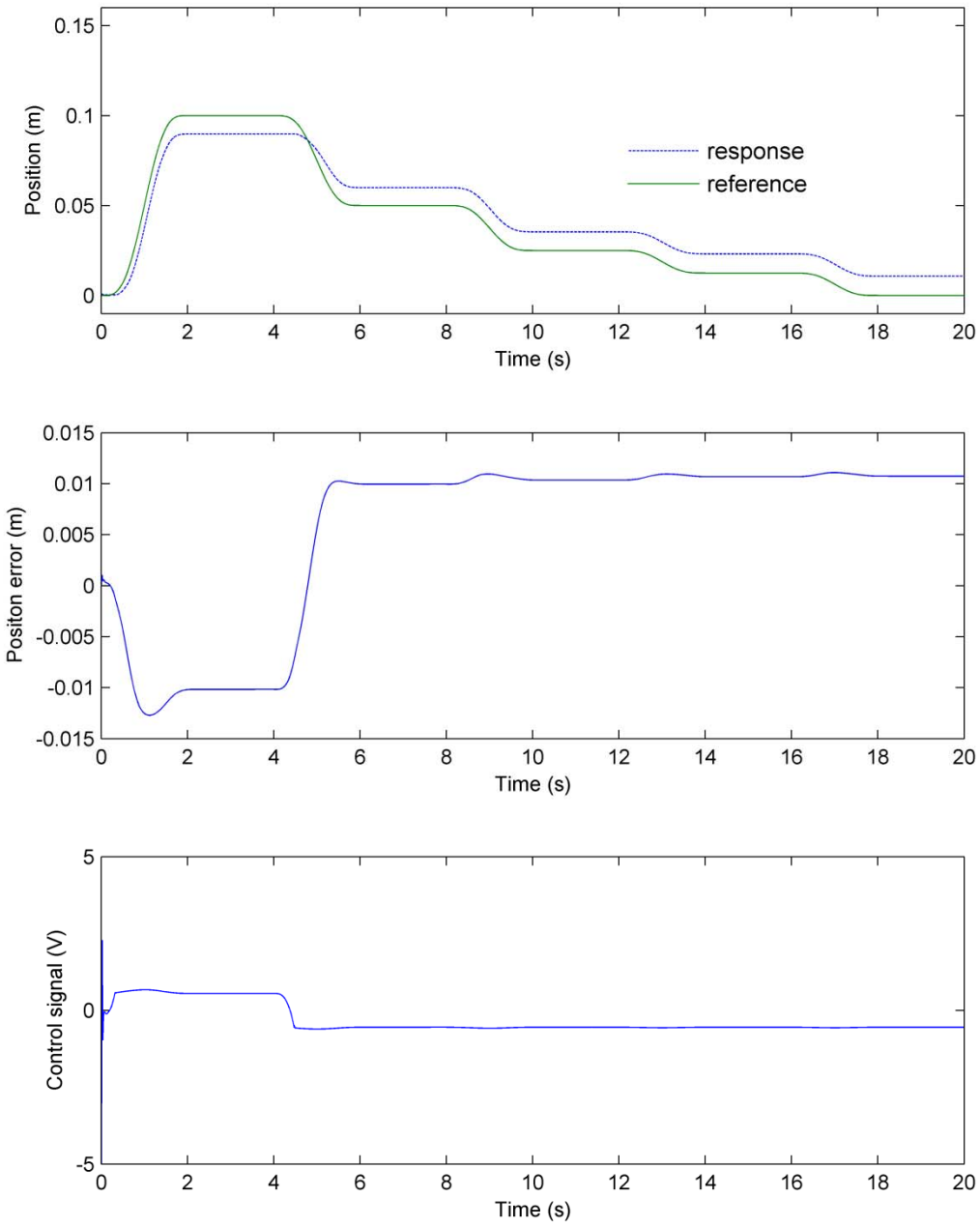

Figure 6.18 Simulated ramp trajectory for cascade control responses without friction compensation in the servo pneumatic actuator with friction.

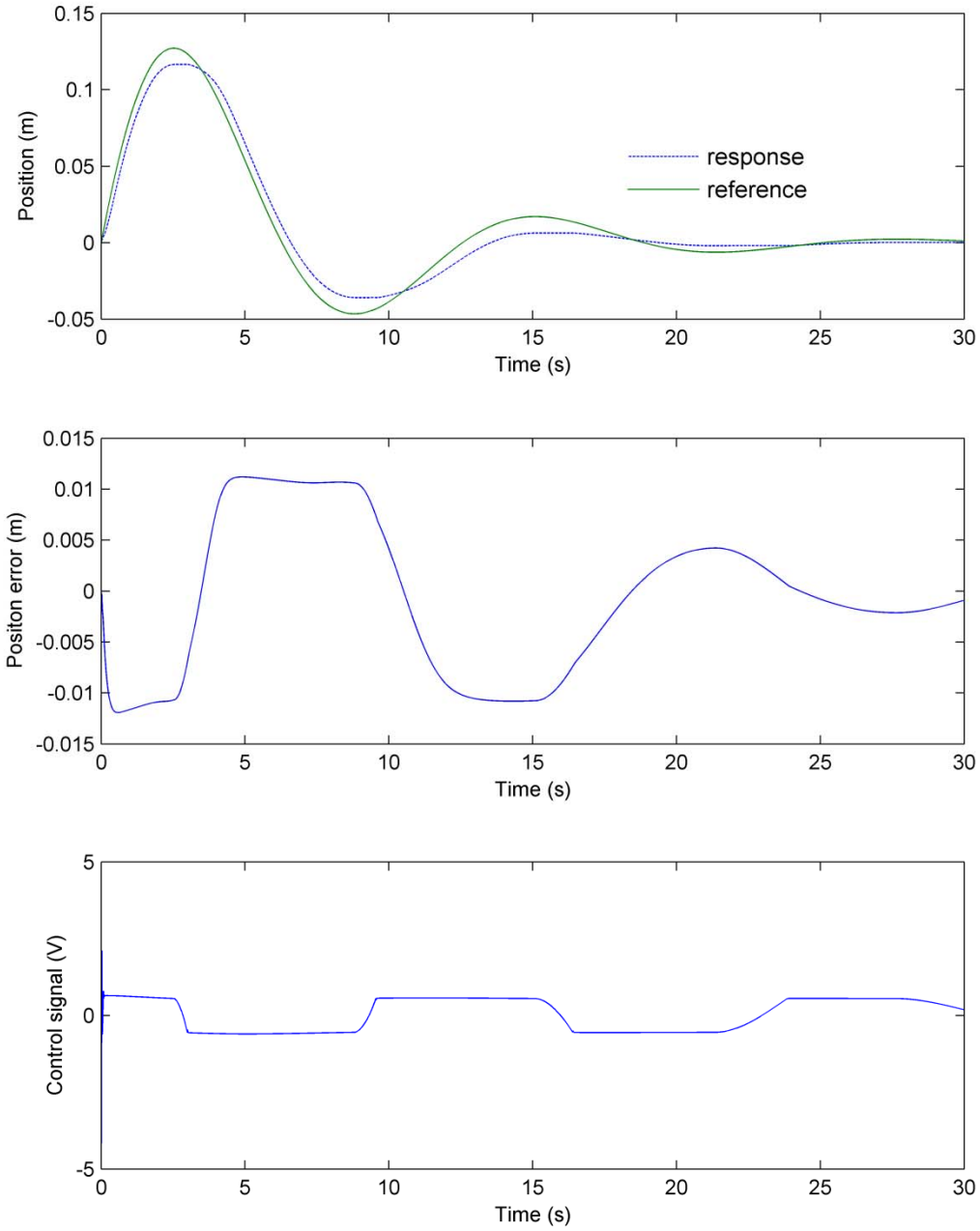

Figure 6.19 Simulated decreasing sine trajectory for cascade control responses without friction compensation in the servo pneumatic actuator with friction.

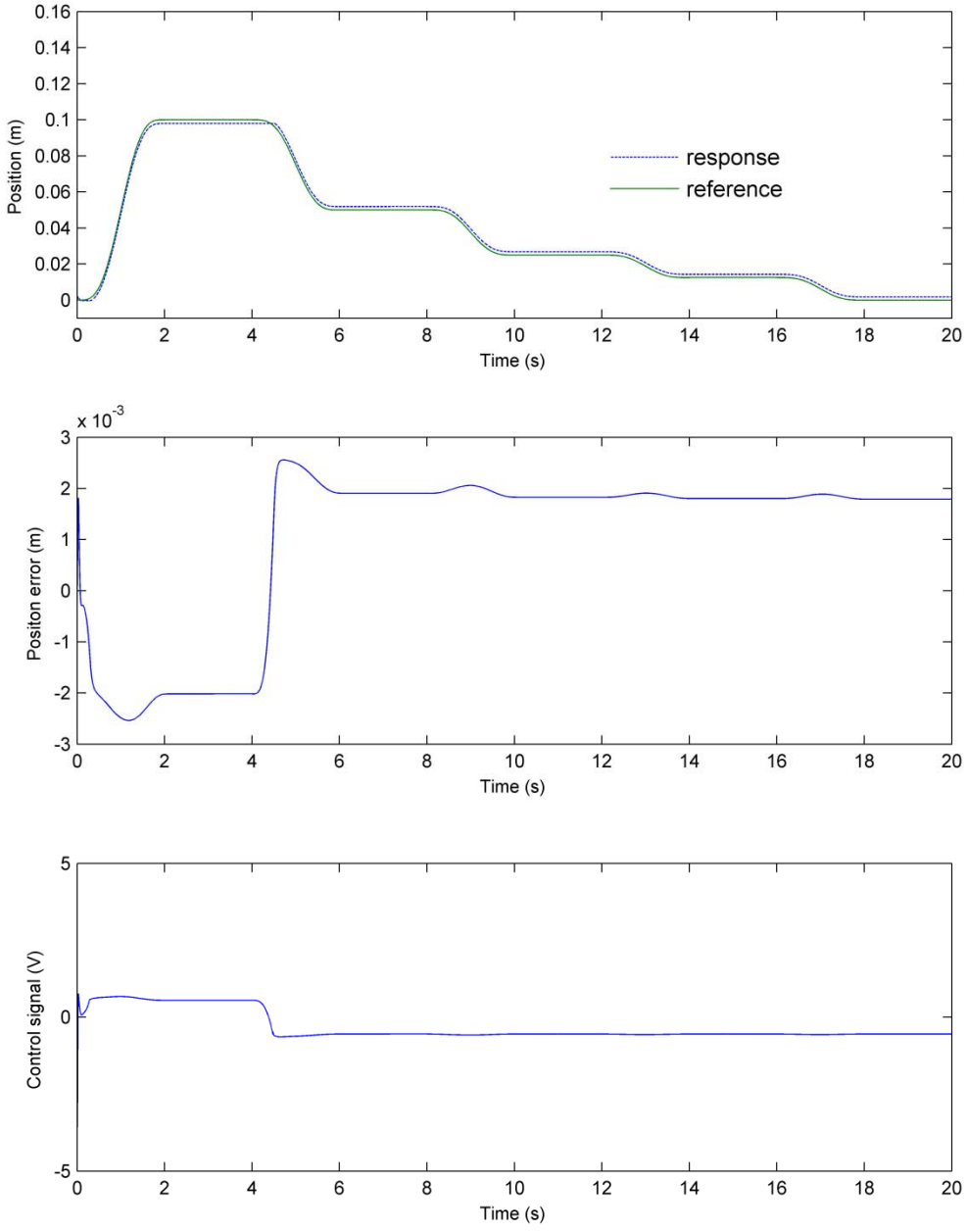

Figure 6.20 Simulated ramp trajectory for cascade control responses with friction compensation in the servo pneumatic actuator with friction.

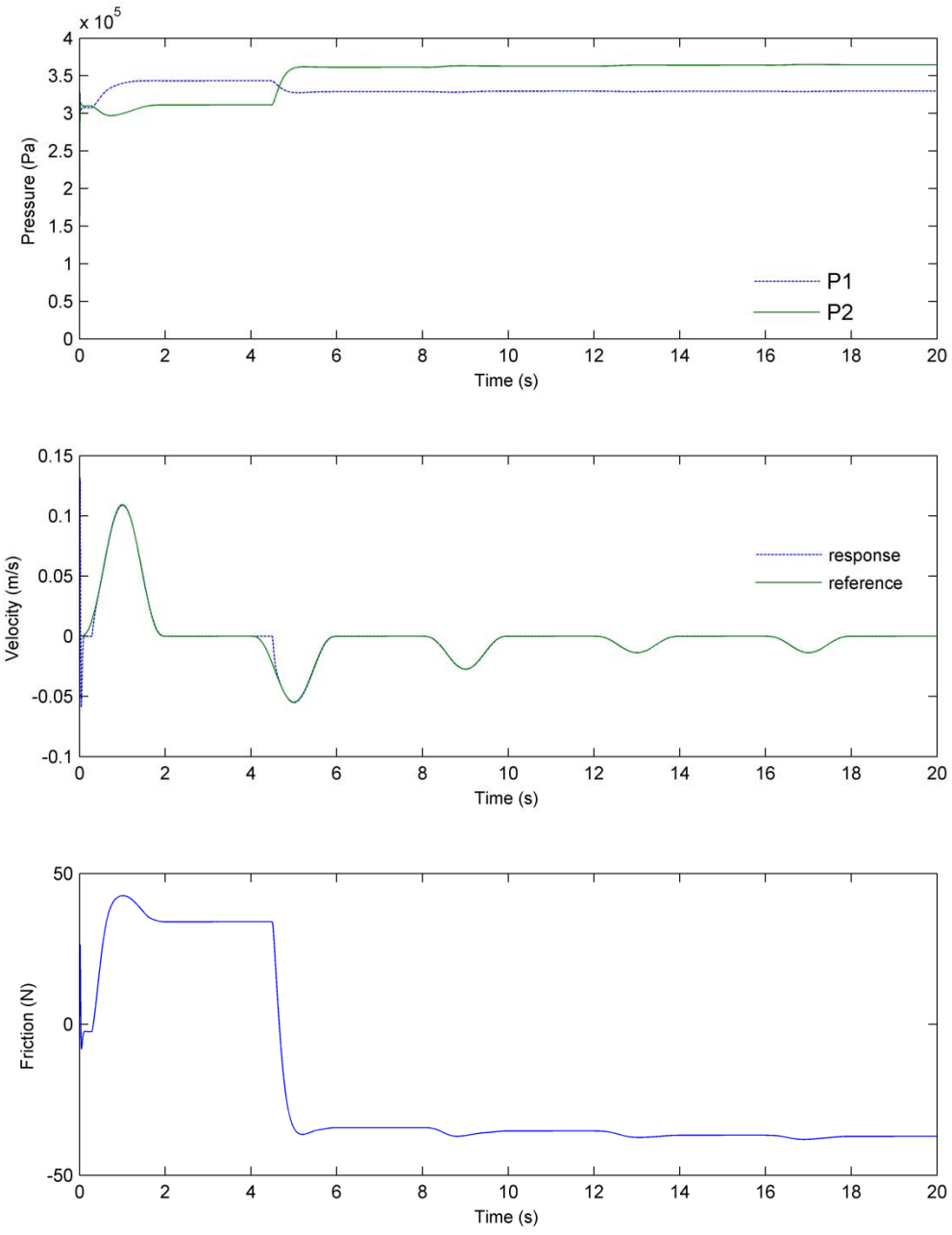

Figure 6.21 Simulated ramp trajectory for cascade control responses with friction compensation in the servo pneumatic actuator with friction (continued).

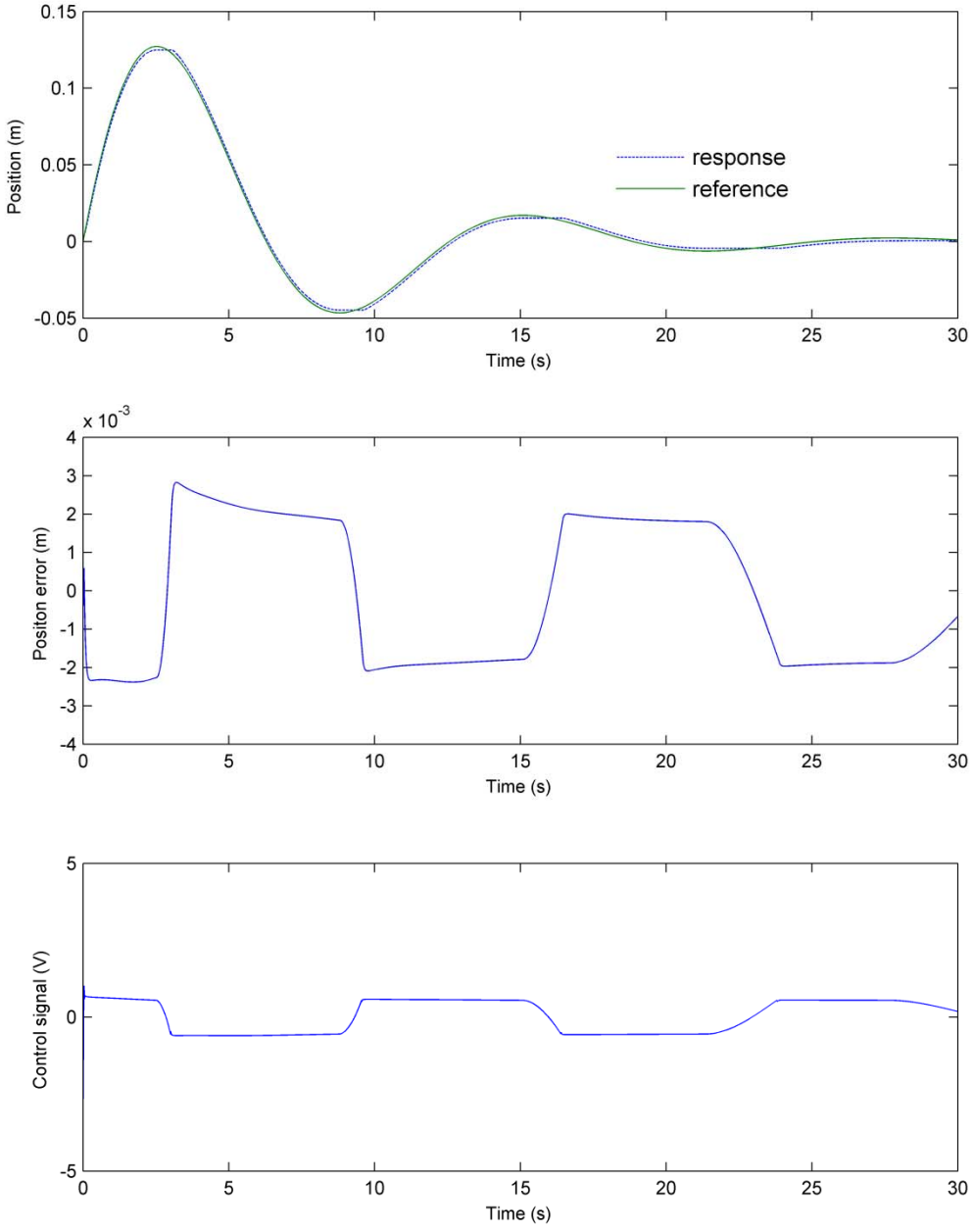

Figure 6.22 Simulated decreasing sine trajectory for cascade control responses with friction compensation in the servo pneumatic actuator with friction.

The same sets of reference tracking test are performed on the backstepping control. The first set of test considers no friction in the pneumatic actuator model. In Figure 6.23 and Figure 6.24, the tracking pattern under backstepping control looks more similar to that of cascade control. This is due to the fact that both control algorithms use pressure differential error to construct the Lyapunov function. The similar tracking pattern also appears in the sinusoidal reference tracking for backstepping control and cascade control in Figure 6.25 and Figure 6.17, respectively.

In the second set of test, friction is introduced to the model. In Figure 6.26, the ramp reference tracking pattern of backstepping control appears more similar to that of cascade control; however, the backstepping controller produces larger tracking errors than those of cascade controller. This suggests that the partial sliding mode control algorithm in the cascade controller helps the controller to perform better than the pure Lyapunov-based backstepping controller when the friction compensation is not considered. This assertion is confirmed from the position error plot of sinusoidal reference tracking in Figure 6.27.

The third set of test examines the performance of backstepping controller that includes the friction compensation. In Figure 6.28, the ramp reference tracking errors are restored almost back to those when the model does not include friction (see Figure 6.23). Meanwhile, the initial oscillation is removed completely due the damping effect created by the viscous friction. With respect to Figure 6.29, the pressure differential in the pressure plot suggests that the additional actuation force is created to counteract the friction, which exists throughout the ramp reference tracking. With reference to Figure 6.30, the sinusoidal reference tracking shows satisfactory performance through a smooth control signal.

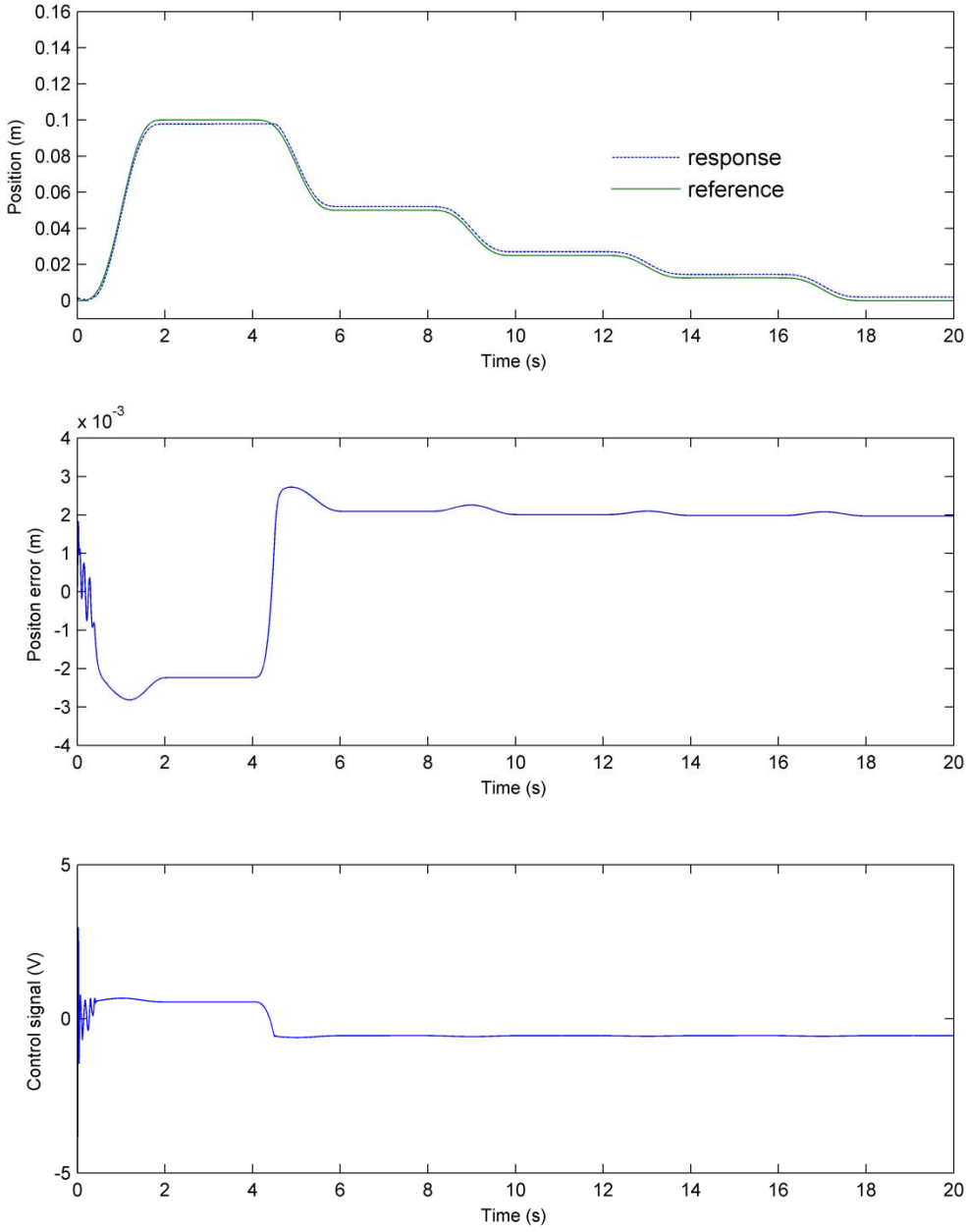

Figure 6.23 Simulated ramp trajectory for backstepping control responses with the assumption of no friction in the servo pneumatic actuator.

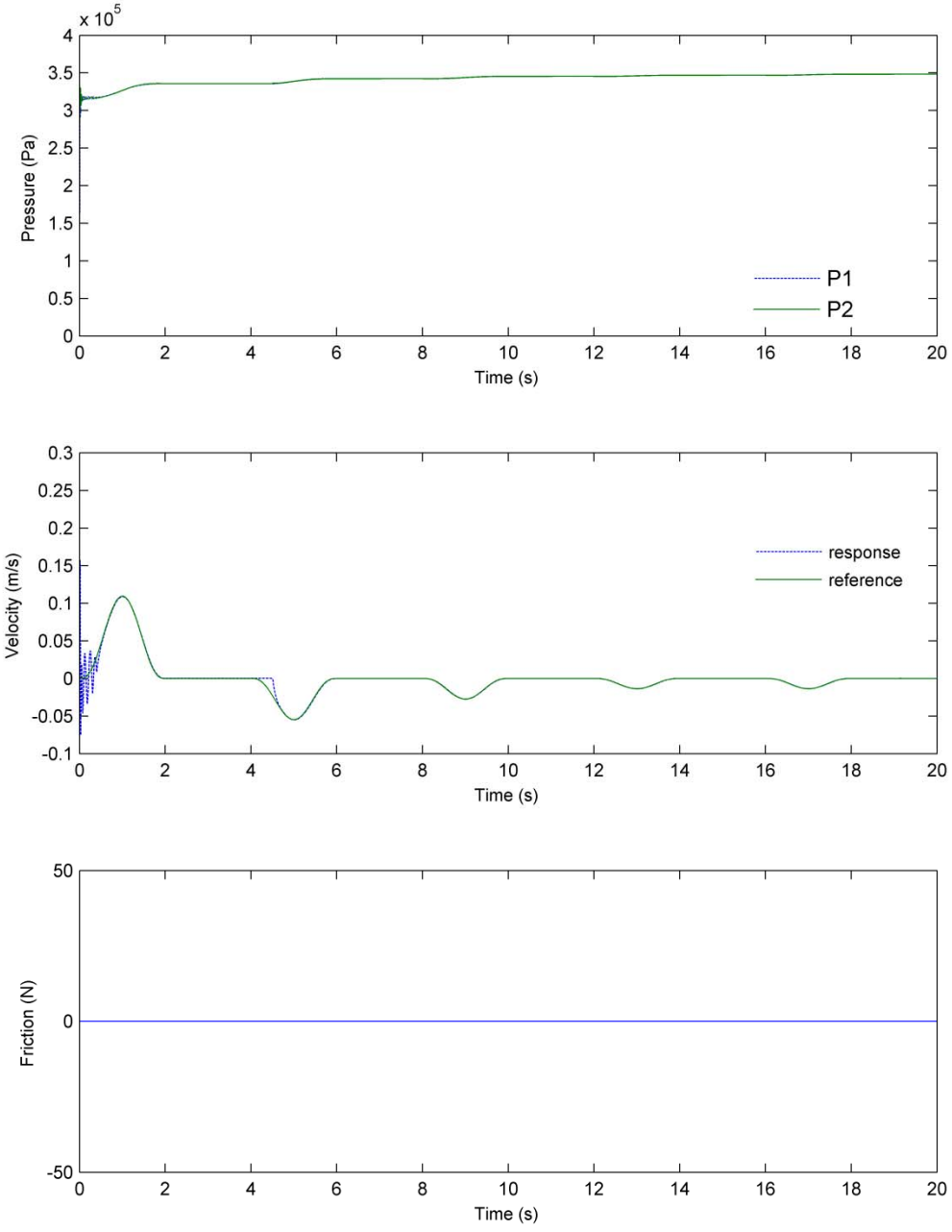

Figure 6.24 Simulated ramp trajectory for backstepping control responses with the assumption of no friction in the servo pneumatic actuator (continued).

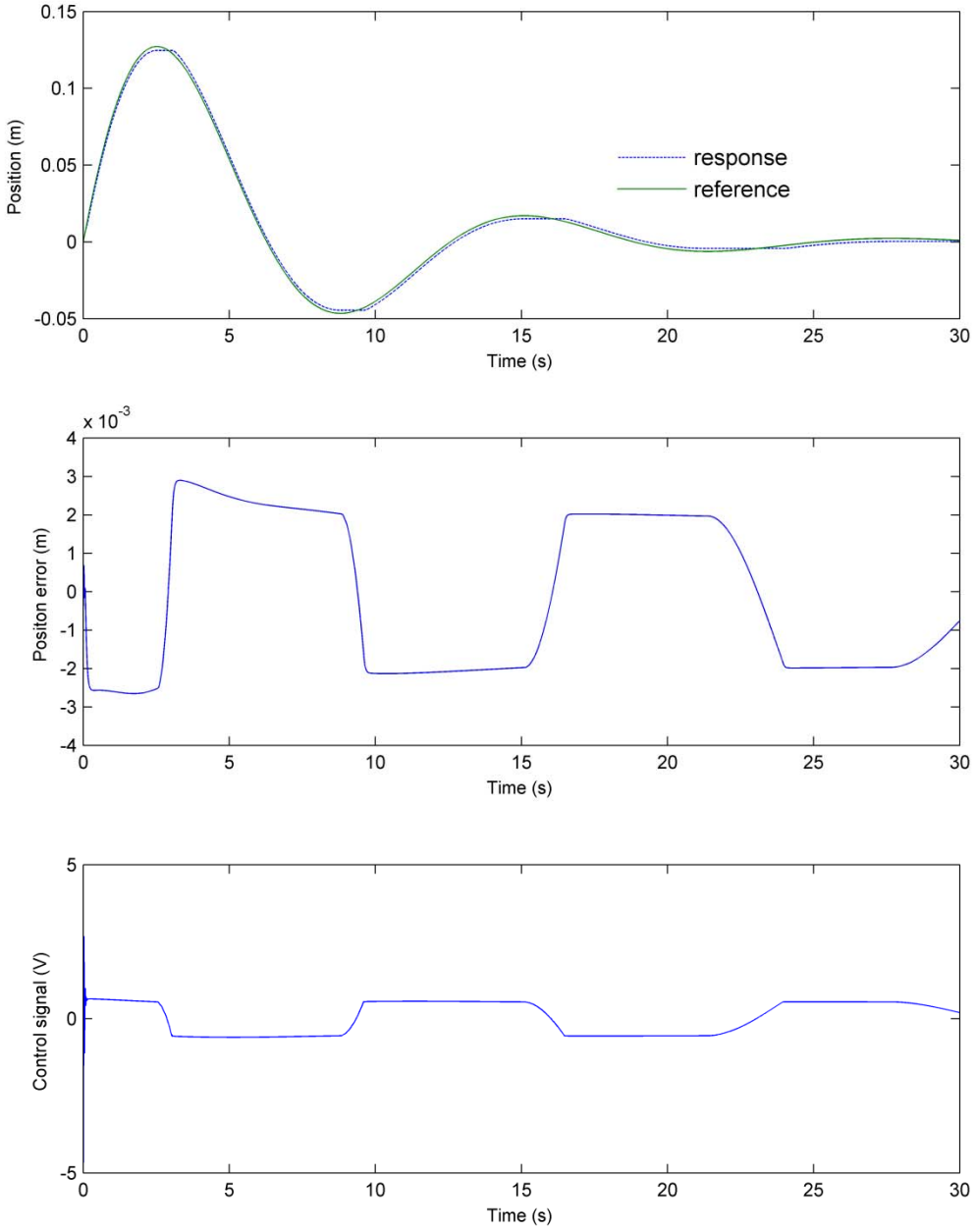

Figure 6.25 Simulated decreasing sine trajectory for backstepping control responses with the assumption of no friction in the servo pneumatic actuator.

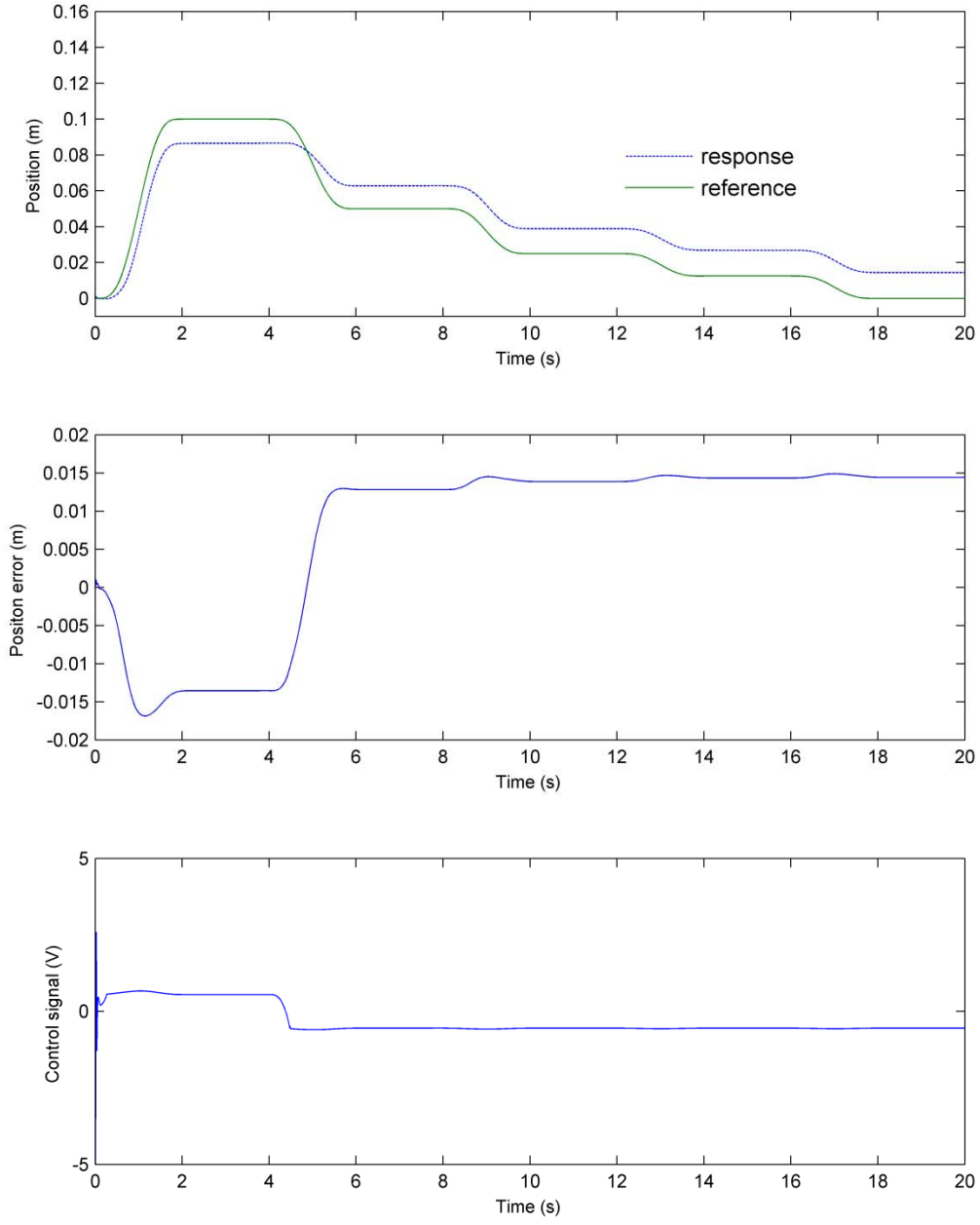

Figure 6.26 Simulated ramp trajectory for backstepping control responses without friction compensation in the servo pneumatic actuator with friction.

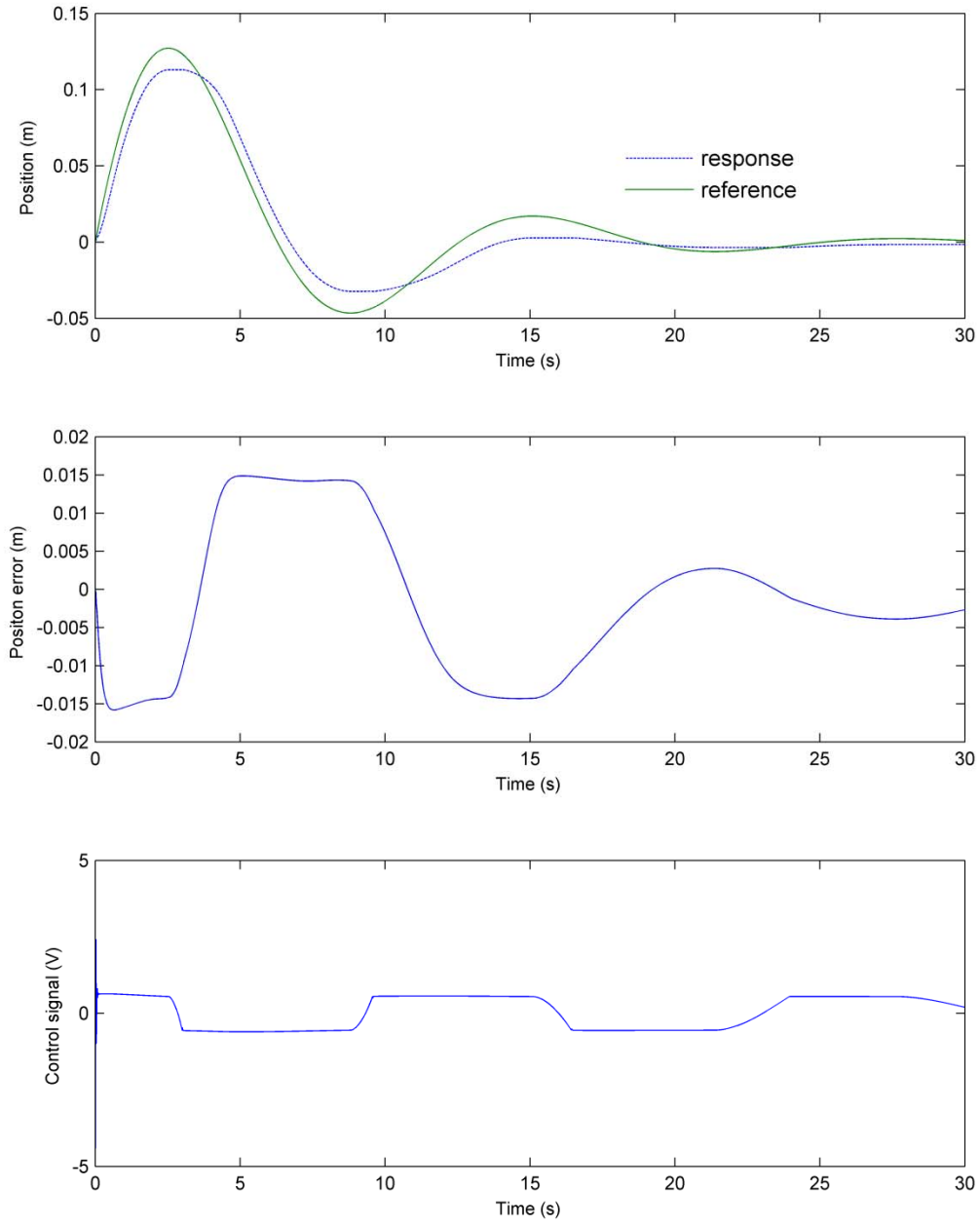

Figure 6.27 Simulated decreasing sine trajectory for backstepping control responses without friction compensation in the servo pneumatic actuator with friction.

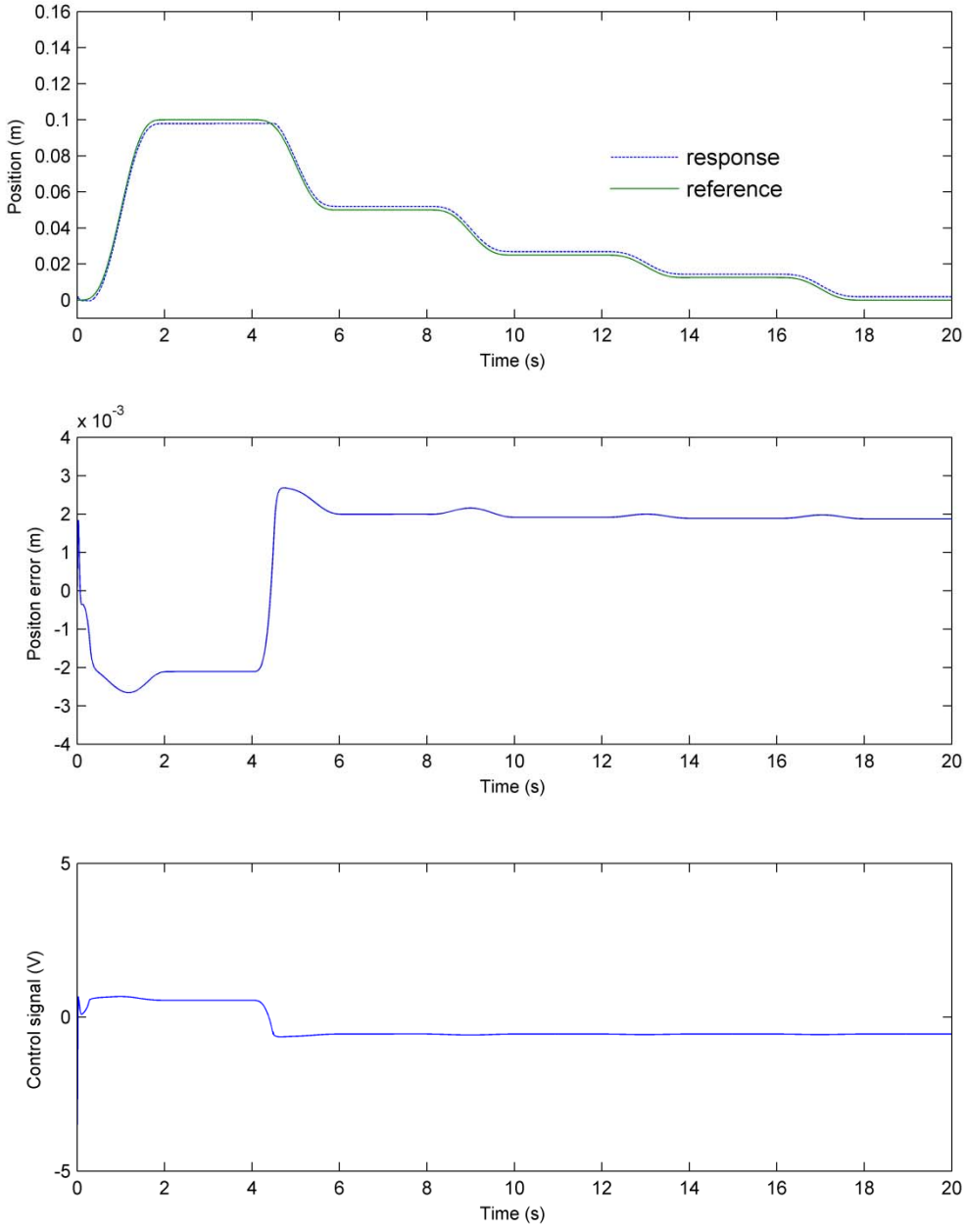

Figure 6.28 Simulated ramp trajectory for backstepping control responses with friction compensation in the servo pneumatic actuator with friction.

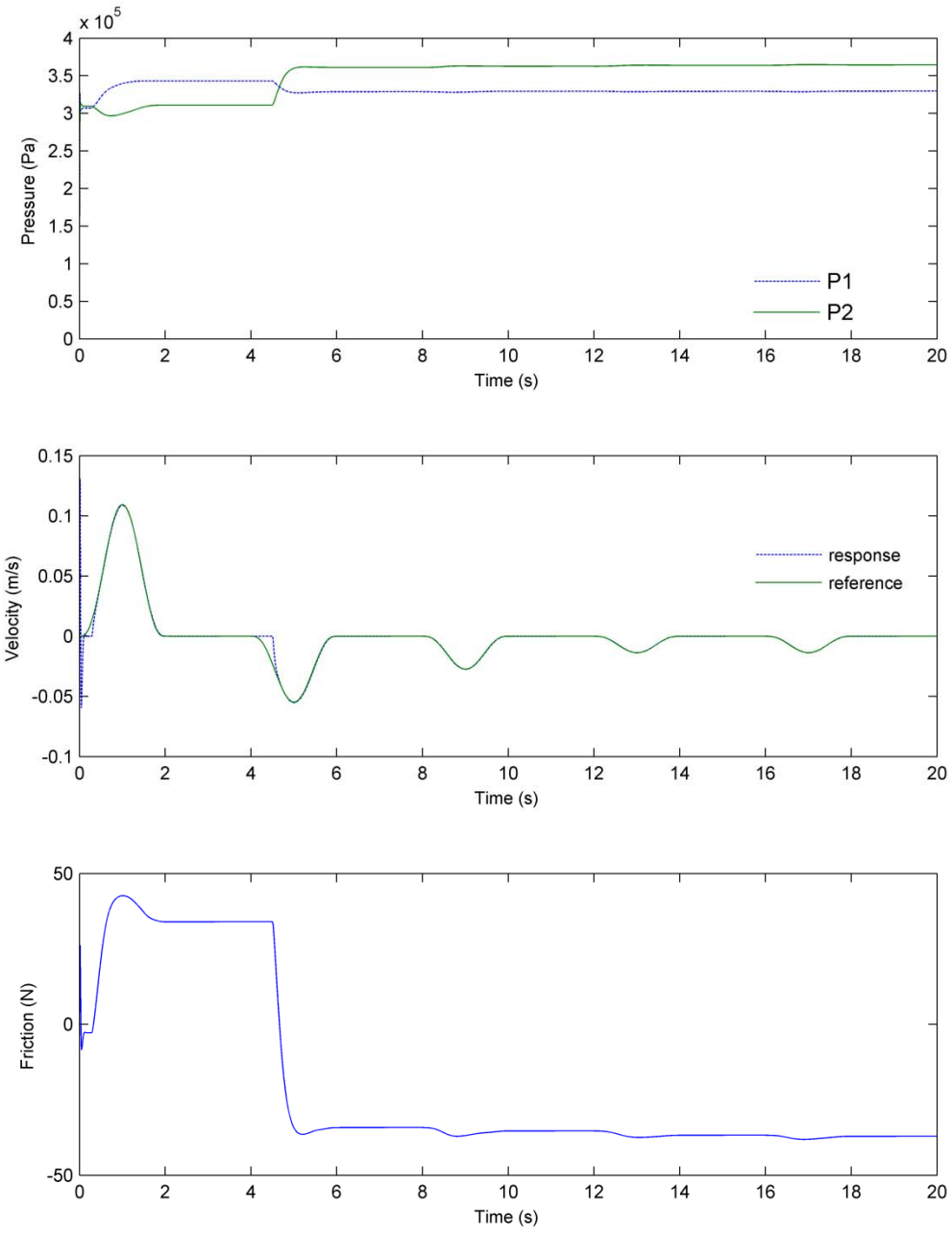

Figure 6.29 Simulated ramp trajectory for backstepping control responses with friction compensation in the servo pneumatic actuator with friction (continued).

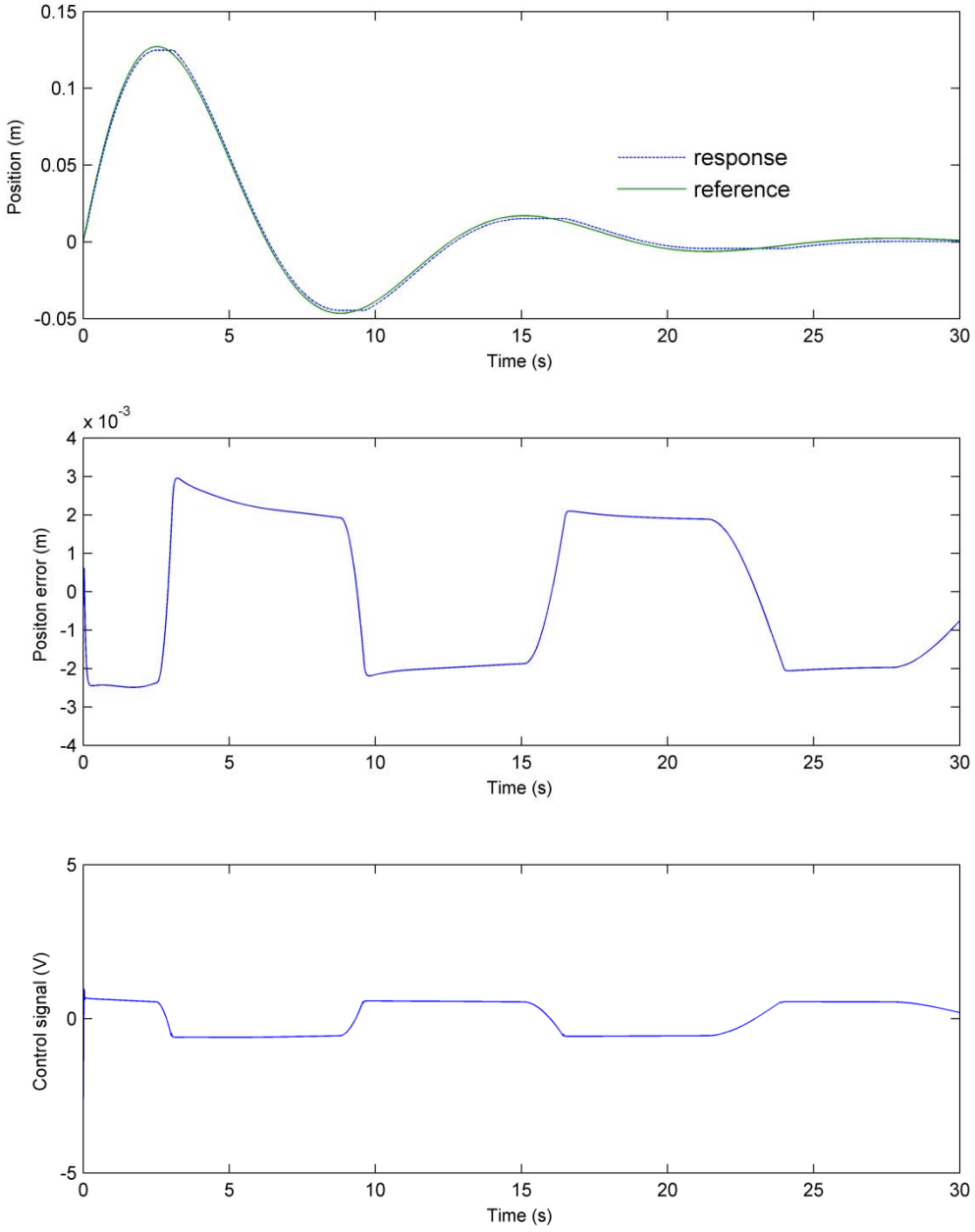

Figure 6.30 Simulated decreasing sine trajectory for backstepping control responses with friction compensation in the servo pneumatic actuator with friction.

6.3 Dynamical Adaptive Backstepping-Sliding Mode Controller Simulation

The newly developed DAB-SMC is tested in simulation in this section to give satisfactory tracking for the given reference trajectories. With reference to the control law and adaptive law given in equation (5.131) through (5.134), control gains associated with sliding mode, adaptive law, and acceleration observer are set to zero. The only control gains that are turned on and tuned at this stage are k_1, k_2, and k_3.In Figure 6.31, the tracking errors have some initial oscillations as those shown in the backstepping controller; afterward, the actuator system is able to track the reference in a stable manner. The control signal in Figure 6.31 also shows reduced control efforts after the initial oscillation. With respect to Figure 6.32, the pressures in the two actuator chambers become close to each other due to the fact that friction is not included in the system model. This pressure differential creates the only force acting on the piston to influence the motion of the actuator. The velocity plot in Figure 6.32 confirms that controller initially takes more efforts to force the system velocity to track the reference velocity. With respect to Figure 6.33, the controller takes fewer efforts to track the sinusoidal reference trajectory than ramp reference trajectory, and the tracking error has the tendency to reduce as the amplitude of the sinusoidal reference signal reduces.

As friction is added to the simulation, the system responses for DAB-SMC controller without the activation of friction adaptive law show significant large steady state tracking errors similar to those of the backstepping controller without friction compensation. With reference to Figure 6.34, despite the large steady state tracking error, the initial oscillation in the system response is reduced significantly due to the damping effect created by the viscous friction, and the controller takes fewer efforts to reach the steady state tracking. With respect to Figure 6.35, pressure differential of the two chambers is shown in the pressure plots, and the actuator force created from the pressure differential is used to counteract the friction created during the tracking. The friction plot in Figure 6.35 confirms that the friction exists all the time during the reference tracking. With reference to Figure 6.36, large tracking error has also shown in the position error plot for the sinusoidal reference tracking, and the position error has the tendency to become smaller as the amplitude of the sinusoidal reference trajectory reduces.

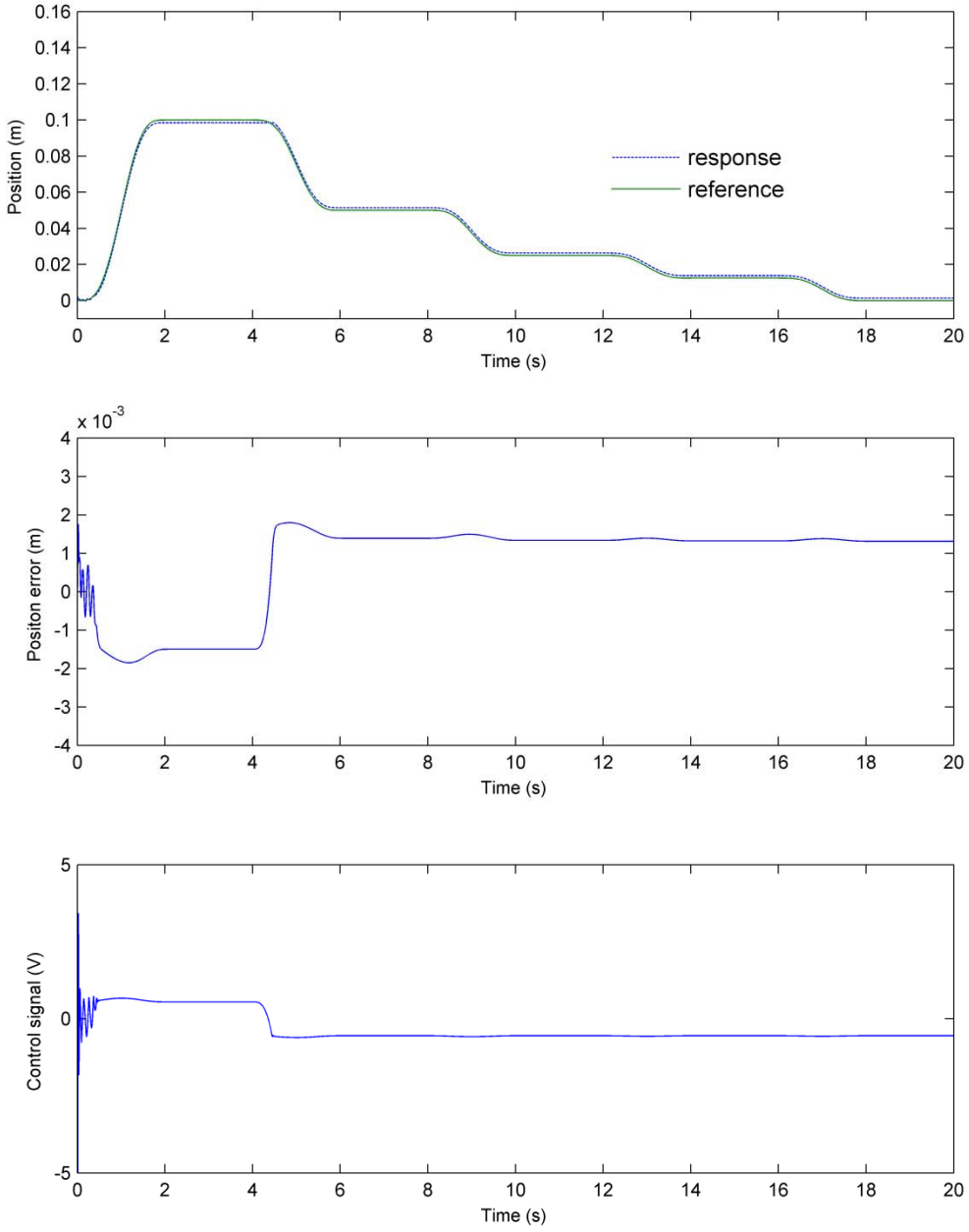

Figure 6.31 Simulated ramp trajectory for dynamical adaptive backstepping-sliding mode control responses with the assumption of no friction in the servo pneumatic actuator.

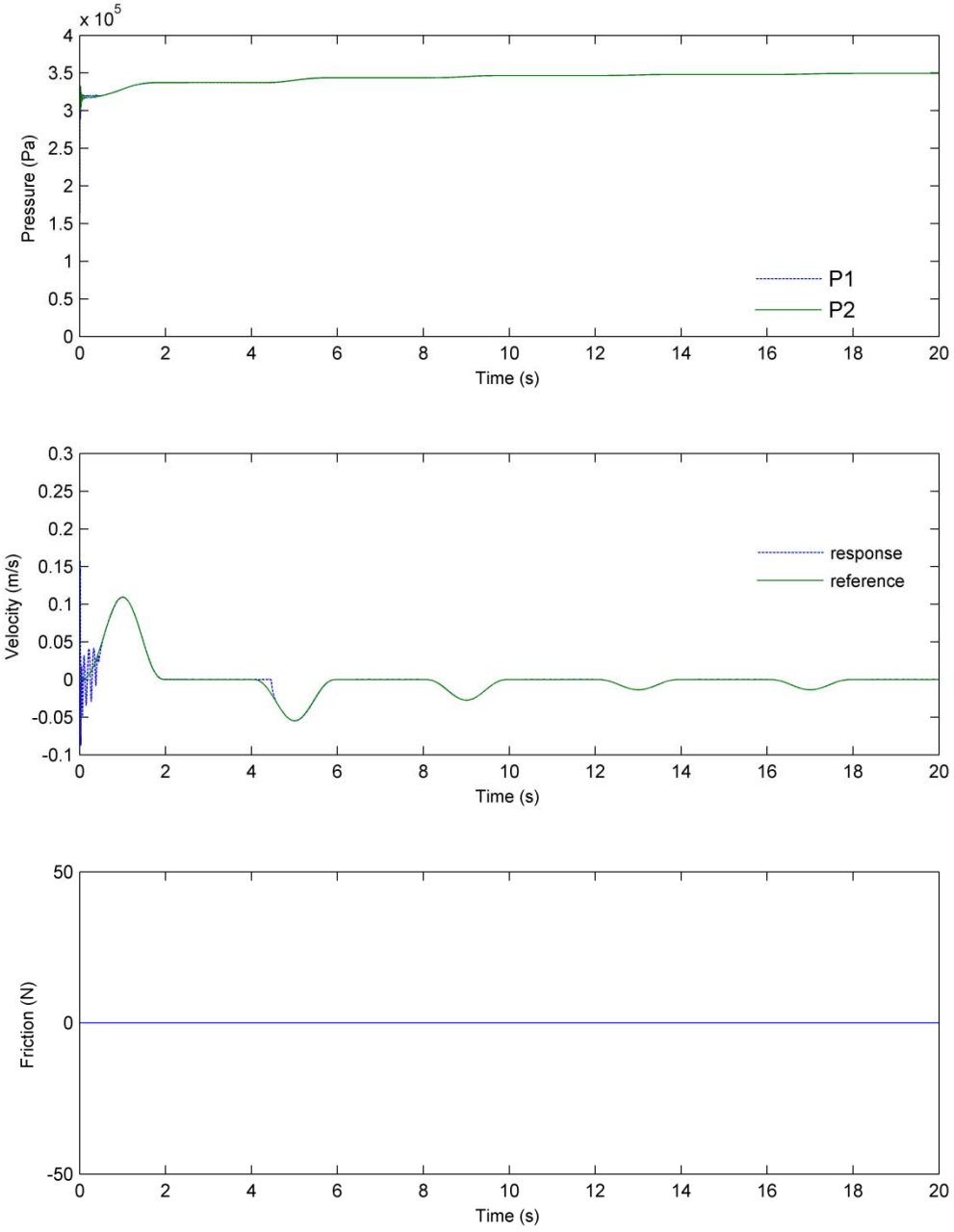

Figure 6.32 Simulated ramp trajectory for dynamical adaptive backstepping-sliding mode control responses with the assumption of no friction in the servo pneumatic actuator (continued).

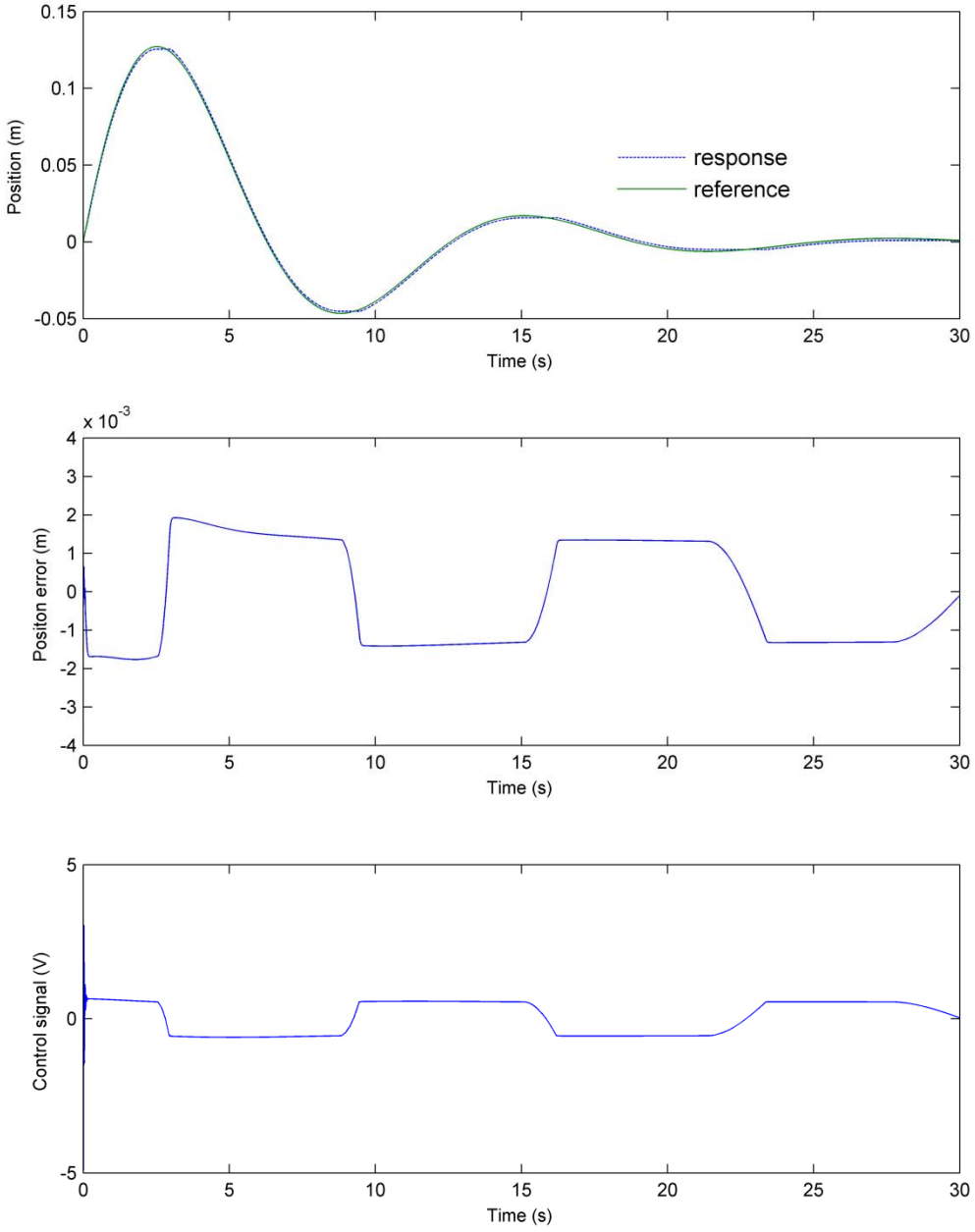

Figure 6.33 Simulated decreasing sine trajectory for dynamical adaptive backstepping-sliding mode control responses with the assumption of no friction in the servo pneumatic actuator.

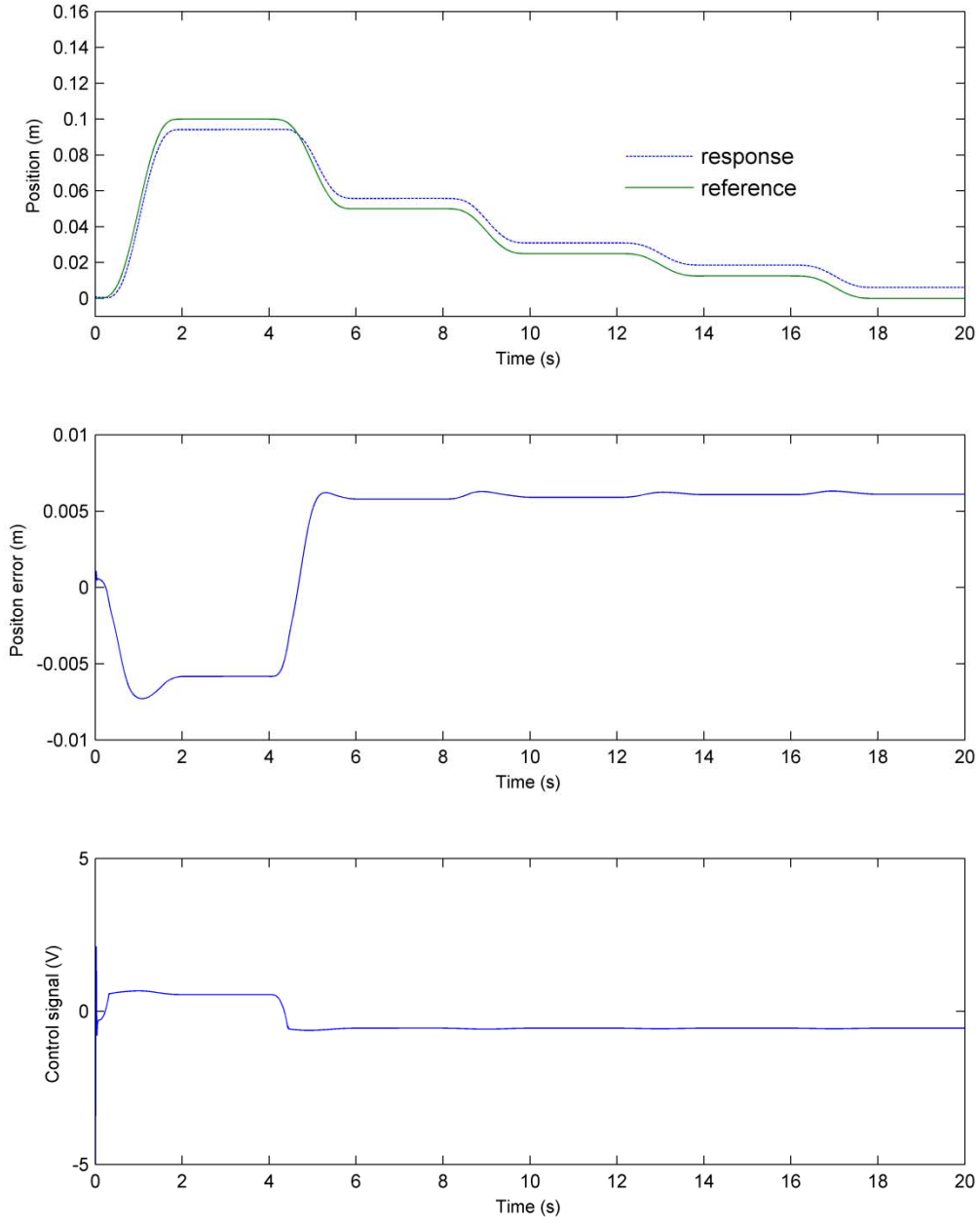

Figure 6.34 Simulated ramp trajectory for dynamical adaptive backstepping-sliding mode control responses without friction compensation in the servo pneumatic actuator with friction.

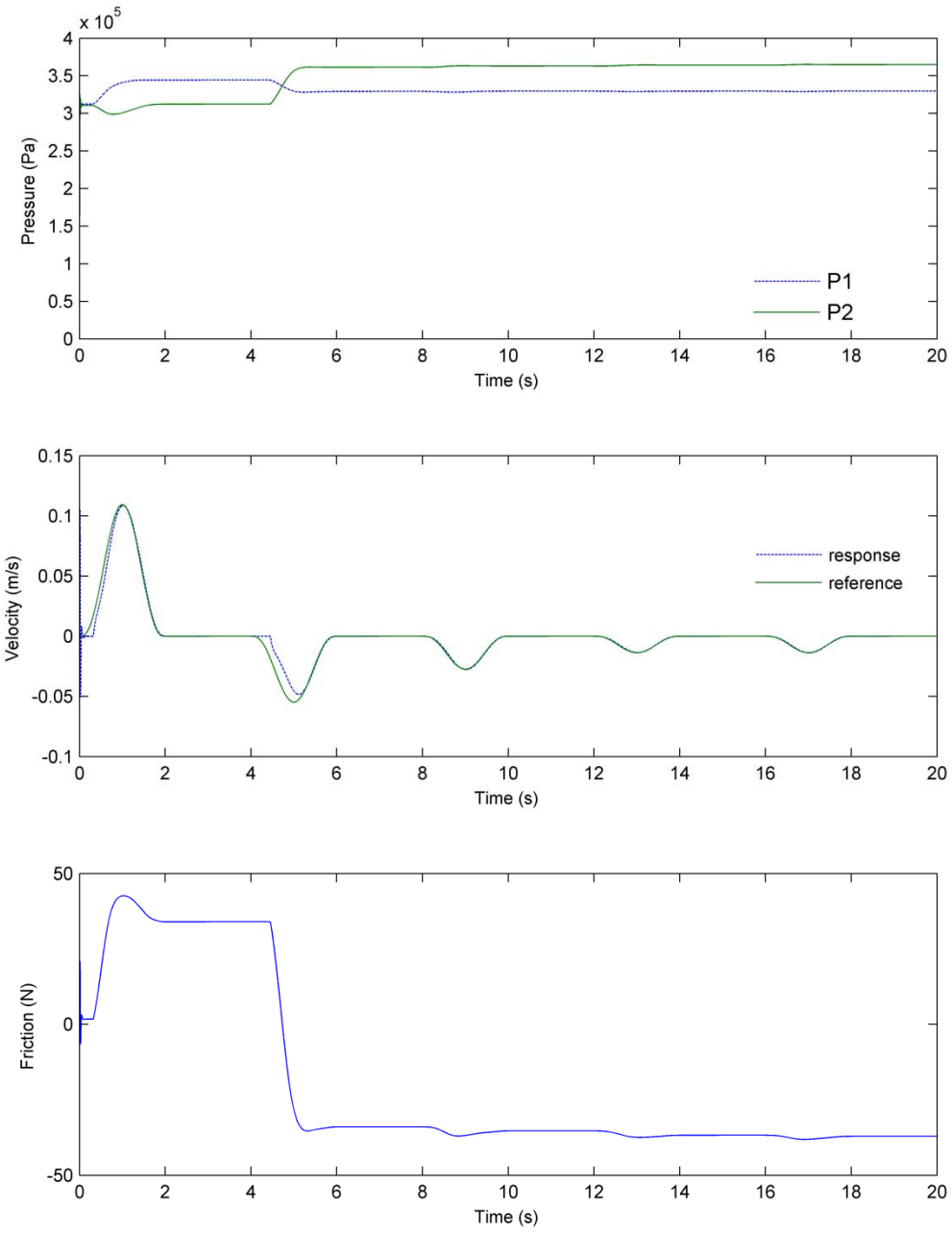

Figure 6.35 Simulated ramp trajectory for dynamical adaptive backstepping-sliding mode control responses without friction compensation in the servo pneumatic actuator with friction (continued).

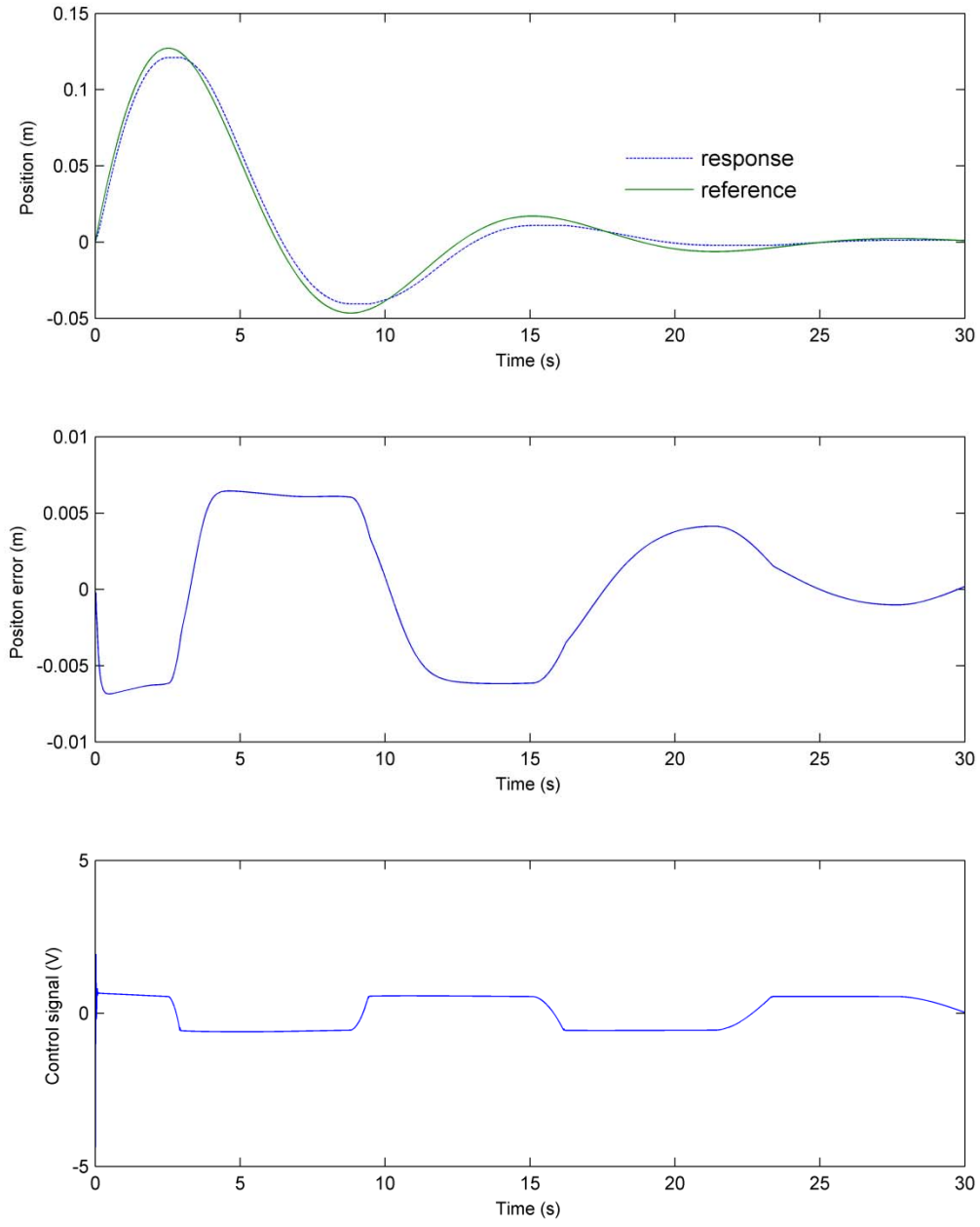

Figure 6.36 Simulated decreasing sine trajectory for dynamical adaptive backstepping-sliding mode control responses without friction compensation in the servo pneumatic actuator with friction.

At this stage, the backstepping control gains in DAB-SMC controller are kept the same as the previous test, and the gains γ_1 , γ_2, and γ_3 in friction adaptive law is activated to compensate for the friction. With reference to Figure 6.37, there is significant reduction in the system tracking error as shown in the position error plot; this is due to the fact that friction is estimated on-line through the dynamical adaptive laws, and these laws are constructed in such a way that they further reduces the tracking errors. In Figure 6.38, the simulated friction and estimated friction are compared, and the friction estimation plot shows that the estimate error of friction is in the range of -15 N to +15 N. With respect to Figure 6.39, the performance of sinusoidal reference tracking in the position plot is satisfactory; however, position error plot shows significant oscillation during the initial tracking, and this is due to the fact that the adaptive laws take efforts to adapt the friction initially. The position error plot frequently shows peaks, which occur when the actuator changes direction of motion, and this is due to the fact that the adaptive law re-adapts to the friction when the friction changes its direction. In Figure 6.40, the comparison of simulated and estimated friction confirms that the oscillations in the tracking errors are due to initial friction adaptation.

Finally, gains Γ_1 and Γ_2 associated with the sliding surface and the control gain Γ_3 for the acceleration observer are turned on and tuned to replace the acceleration feedback. With reference to the simulation results of ramp reference tracking in Figure 6.41, one of the significant contributions of the acceleration observer to the DAB-SMC controller is the reduction the maximum position error. The acceleration observer is a by-product of the sliding mode control algorithm in the DAB-SMC controller, and the acceleration estimate is constructed such that it is forced onto the sliding surface. The acceleration estimate utilizes the friction estimation given by the friction adaptive law and assumes that the friction estimate converges to the simulated friction. In Figure 6.42, the acceleration estimate shows large estimation errors; this is due to the fact that the friction estimate, which is used to produce the acceleration estimate, does not estimate the simulated friction perfectly (see Figure 6.38). With respect to simulation results of sinusoidal reference tracking in Figure 6.43, significant reduction in the maximum tracking error is observed in the position error plot after the introduction of the acceleration observer to the controller. With reference to Figure 6.44, the explanation used to explain the large

acceleration estimate errors in ramp reference tracking can be reused to explain the large acceleration estimate errors in the sinusoidal reference tracking.

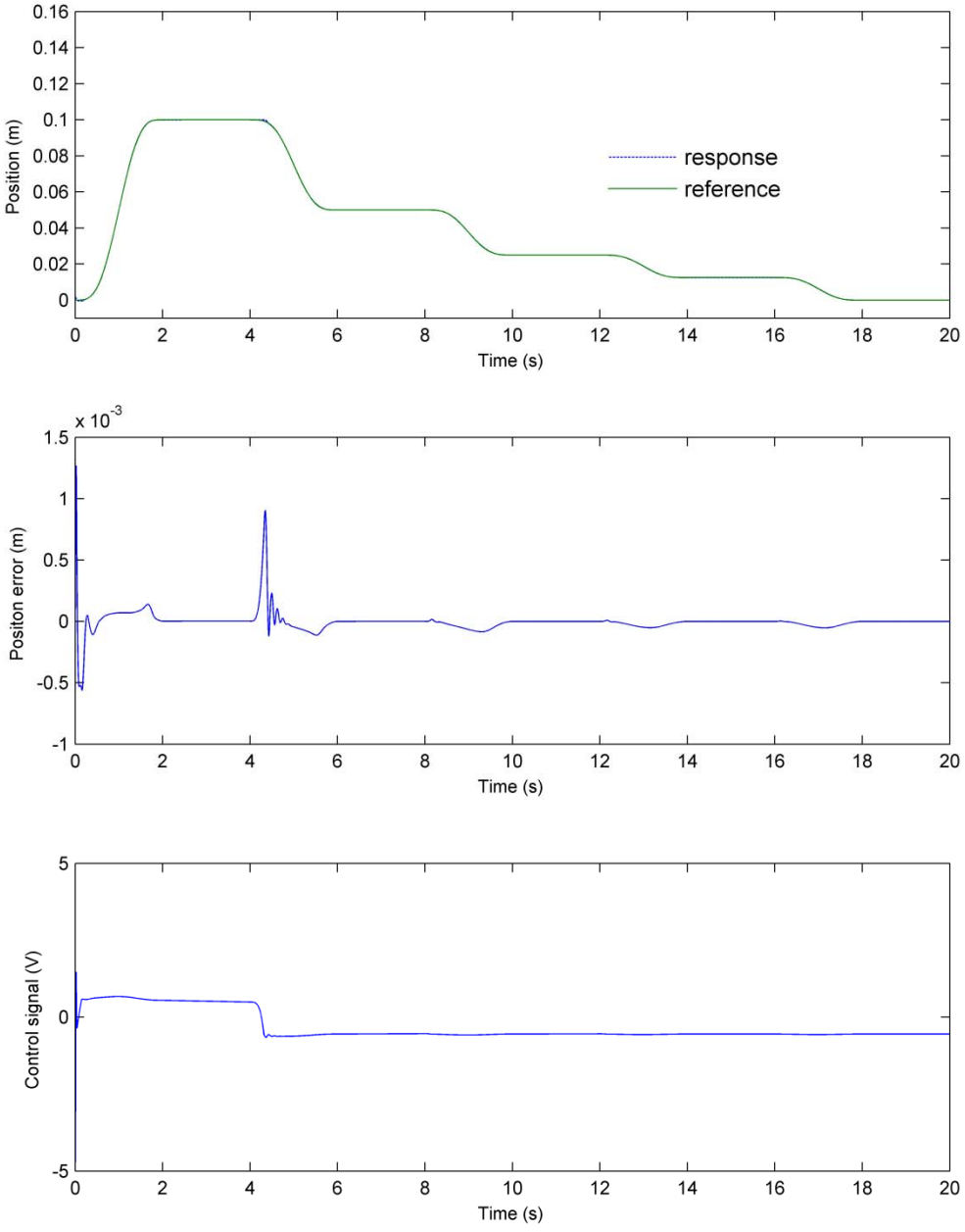

Figure 6.37 Simulated ramp trajectory for dynamical adaptive backstepping-sliding mode control responses with adaptive friction compensation in the servo pneumatic actuator with friction.

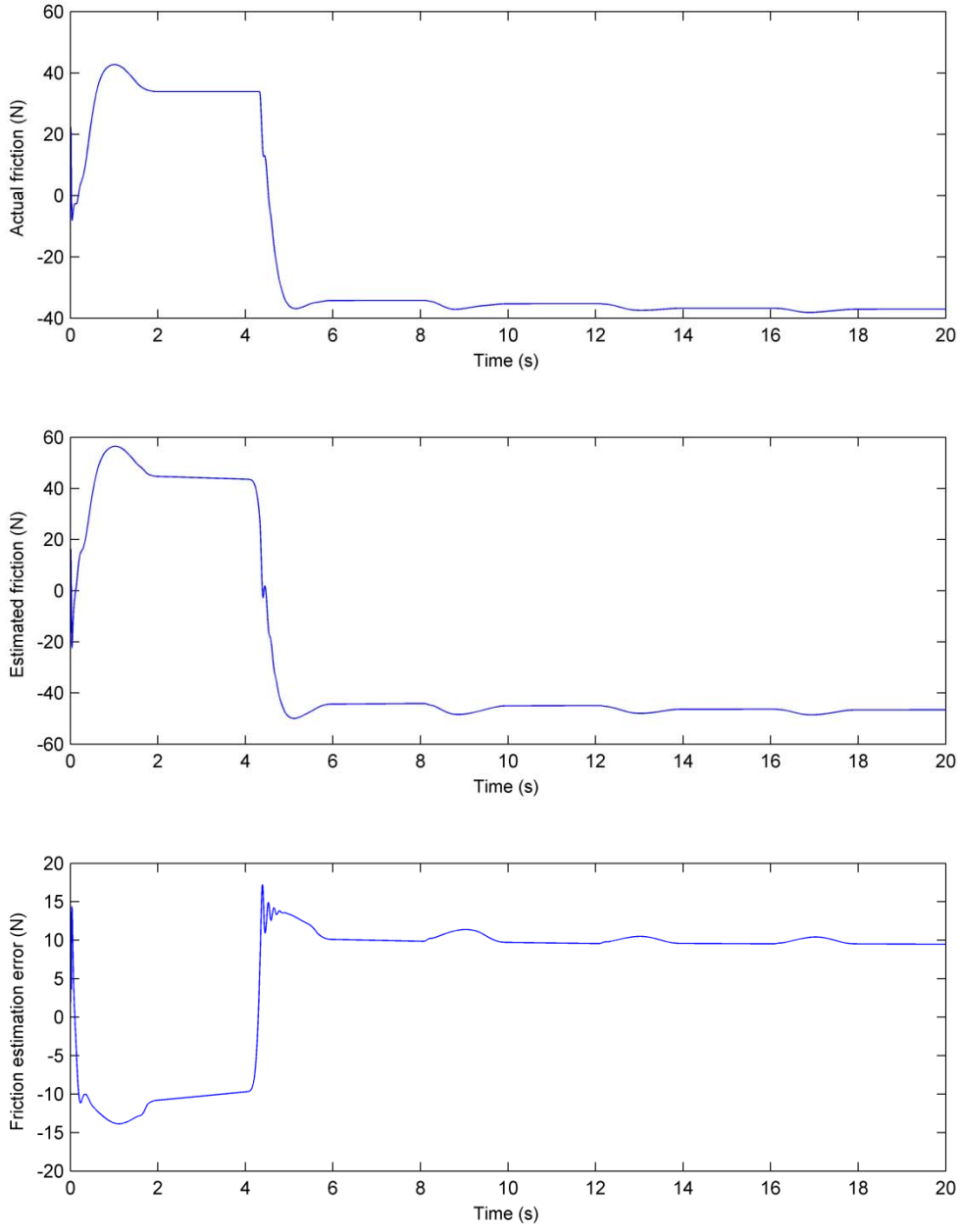

Figure 6.38 Friction estimation to ramp trajectory of dynamical adaptive backstepping-sliding mode control responses with adaptive friction compensation in the servo pneumatic actuator with friction.

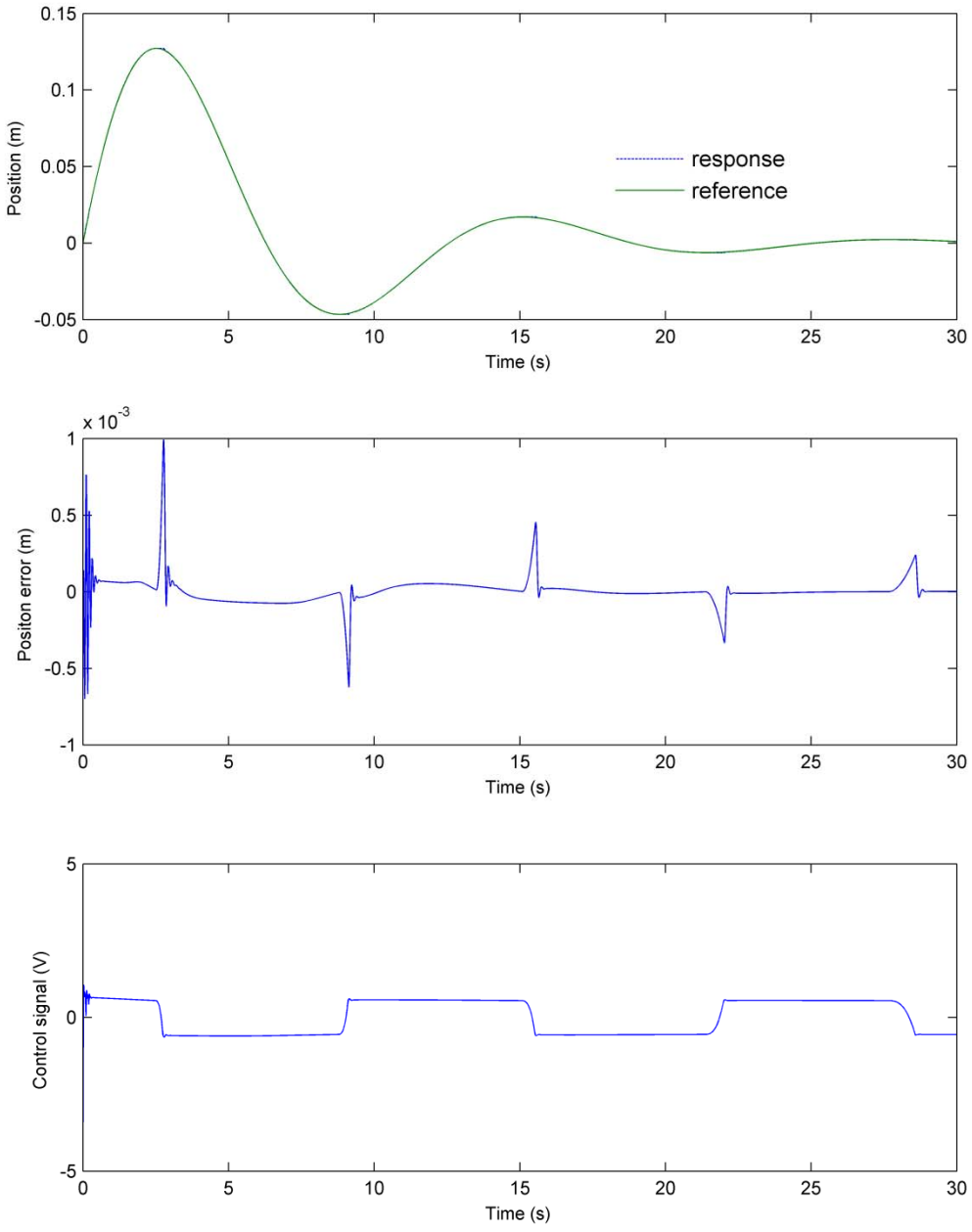

Figure 6.39 Simulated decreasing sine trajectory for dynamical adaptive backstepping-sliding mode control responses with adaptive friction compensation in the servo pneumatic actuator with friction.

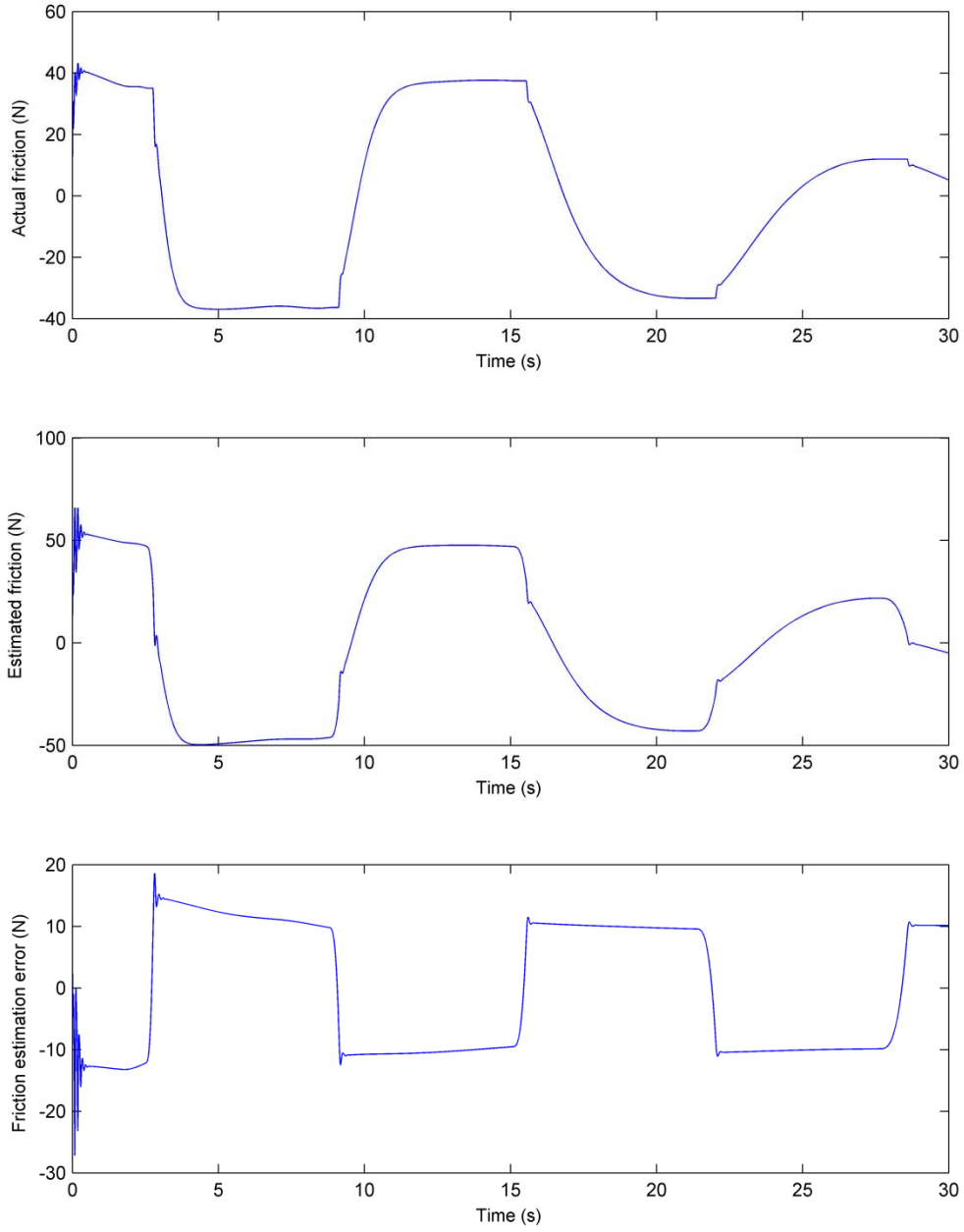

Figure 6.40 Friction estimation to decreasing sine trajectory of dynamical adaptive backstepping-sliding mode control responses with adaptive friction compensation in the servo pneumatic actuator with friction.

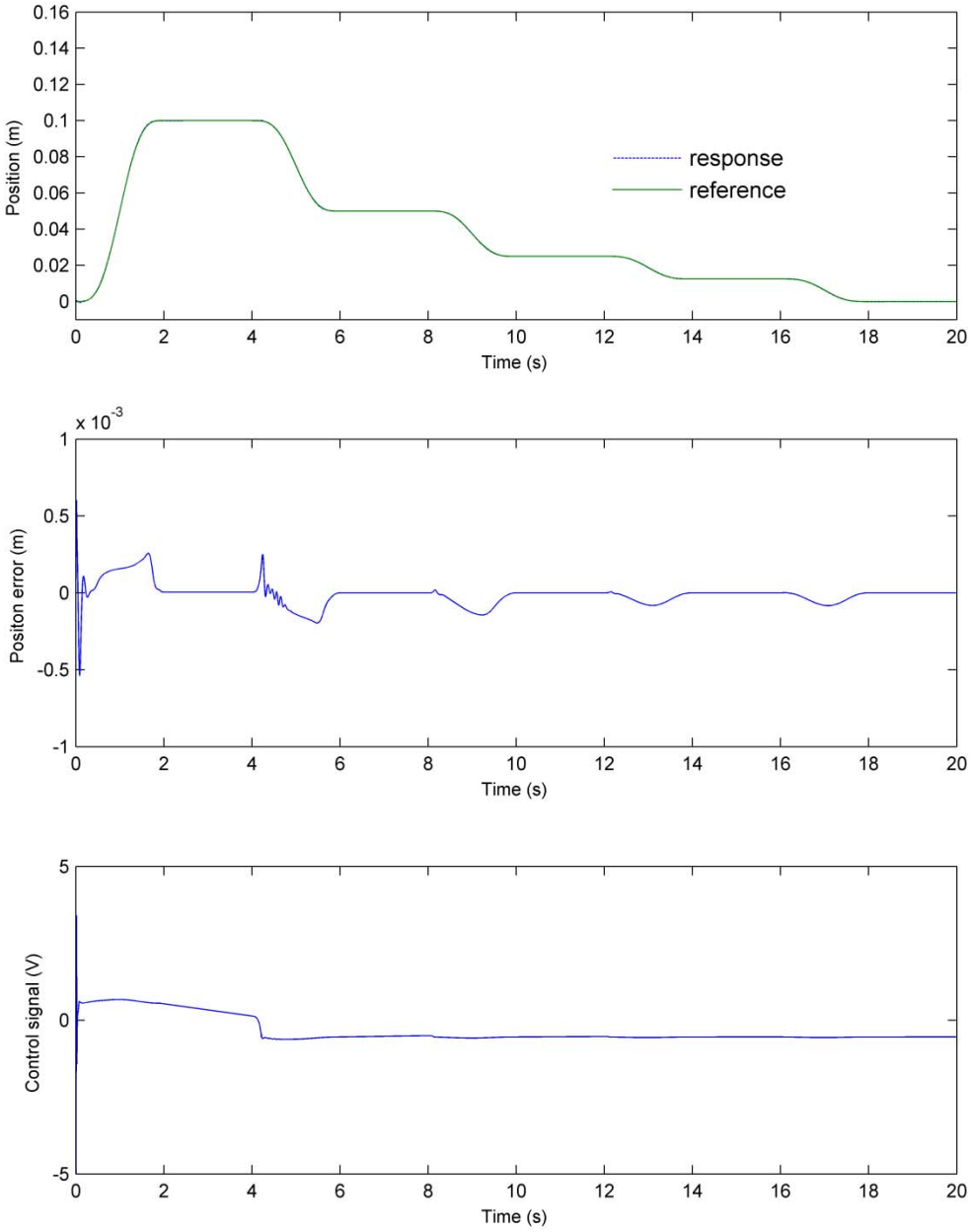

Figure 6.41 Simulated ramp trajectory for dynamical adaptive backstepping-sliding mode control responses with adaptive friction compensation, acceleration observer, and sliding mode control in the servo pneumatic actuator with friction.

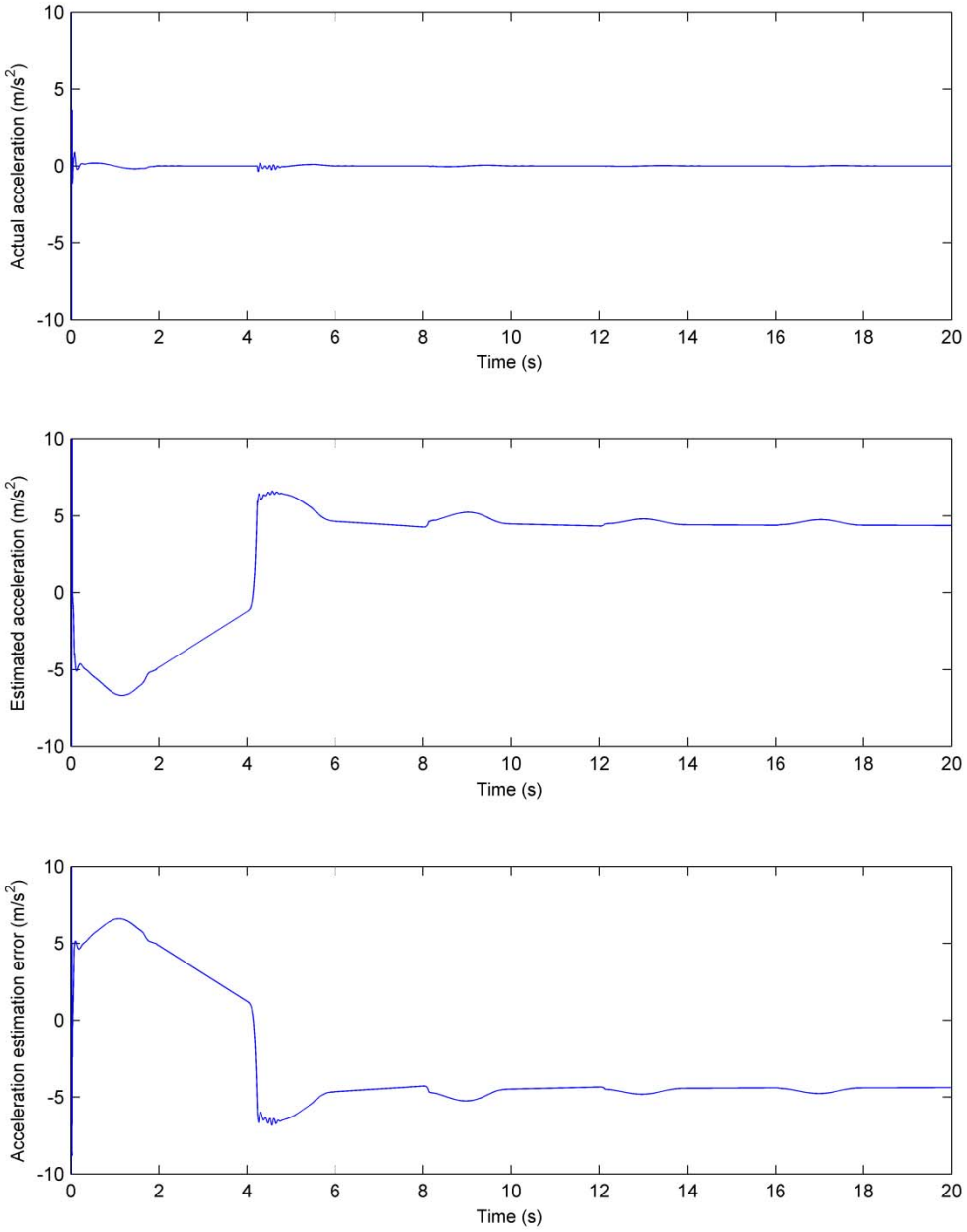

Figure 6.42 Acceleration estimation to ramp trajectory of dynamical adaptive backstepping-sliding mode control responses with adaptive friction compensation, acceleration observer, and sliding mode control in the servo pneumatic actuator with friction.

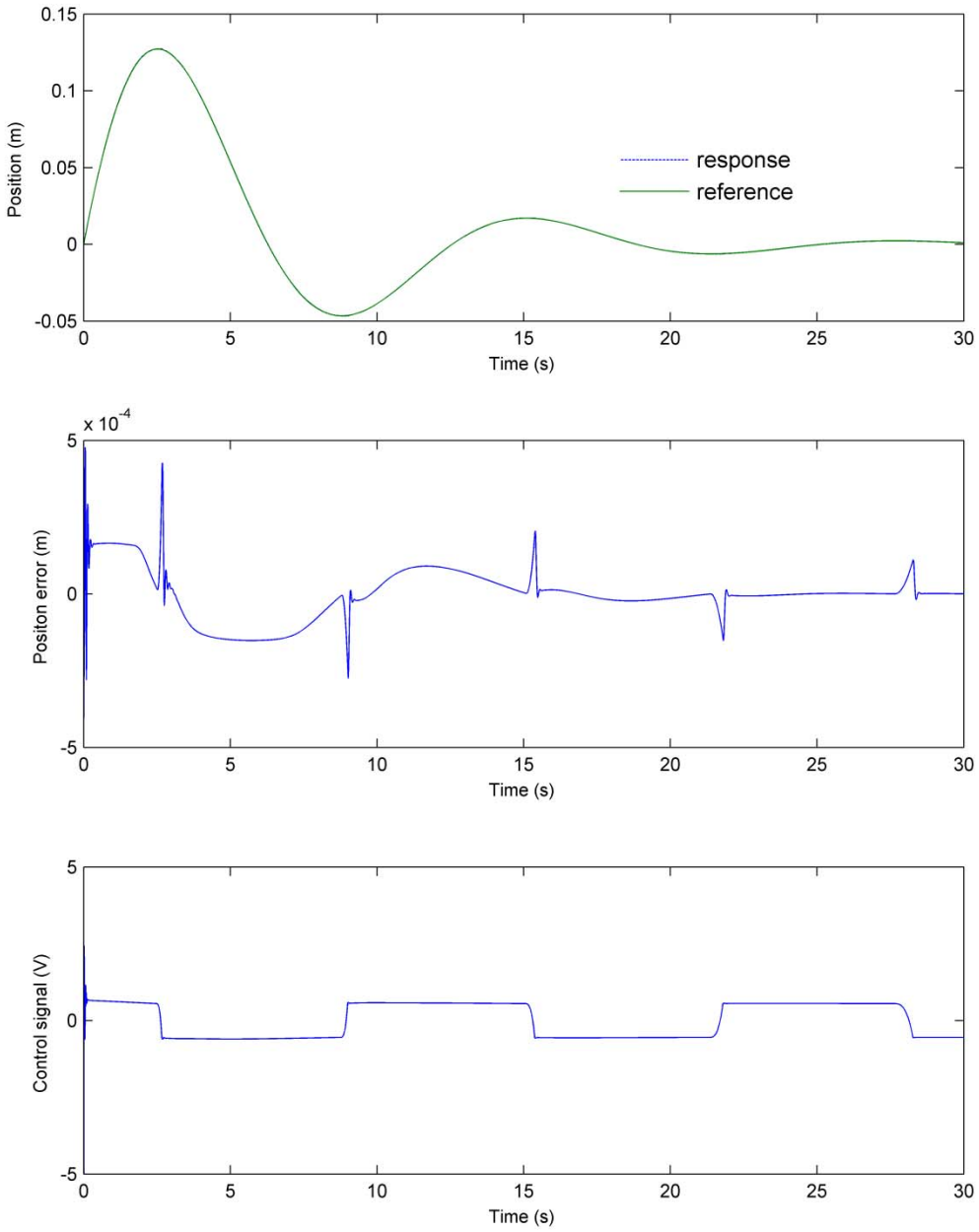

Figure 6.43 Simulated decreasing sine trajectory for dynamical adaptive backstepping-sliding mode control responses with adaptive friction compensation, acceleration observer, and sliding mode control in the servo pneumatic actuator with friction.

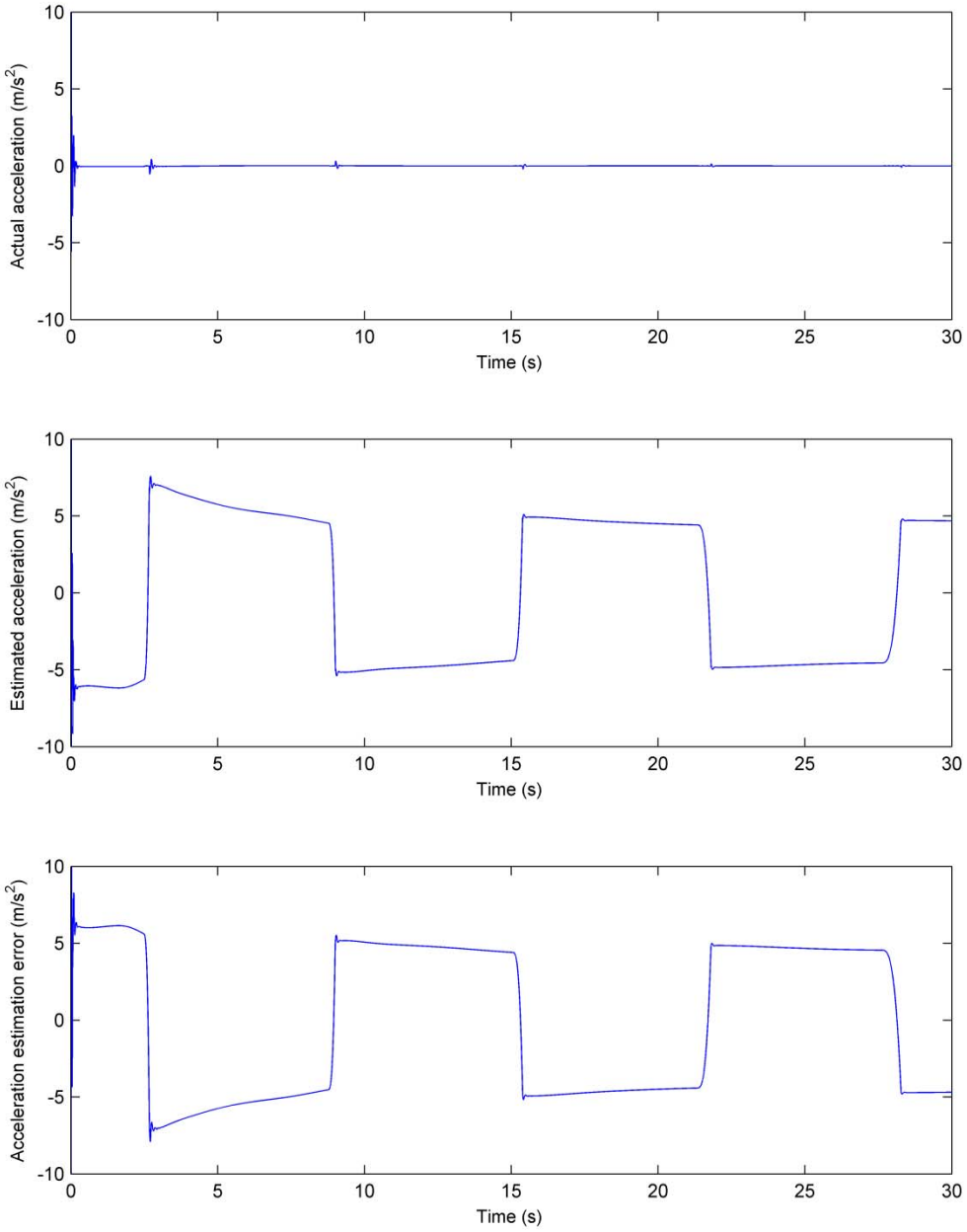

Figure 6.44 Acceleration estimation to decreasing sine trajectory of dynamical adaptive backstepping-sliding mode control responses with adaptive friction compensation, acceleration observer, and sliding mode control in the servo pneumatic actuator with friction.

6.4 Integration of Dynamical Adaptive Backstepping-Sliding Mode Control with Lyapunov-based Pressure Observer

A typical servo pneumatic actuator system employs two pressure sensors for pressure states feedback. The requirement for pressure sensing in the servo pneumatic actuator is burdensome. A globally stable Lyapunov-based pressure observer design is proposed by Gulati et al. [12]. The pressure observer utilizes displacement and velocity states and the control signal to estimate the pressures in the pneumatic cylinder chambers. A brief convergence proof of the pressure observer is provided for the reader's convenience.

The pressure observer is given in the form of

$$\dot{\hat{P}} = \alpha \frac{RT}{V} \dot{\hat{m}} - \alpha \frac{\dot{V}}{V} \hat{P}, \tag{6.9}$$

where $\dot{\hat{P}}$ is the estimated pressure dynamics, $\dot{\hat{m}}$ is the estimated mass flow rate, V is the chamber volume , and $\dot{V}$ is volumetric change rate of the chamber.

In order to show the convergence between the simulated and estimated pressure, the positive definite Lyapunov function V_l for the pressure observer is given as

$$V_l = \frac{1}{2}\left(PV - \hat{P}V\right)^2. \tag{6.10}$$

In the derivation of the pressure dynamics of the actuator model, the pressure dynamics is derived with the assumption of air in adiabatic process; hence, the thermal expansion coefficient $\alpha = r = 1.4$ is used. With reference to [12], the thermodynamics process in the actuator can vary from isothermal ($\alpha = 1$) process to adiabatic process ($\alpha = 1.4$). Hence, the actual pressure dynamics can be written as

$$\dot{P} = \alpha \frac{RT}{V} \dot{m} - \alpha \frac{\dot{V}}{V} P. \tag{6.11}$$

The time derivative of equation (6.10) gives

$$\dot{V}_l = \frac{1}{2}\left(PV - \hat{P}V\right)\left(\dot{P}V + \alpha P\dot{V} - \dot{\hat{P}}V - \alpha\hat{P}\dot{V}\right) \tag{6.12}$$

Substituting equations (6.9) and (6.11) into equation (6.12),

$$\dot{V}_l = \alpha RTV\left(P - \hat{P}\right)\left(\dot{m} - \dot{\hat{m}}\right) \tag{6.13}$$

The proof of $\dot{V}_l \leq 0$ is shown graphically by the valve flow dynamics (see Figure 6.45). Both charging and discharging process shows that the relation between chamber pressure and mass flow rate possess the monotone property, i.e., $\left(P - \hat{P}\right)\left(\dot{m} - \hat{\dot{m}}\right) \leq 0$ holds all the time. In addition, the thermal expansion coefficient α varies from isothermal process to adiabatic process but is always greater than zero; therefore, $\dot{V}_l \leq 0$. This ends the proof of the convergence of the pressure observer.

With reference to the simulation results of ramp reference tracking in Figure 6.46, the system performance after the integration of DAB-SMC controller with the pressure observer does not show significant variations from that of the system prior to integration. This suggests that the system after integration can provide equivalent performance for ramp reference tracking. With respect to Figure 6.47, the pressure estimation error plot shows the convergence property of pressure estimate for one of the actuator chambers. The simulation results shown in Figure 6.48 confirm that satisfactory performance also can be obtained for sinusoidal reference tracking. With respect to Figure 6.49, the pressure observer shows the convergence property for sinusoidal reference tracking as well.

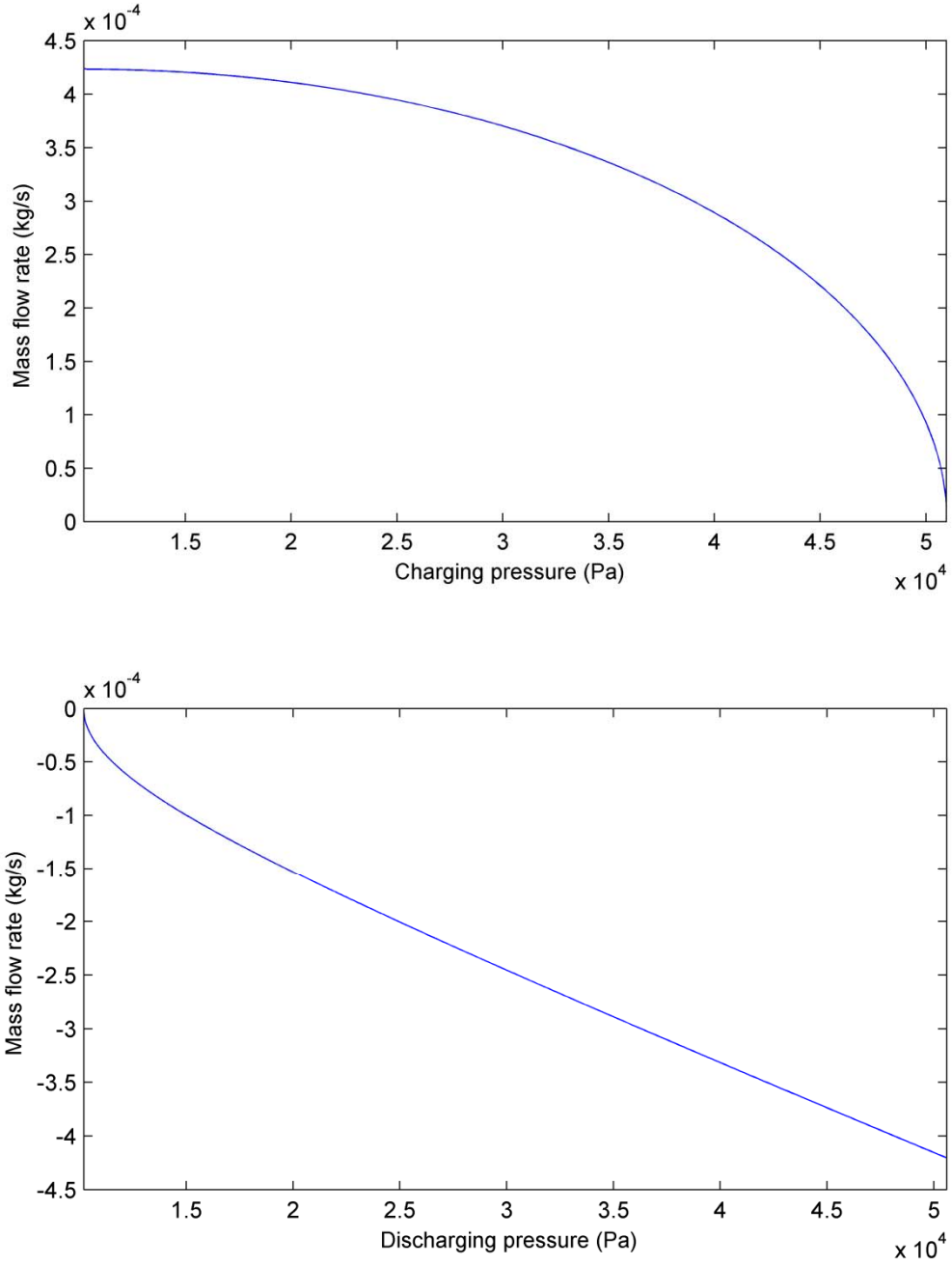

Figure 6.45 (a) mass flow for charging process, (b) mass flow for discharging process.

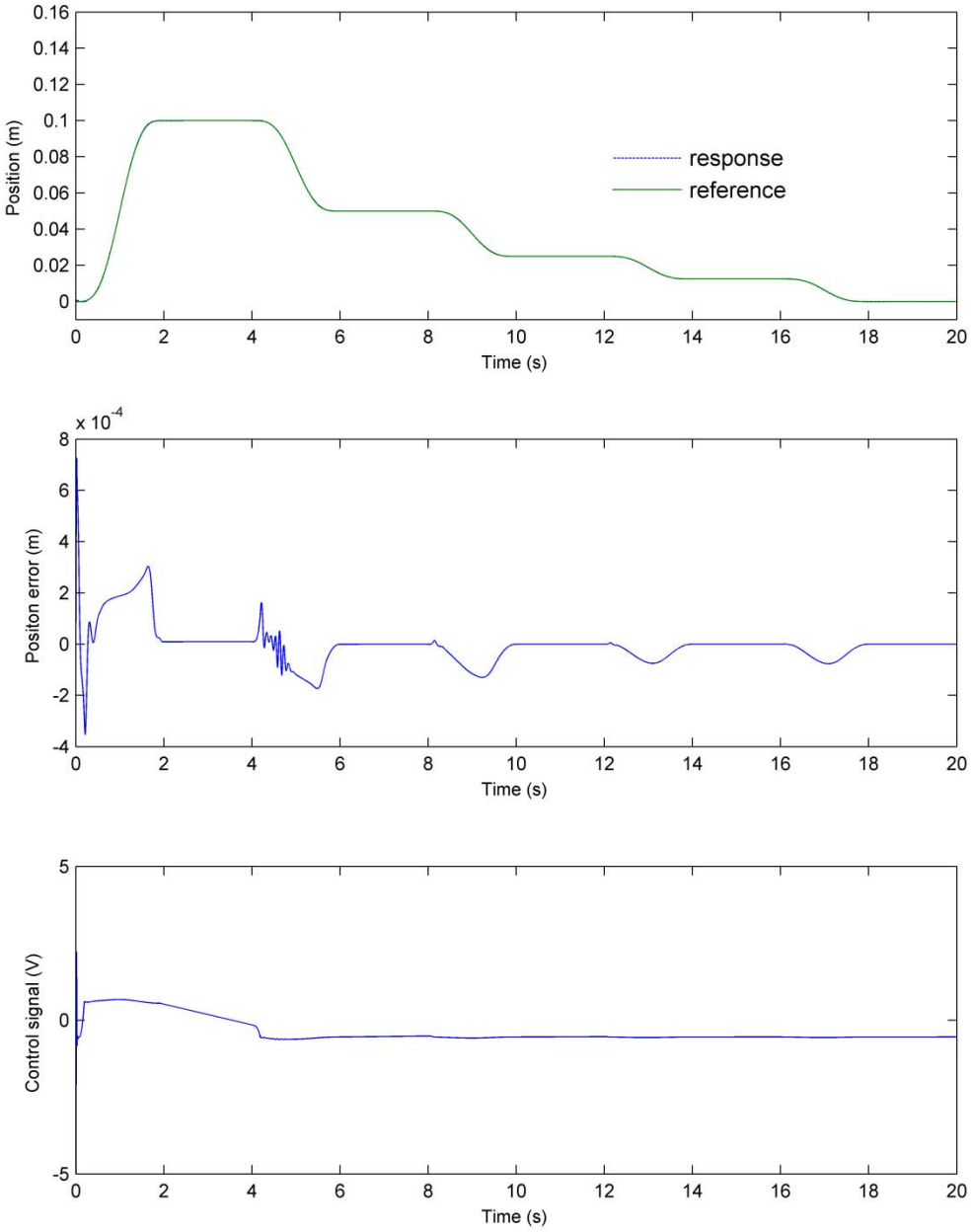

Figure 6.46 Simulated ramp reference tracking for dynamical adaptive backstepping-sliding mode control responses with pressure observer in the servo pneumatic actuator with friction.

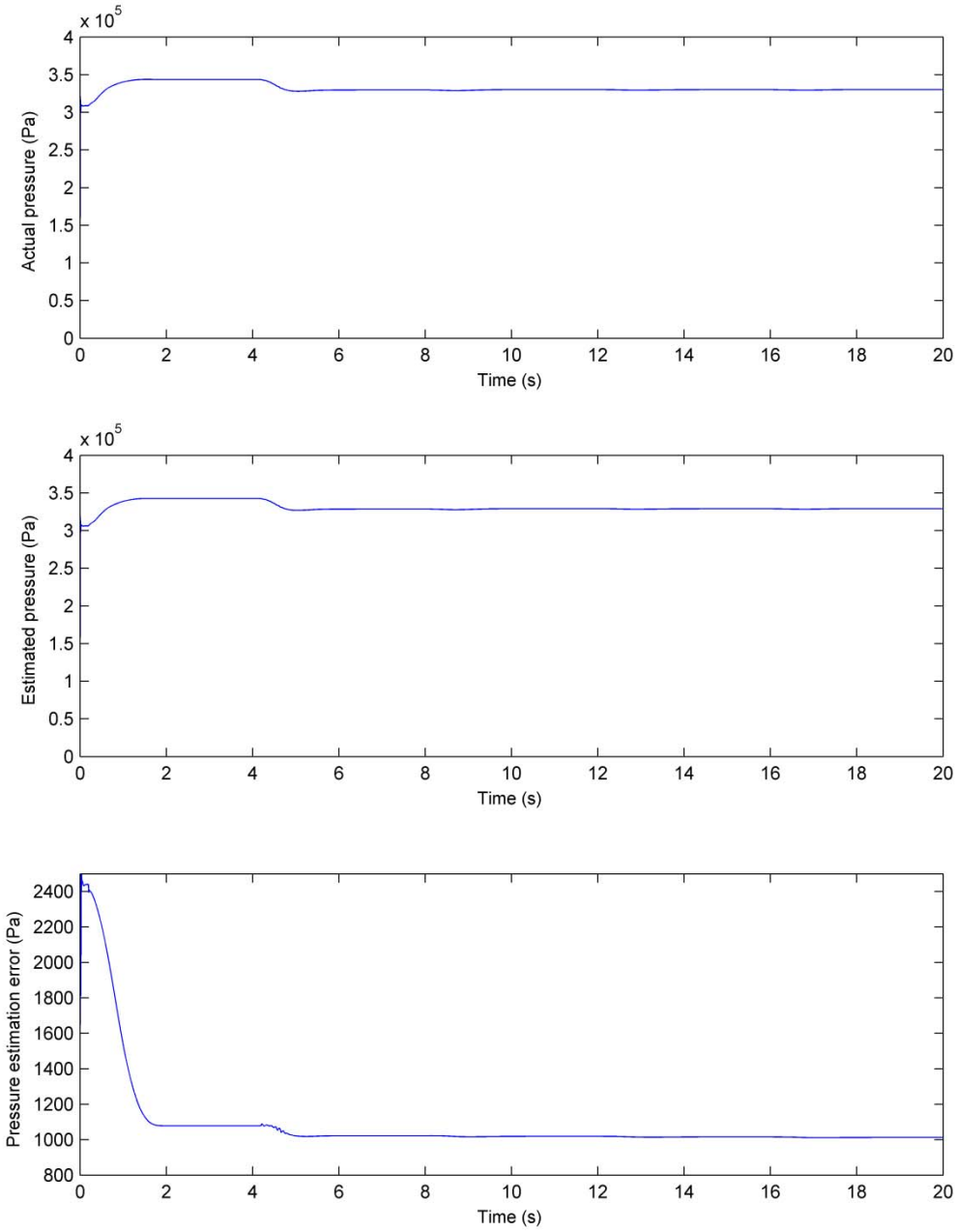

Figure 6.47 Pressure estimation to ramp reference tracking of dynamical adaptive backstepping-sliding mode control of the servo pneumatic actuator with friction.

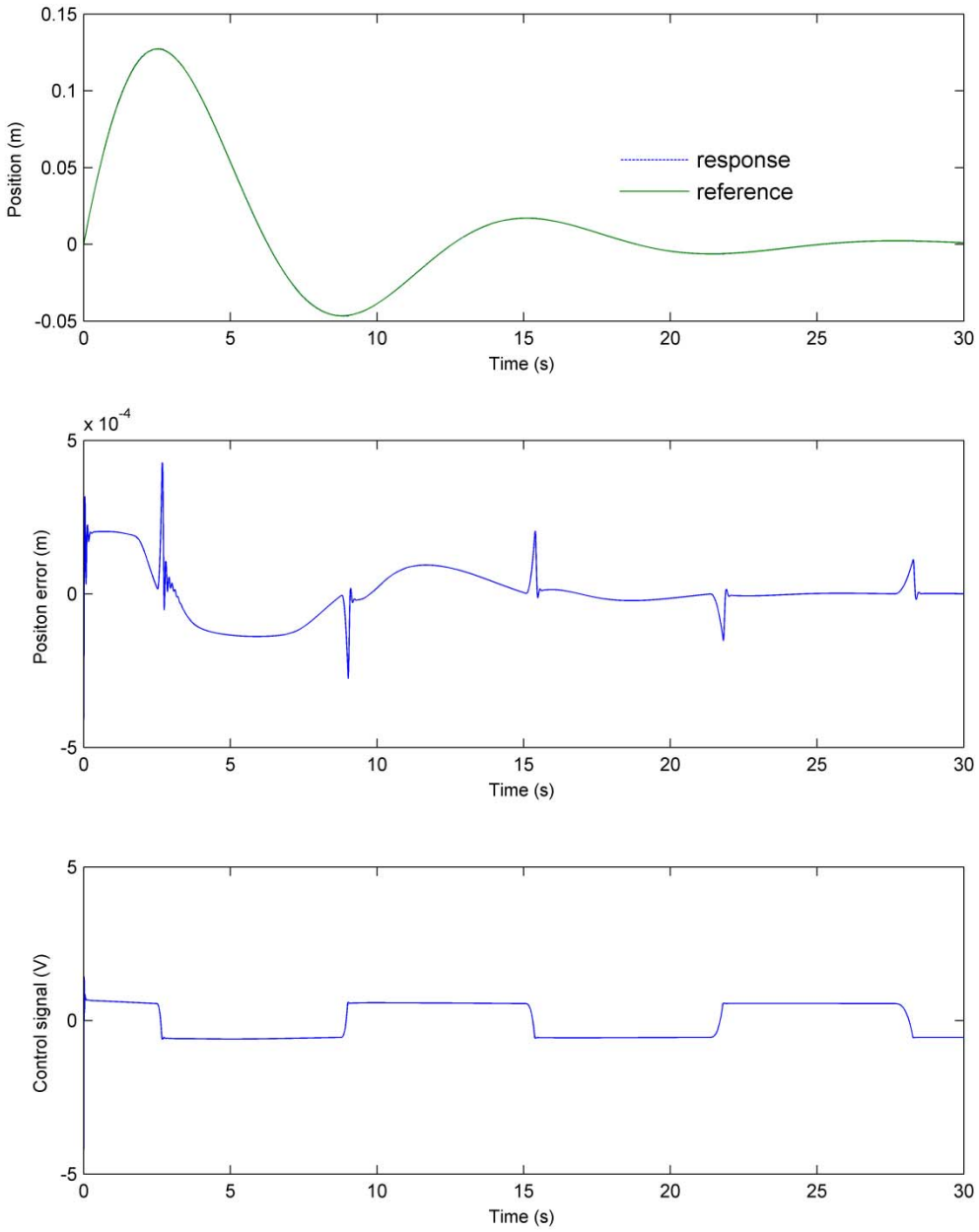

Figure 6.48 Simulated decreasing sine reference tracking for dynamical adaptive backstepping-sliding mode control responses with pressure observer in the servo pneumatic actuator with friction.

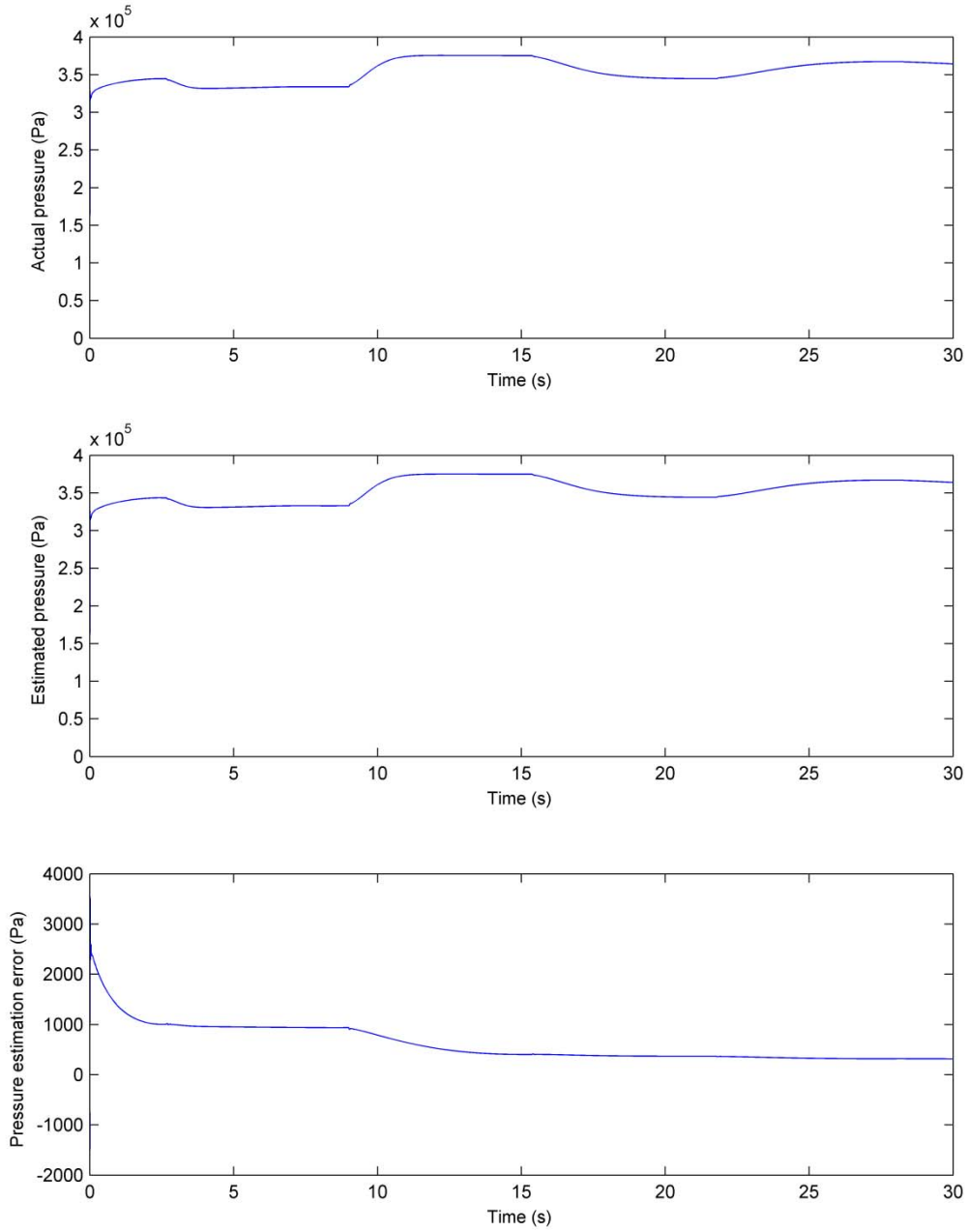

Figure 6.49 Pressure estimation to decreasing sine reference tracking of dynamical adaptive backstepping-sliding mode control responses with pressure observer in the servo pneumatic actuator with friction.

6.5 Summary

In this chapter, the validity of the mathematical model developed for servo pneumatic actuator is verified, and reference test trajectories are constructed to evaluate the performance of the controllers developed in Chapter 5. The nonlinear controllers from previous works are simulated and the results are compared. The results suggest that sliding mode controller performs better than cascade controller, and cascade controller performs better than backstepping controller. Then, the newly developed dynamical adaptive backsteping-sliding mode controller (DAB-SMC) is evaluated using the same testing trajectories, and the results shows that the new controller performs better than all previous controllers in terms reference tracking. Finally, the integration of a Lyapunov-based pressure observer and the DAB-SMC is considered for the control system and the simulation results show no significant changes in comparison with the control system before the integration. The controller gains used in the simulations are summarized in Table 6.3.

With the integration of the pressure observer, the prerequisites for the implementation of DAB-SMC controller are as follows: (1) the identification of the static friction, Coulomb friction, and Stribeck velocity is required for the type of pneumatic actuator used in the implementation; (2) an optical sensor is required for the measurement of the actuator displacement; (3) the velocity of the actuator is required and can be estimated numerically from a regression function on the displacement feedback data.

Table 6.3 Controller parameters.

Controller parameters in sliding mode control	**Value**
λ	150
η	$5e^{-5}$
φ	20
Controller parameters in cascade control	**Value**
k_p	150
k_v	40
λ	50
Controller parameters in Backsteping control	**Value**
k_1	80
k_2	20
k_3	200
Controller parameters in DAB-SMC	**Value**
k_1	80
k_2	20
k_3	200
Γ_1	0.001
Γ_2	0.02
Γ_3	0.001
η	0.001
γ_0	0.08
γ_1	0.08
γ_{12}	0.08

Chapter 7. Conclusions

In order to provide good reference tracking, control engineers designing tracking control systems need to be aware of the friction induced adverse effects; hence, a comprehensive review of the friction associated with mechanical system is provided in this study. To analyze systems with friction, the approach taken in this study is through a simplified non-smooth system model of friction. This approach allows the analysis of complex system to be completed in a simplified fashion. The results of the analysis suggest that it is absolutely necessary to provide friction compensation to the systems with friction so as to avoid friction induced instability and low performance.

In spite of existence of many references regarding pneumatic tracking systems, the literature in the area of incorporating the friction effect in pneumatic tracking system is still sparse. Particularly, prior to this study there is no publication on the survey of using Lyapunov-based nonlinear control techniques in servo pneumatic actuators. This thesis has made a number of contributions to the development, implementation, and simulation evaluation of nonlinear adaptive and robust control laws for pneumatic actuator moving at low speed. A dynamical adaptive backstepping-sliding mode controller (DAB-SMC) is developed and verified for servo pneumatic actuator through the simulation of its mathematical model. The simulation is accomplished by introducing the friction to the actuator simulator through the LuGre friction model. The simulation program can simulate the following scenarios: (1) tracking control without the consideration of friction in the system model, (2) tracking control with feedforward model-based friction compensation, (3) tracking control with adaptive compensation of friction, and (4) tracking control with the integration of the developed controller and a Lyapunov-based pressure observer.

The DAB-SMC controller in this study is able to provide good performance for reference tracking despite the friction disturbance to the pneumatic actuator model. The controller also inherits robustness due to the incorporation of sliding mode control law. The integration of the controller with the Lyapunov-based pressure observer is able to reduce the state feedback of servo pneumatic system to only piston displacement.

References

[1] W.S. Owen, *An Investigation into the Reduction of Stick-slip Friction in Hydraulic Actuator (M. Sc. Thesis)*. Vancouver, BC: University of British Columbia, 2001.

[2] B. Armstrong-Helouvry, "Survey of models, analysis tools and compensation methods for control of machines with friction," *Automatica*, vol. 30, pp. 1083-138, 1994.

[3] H. Olsson, K.J. Astrom, D.W. Canudas, M. Gafvert and P. Lischinsky, "Friction models and friction compensation," *Eur. J. Control*, vol. 4, pp. 176-95, 1998.

[4] P. Dahl, *A Solid Friction Model (Tech. Rep. TOR-0158(3107-18)-1)*. EL Segundo, CA: Aerospace Corporation, 1968.

[5] D.W. Canudas, H. Olsson, K.J. Astrom and P. Lischinsky, "A new model for control of systems with friction," *IEEE Trans. Autom. Control*, vol. 40, no. 3, pp. 419-25, 1995.

[6] D.W. Canudas and P. Lischinsky, "Adaptive friction compensation with partially known dynamic friction model," *Int. J. Adapt. Control Signal Process.*, vol. 11, no. 1, pp. 65-80, 1997.

[7] A.F. Filippov, "Differential equations with discontinuous right-hand side," *Amer. Math. Soc. Translations*, vol. 42, pp. 199-231, 1964.

[8] Q. Wu and N. Sepehri, "On Lyapunov's stability analysis of non-smooth systems with applications to control engineering," *Int. J. Non Linear Mech.*, vol. 36, no. 10, pp. 1153-61, 2001.

[9] R.I. Leine and N. Van De Wouw, *Stability and Convergence of Mechanical Systems with Unilateral Constraints.* Berlin, Germany: Springer-Verlag, 2008.

[10] Z. Rao and G.M. Bone, "Nonlinear modeling and control of servo pneumatic actuators," *IEEE Trans. Control Syst. Technol.*, vol. 16, no. 5, pp. 562-9, 2008.

[11] R. Guenther, E.C. Perondi, E.R. Depieri and A.C. Valdiero, "Cascade controlled pneumatic positioning system with LuGre model based friction compensation," *J. Braz. Soc. Mech. Sci. Eng.*, vol. 28, pp. 48-57, 2006.

[12] N. Gulati and E.J. Barth, "A globally stable load-independent pressure observer for the servo control of pneumatic actuators," *IEEE/ASME Trans. Mechatron.*, vol. 14, no. 6, pp. 295-306, 2009.

[13] J.J. Slotine and W. Li, *Applied Nonlinear Control.* Englewood Cliffs, NJ: Prentice-Hall, 1991.

[14] V.I. Utkin, "Discontinuous control system: state of art in theory and applications," *Automatic Control-World Congress,* vol. 1, pp. 25-44, 1988.

[15] M. Krstic, I. Kanellakopoulos and P. Kokotovic, *Nonlinear and Adaptive Control Design.* New York, NY: Wiley, 1995.

[16] M. Rios-Bolivar, H. Sira-Ramirez and A.S.I. Zinober, "Output tracking control via adaptive input-output linearization: a backstepping approach," *IEEE Conf. Decis. Control,* vol. 2, pp. 1579-84, 1995.

[17] M. Rios-Bolivar, *Adaptive Backstepping and Sliding Mode Control of Uncertain Nonlinear Systems (Ph.D. Thesis).* Sheffield, UK: University of Sheffield, 1997.

[18] M. Rios-Bolivar and A.S.I. Zinober, "Dynamical adaptive sliding mode control of observable minimum-phase uncertain nonlinear systems," *Proceedings of Variable Structure Systems, Sliding Mode and Nonlinear Control,* pp. 211-35, 1999.

[19] S. Ning and G.M. Bone, "High steady-state accuracy pneumatic servo positioning system with PVA/PV control and friction compensation," *IEEE Int. Conf. Rob. Autom.,* pp. 2824-9, 2002.

[20] S. Liu and J.E. Bobrow, "An analysis of a pneumatic servo system and its application to a computer-controlled robot," *Trans ASME, J. Dyn. Syst. Meas. Control,* vol. 110, no. 3, pp. 228-35, 1988.

[21] J. Wang, J. Pu and P. Moore, "A practical control strategy for servo-pneumatic actuator systems," *Control Eng. Pract.,* vol. 7, no. 12, pp. 1483-8, 1999.

[22] M. Karpenko, *Design of A Nonlinear Position Controller for A Pneumatic Actuator with Friction (Report).* Winnipeg, MB: University of Manitoba, 2003.

[23] D. Ben-Dov and S.E. Salcudean, "A force-controlled pneumatic actuator," *IEEE Trans. Rob. Autom.,* vol. 11, no. 12, pp. 906-11, 1995.

[24] J. Halling, *Principle of Tribology.* London, UK: Macmillan Press, 1975.

[25] B. Armstrong-Helouvry, *Control of Machines with Friction.* Boston, MA: Kluwer Academic Publisher, 1991.

[26] D. Karnopp, "Computer simulation of stick-slip friction in mechanical dynamic system," *J. Dyn. Syst. Meas. Control Trans. ASME,* vol. 107, no. 1, pp. 100-103, 1985.

[27] N. Sepehri, F. Sassani and P. Lawrence, "Simulation and experimental studies of gear backlash and stick-slip friction in hydraulic excavator swing motion," *ASME J. Dyn. Syst. Meas. Control,* vol. 118, pp. 463-7, 1996.

[28] V. Johanes, M. Green and C. Brockey. "The role of the rate of application of the tangential force in determining the static friction coefficient," *Wear,* vol. 24, no. 3, pp. 381-85, 1973.

[29] D.P. Hess and A. Soom, "Friction at a lubricated line contact operating at oscillating sliding velocities," *J. Tribology,* vol. 112, no. 1, pp. 147-52, 1990.

[30] H. Zeng and N. Sepehri, "Tracking control of hydraulic actuators using a LuGre friction model compensation," *J. Dyn. Syst. Meas. Control,* vol. 130, no. 1, pp. 014502-1-7, 2008.

[31] N. Rouche, P. Habets and M. Laloy, *Stability Theory by Liapunov's Direct Method.* Berlin, Germany: Springer-Verlag, 1977.

[32] L.M. Timothy, *Nonlinear Control System Stability via the Second Method of Lyapunov (Ph.D. Thesis).* Ann Arbor, MI: University of Utah, 1960.

[33] M. Vidyasagar, *Nonlinear Systems Analysis.* Englewood Cliffs, NJ: Prentice-Hall, 1993.

[34] M. Karpenko and N. Sepehri, "Development and experimental evaluation of a fixed-gain nonlinear control for a low-cost pneumatic actuator," *IEE Proc., Control Theory Appl.,* vol. 153, no. 6, pp. 629-40, 2006.